Interactions entre la supraconductivité et la criticité quantique, dans les composés CeCoIn5, URhGe et UCoGe

Ludovic Howald

▶ **To cite this version:**

Ludovic Howald. Interactions entre la supraconductivité et la criticité quantique, dans les composés CeCoIn5, URhGe et UCoGe. Autre [cond-mat.other]. Université de Grenoble, 2011. Français. NNT : 2011GRENY010 . tel-00584598v2

HAL Id: tel-00584598

https://theses.hal.science/tel-00584598v2

Submitted on 11 Apr 2011

HAL is a multi-disciplinary open access archive for the deposit and dissemination of scientific research documents, whether they are published or not. The documents may come from teaching and research institutions in France or abroad, or from public or private research centers.

L'archive ouverte pluridisciplinaire **HAL**, est destinée au dépôt et à la diffusion de documents scientifiques de niveau recherche, publiés ou non, émanant des établissements d'enseignement et de recherche français ou étrangers, des laboratoires publics ou privés.

UNIVERSITÉ DE GRENOBLE

THÈSE
pour obtenir le grade de:
DOCTEUR DE L'UNIVERSITÉ DE GRENOBLE
Spécialité: **Physique de la matière condensée et du rayonnement**
Arrêté ministériel: 7 août 2006

Présentée par

Ludovic Howald

Thèse dirigée par **Jean-Pascal Brison**
préparée au sein du **Service de Physique Statistique, Magnétisme et Supraconductivité (SPSMS)**
dans **l'École Doctorale de Physique, Grenoble**

Interactions entre la supraconductivité et la criticité quantique, dans les composés $CeCoIn_5$, URhGe et UCoGe

Thèse soutenue publiquement le **11 février 2011,**
devant le jury composé de:

Dr. Claude BERTHIER
Laboratoire National des Champs Magnétiques Intenses (Président)
Prof. Hermann SUDEROW
Universidad Autónoma de Madrid (Rapporteur)
Dr. Christoph MEINGAST
Karlsruhe Institute of Technology (Rapporteur)
Dr. Jean-Pascal BRISON
Commissariat l'Énergie Atomique (Directeur de thèse)

Interactions between Superconductivity and Quantum Criticality in $CeCoIn_5$, URhGe and UCoGe

Abstract

The subject of this thesis is the analyze of the superconducting upper critical field (Hc2) and the interaction between superconductivity and quantum critical points (QCP), for the compounds CeCoIn5, URhGe and UCoGe. In CeCoIn5, study by mean of resistivity of the Fermi liquid domain allows us to localize precisely the QCP at ambient pressure. This analyze rule out the previously suggested pinning of Hc2(0) at the QCP. In a second part, the evolution of Hc2 under pressure is analyzed. The superconducting dome is unconventional in this compound with two characteristic pressures: at 1.6GPa, the superconducting transition temperature is maximum but it is at 0.4GPa that physical properties (maximum of Hc2(0), maximum of the initial slope dHc2/dT, maximum of the specific heat jump DC/C,...) suggest a QCP. We explain this antagonism with pair-breaking effects in the proximity of the QCP. With these two experiments, we suggest a new phase diagram for CeCoIn5.

In a third part, measurements of thermal conductivity on URhGe and UCoGe are presented. We obtained the bulk superconducting phase transition and confirmed the unusual curvature of the slope dHc2/dT observed by resistivity. The temperatures and fields dependence of thermal conductivity allow us to identify a non-electronic contribution for heat transport down to the lowest temperature (50mK) and probably associated with magnon or longitudinal fluctuations. We also identified two different domains in the superconducting region, These domains are compatible with a two bands model for superconductivity. Thermopower measurements on UCoGe reveal a strong anisotropy to current direction and several anomaly under field applied in the b direction. We suggest a Lifshitz transition to explain our observations in these two compounds.

Keywords

heavy fermion
unconventional superconductivity
$CeCoIn_5$
resistivity
quantum critical point (QCP)
upper critical field (H_{c2})
ferromagnetic supercondctor
URhGe
UCoGe
thermal conductivity
thermoelectric power

Résumé

Le sujet de cette thèse est l'analyse du second champ critique supraconducteur (Hc2) ainsi que l'interaction entre la supraconductivité et les points critiques quantiques (PCQ), pour les composés CeCoIn5, URhGe et UCoGe. Dans le composé CeCoIn5, l'étude par résistivité du domaine de liquide de Fermi a permis la localisation précise du PCQ a pression ambiante. Cette analyse permet d'invalider l'hypothèse d'une coïncidence entre Hc2(0) et le PCQ. Dans une deuxième partie, l'évolution sous pression de Hc2 est analysée. Le dôme supraconducteur de ce composé est non-conventionnel avec deux pressions caractéristiques différentes: à 1.6GPa, la température de transition supraconductrice est maximum alors que c'est à 0.4GPa que la plupart des grandeurs physiques (maximum de Hc2(0), maximum de la pente dHc2/dT, maximum du saut de chaleur spécifique DC/C, ...) suggèrent la présence d'un PCQ. Nous expliquons cet antagonisme par l'importance des processus de brisure de pairs liés a la proximité du PCQ. Ces deux observations nous permettent de proposer un nouveau diagramme de phase pour CeCoIn5.

Dans une troisième partie, les mesures de conduction thermique sur les composés URhGe et UCoGe sont présentées. Elles nous permettent dans un premier temps d'obtenir la transition "bulk" supraconductrice et de confirmer la forme in-habituelle de Hc2 observée en résistivité. La dépendance en températures et en champs de la conduction thermique nous permet d'identifier une contribution non-électronique au transport de chaleur jusqu'aux plus basses températures. D'autre part, nous identifions deux différents domaines supraconducteurs a bas et hauts champs appliqués selon l'axe b. Ces deux domaines sont compatibles avec un modèle de supraconductivité multigaps. Suivant ces observations et des mesures de pouvoir thermoélectrique, nous proposons un modèle de transition de Lifshitz pour ces deux composés.

Mots Clés

fermions lourds
supraconductivité non-conventionelle
$CeCoIn_5$
resistivité
point critique quantique
champ critique
supraconducteurs ferromagnétiques
URhGe
UCoGe
conductivité thermique
pouvoir thermoelectrique

Merci

Merci a tous ceux qui m'ont soutenu pour cette thèse et sans qui elle n'aurait pas été possible:

Je tiens premièrement à remercier Hermann Suderow qui m'a fait découvrir et m'a conseillé la physique des fermions lourds à Grenoble. Merci à lui aussi d'avoir accepté d'être rapporteur de ma thèse. Je veux aussi remercier Christoph Meingast d'avoir été rapporteur de ma thèse et pour ces intéressantes remarques. Merci aussi à Claude Berthier d'avoir présider le Jury de ma thèse.

Merci a Jean-Pascal Brison de m'avoir initié à la physique des fermions lourds, de m'avoir enseigner les techniques de mesures de résistivité, conduction thermique, de la physique à basse températures et à la thermométrie. J'ai beaucoup apprécié ces trois années passées à Grenoble.

Cette thèse n'aurait pas été aussi intéressantes sans les grandes discussions en partie de physique avec Valentin Taufour et Elena Hassinger ainsi que les fondues, raclette, bières et autres avec également Atsushi, Tatsuma, Tristan, Mathieu, Amalia, Pierre-Jean, Liam, Giorgos, Pana, Alex

Je remercie également Liam Malone, pour ça relecture attentive du manuscrit.

Merci à Jean-Michel Martinod pour son aide précieuse en cryogénie et pour les améliorations de la Manip. Merci aussi à Michel, Maire-Jo, Frederic, Jean-Luc, Marielle, Pierre, Frédéric, pour leurs grandes aides techniques et administratives.

Cette thèse n'aurait pas été possible sans les excellents cristaux fourni par Gérard Lapertot, Dai Aoki et Valentin Taufour.

Merci à Gerog Knebel, pour m'avoir transmis un peu de sa grande expertise dans les composés 115 et pour ces nombreuses heures de course à pied partagée également avec Elena, Giorgos, Alain, Tatsuma, Mario, ... sans lesquelles, il serait impossible de rester de nombreuses heures dans le labo à chercher ce qui (ne) fonctionne (pas) et rester en forme!

Vincent Michal et Vladimir Mineev m'ont aussi apportés une aides théorique précieuses, ainsi que toutes les personnes avec qui j'ai eu la chance de pouvoir discuter pendant ces trois années dans le labo ou en conférences.

Finalement, un grand Merci à mes parents, ma famille, Erika de m'avoir soutenu pendant ces années de thèse. Merci aussi à tous ceux qui m'ont accompagné en montagne et a celle-ci d'avoir été là pour profiter de la vie à Grenoble.

Contents

Once upon a time, in the heart of a dying star was formed a Ce nucleus. Soon after it mother star explode, the Ce nucleus cool down and attract 58 electrons to get a neutral charge. The electronic world is not fair, the first electrons joining the nucleus will reach some stable low energy orbitals in the vicinity of the nucleus, while the last one may get an exciting interacting life on the top partially empty level. Following the law of gravity our Ce atoms, and it cloud of electrons, collapses in the following years together with a bunch of other atoms created by it mother star to form a planet. In this process, the Ce atoms will approach their neighborings pairs and the curious high energy electrons, feeling lonely in their unfilled orbital, may choose to form join orbitals with other electrons in an equivalent situation. On lowering the environment energy this process may eventually end up with the creation of a solid material. In this situation the distance between two next neighbor atoms in the material is given by the minimum energy of their join orbital. But for our Ce atoms their is a dilemma as several layer have comparable energy and will compete to form or not orbital layer in the compound. This bring to the study of strongly interacting systems.

Plan of this thesis

Here are some of the questions I want to discuss in this thesis, first starting quite generally in the introduction with the heavy fermion, why can they have "heavy" masses? Then I will discuss why f shell electrons can be either "localized" or "delocalized"? What are the expected physical laws, for the quantities we will measured, in the normal state and in the quantum critical region of a heavy fermion? What is a quantum critical point in heavy fermion and why it is important for magnetic superconducting pairing? And finally how can superconductivity and magnetism coexist?

In the second chapter the two experimental setups used in this thesis will be presented, with the question of what are the technological challenges and limitations?

In the third chapter, we analyze the following problems: Is there a quantum critical point in $CeCoIn_5$ at the upper critical field ($H_{c2}(0)$) at ambient pressure? How can we explain the unusual phase diagram of $CeCoIn_5$ that appears to have two critical pressures, one where T_{SC} is maximum and the other where most of the physical quantities: C/T, $H_{c2}(0)$, $\partial H_{c2}/\partial T$, ρ_0, ... show an anomaly. With these two experiments we were able to draw a new phase diagram (H,P,T) for $CeCoIn_5$.

In the fourth chapter, we present our thermal conductivity data on UCoGe and URhGe. It is the first attempt to reveal the symmetry of the superconducting order parameter in the different part of the (T,H) phase diagram of these compounds. These measurements also allow the detection of the bulk superconducting and ferromagnetic transitions. We were therefore able to confirm the unusual field dependence of H_{c2} in these compounds.

Together all these experiments allow us to study the interplay between superconductivity and magnetism. Through a quantitative analysis of H_{c2} and the position of quantum criticality in these systems, we can better understand how superconductivity is affect by a quantum critical point.

1 Introduction

1.1 Motivations

The challenge in the physics of heavy fermion materials is to understand the electronic properties of metallic compounds made of elements with more than one unfilled electronic shell giving rise to a complicated band structure and strong correlations between the electrons. Another one, is related to the intimate interplay between superconductivity and magnetism. This interest is due to the important possible applications of the superconducting state and because in heavy fermion the phase diagrams strongly suggest that magnetism and superconductivity are related. So if no direct potential applications of the heavy fermion have been suggested up to now, the heavy fermion problem can be an important piece to understand the puzzle of unconventional superconductivity.

The experiments presented in this thesis are in continuity to the long work done in the physics of heavy fermion. This physics is quite complicated with an enormous amount of experiments and ideas that have been made and suggested in the last years. So many that a three years Phd is certainly not long enough to understand all the different issues. Nevertheless, in the introduction I will try to present the "big picture" on heavy fermion physics and unconventional superconductivity.

In most of the heavy fermion compounds, the superconducting state has a maximum critical temperature at an anti-ferromagnetic (AFM) phase transition. In the vicinity of the transition, the physical properties like resistivity show non-Fermi liquid behaviour. For this reason, it is believed that the transition would end with a quantum critical point (QCP) at $T = 0$ in the absence of superconductivity. As for example in $CePd_2Si_2$ or $CeIn_3$ displayed on figure 1.1. These types of phase diagrams suggest that superconductivity and magnetism are related and that the maximum of superconductivity happens at a magnetic quantum critical point. In this thesis, I present three compounds for which the phase diagram is qualitatively different: in $CeCoIn_5$, the maximum of superconductivity do not correspond to the position of a QCP and in the ferromagnetic superconductors URhGe and UCoGe the maximum of superconductivity observed under magnetic field may not be directly related to a QCP.

Results on $CeCoIn_5$ are discussed in chapter 3, in this compound no antiferromagnetism is directly observed. However, a QCP would exist at $p = 0$ and $T = 0$ in the vicinity of the upper critical field H_{c2} and the maximum of the su-

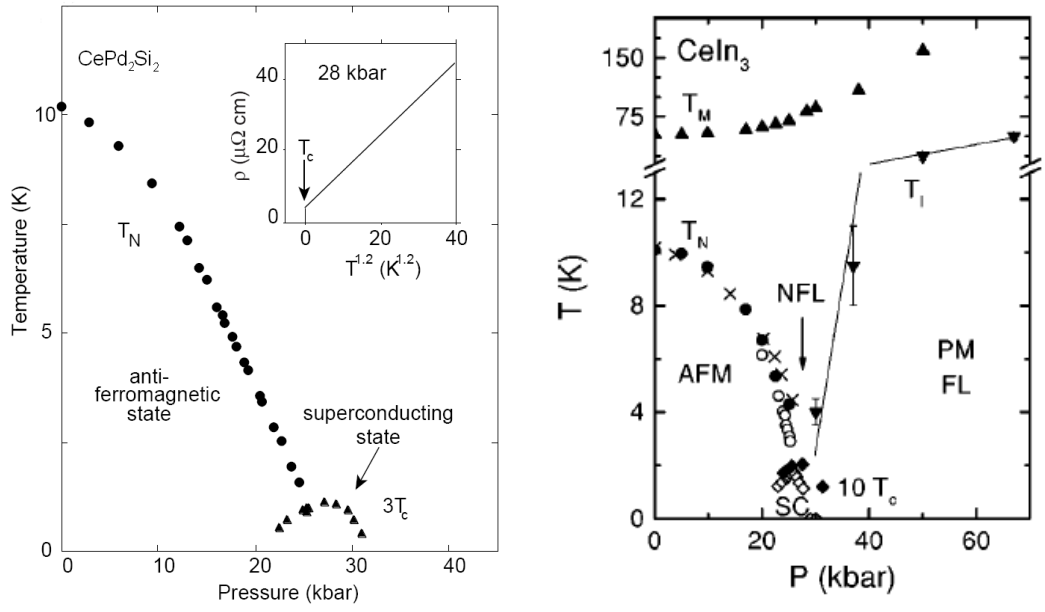

(a) (b)

Figure 1.1: Pressure temperature phase diagrams of two "model" heavy fermion compounds: $CePd_2Si_2$ and $CeIn_3$ from [Mathur 98] and [Knebel 01]. Under pressure, the AFM state is suppress, a QCP is obtained when $T_N = 0$ as demonstrated by the vanishing of the Fermi liquid domain or non-Fermi liquid behavior of $\rho(T)$ at this pressure. In the vicinity of the QCP, the superconducting state is realized.

perconducting transition T_{SC}, under pressure, does not correspond to anomalies in the normal phase (maximum of $m^\star$, NFL regime, ...) characterizing the presence of a QCP. Our analysis of this phase diagram revises this picture and may also give some clues on the type of QCP found in $CeCoIn_5$.

In the fourth chapter, I will present work on UCoGe and URhGe, two ferromagnetic superconductors. In these compounds an increase of the superconducting transition is observed under magnetic field. The so called "re-entrant phase" is evidence for an increased pairing strength or a decrease of the limitating mechanisms (orbital and paramagnetic limits) under magnetic field. The coexistence of ferromagnetism and superconductivity is well established in these compounds. By means of thermal conductivity, we made the first measurements which were intended to probe the symmetry of the superconducting order parameter and yield a first bulk probe of the upper critical field below 8 T.

1.2 Heavy fermion

It is known since the beginning of quantum physics that the electrons of an atom have discrete energy levels. The energy of these levels depend first on the orbital (i.e. the wave function 1s,2s,2p,3s,3p,3d,...) of the electron. Then, it will depend of it spin configuration: Hund's rule. A 4f orbital can contain 14 electrons, the

lowest energy is the one of minimum quantum number m=-3 then m=-2, ... But due to Coulomb repulsion from other electrons already present in the same orbital and to the crystal field, the hierarchy between energy levels may be modified. For the light atoms, the first contribution is the most important and different orbitals are clearly separated in energy. This can be seen, as their free atoms only have one unfilled electronic layer. When forming a compound, bounding and anti-bounding crystalline (or molecular*) orbitals will be formed on the basis of these unfilled orbitals (plus eventually one or two high energy filled ones if the formed crystalline orbital as a lower energy). The distance between two atoms in the compound is given by the minimum of energy of the crystalline orbital. This scheme works well for light atoms, but starting from chromium the situation is more complex. For some elements, the difference in energy between two orbital level can be smaller than one of the other contribution previously discussed (electronic repulsion or crystal field). In this case the free atom will have more than one unfilled electronic orbital. Cerium and Uranium, that form the compounds discussed in this thesis are in this case, with electronic configuration: [Ce]=[Xe] $4f^1$ $5d^1$ $6s^2$ and [U]=[Rn] $7s^2$ $5f^3$ $6d^1$. [Xe] and [Rn] stand for the electronic configuration of the rare earth Xenon and Radon respectively. When forming a compound, the different unfilled electronic orbitals may form crystalline orbitals, but they will be some frustration for the distance between the atoms as the energy of different crystalline orbitals can not be minimized at the same time. For this reason some crystalline orbitals may not form, their energy being higher than the one of atomic orbitals. This is well known as the reason for the insulating properties of Mott insulators compounds. In case of metallic compounds, it also exists: for Ce and U based compounds the f orbitals can be partially "localized" meaning that they do not form bands. Interactions between the f "localized" electrons and the conduction band lead to strongly correlated electrons systems. Heavy fermion are part of this category.

Kondo effect and Kondo lattice

Generally, the physics of 3D metallic systems, is described in the framework of the Fermi-liquid theory. This theory makes a one to one mapping between the real system and a system of quasi-particles that can be understood theoretically as a weakly interacting gas. Physical properties such as the temperature dependence of: resistivity ($\rho(T)$), specific heat $C(T)$, thermal conductivity $\kappa(T)$ and others can be calculated within this theory. The transition from the real system to the Fermi-liquid induces a renormalization of the masses of the quasi-particles ($m^\star$) compared to the bare electron mass (m_0). In heavy fermion the renormalization can be as large as: $m^\star = 1000 m_0$.

Several effects will enhance the quasi-particles mass. Like in conventional materials, the band structure or an applied magnetic field can cause mass enhancements. For example, in a two-dimensional metal with columnar like Fermi-surface, one expects larger masses out of plane than in plane. But the most important contribution

*This discussion is completely general, as for the molecule or crystalline compounds, but for clarity, I will only discuss the crystalline case from this point.

in heavy fermion masses renormalization comes from the Kondo effect [Kondo 64]. This effect, explains the observed enhancement of the resistivity at low temperature in dilute magnetic alloys. The idea is that in a ground state with magnetic impurities, conduction electrons will locally "screen" the magnetic moments of each impurities. An impurity of spin S=1/2, will be surrounded on average by one electron of the conduction band forming a "collective" singlet state with the impurity.

Kondo considered the so called s-d model, taking into account interactions between magnetic impurities and the conduction electrons:

$$H = \underbrace{\sum_{k,\sigma} \epsilon_{k,\sigma} c^{\dagger}_{k,\sigma}, c_{k,\sigma}}_{\text{conduction electrons}} + \underbrace{J \overrightarrow{S} \overrightarrow{s}}_{\text{interaction with magnetic impurities}} \tag{1.2.1}$$

Using a third order perturbation calculation in J, when $J < 0$ (anti-ferromagnetism), he obtained:

$$\rho(T) = \rho_B(1 - N_0 J \log(\frac{T}{D})) \tag{1.2.2}$$

where N_0 is the density of state of the conduction band, D the bandwidth of the conduction electrons and $\rho_B \propto T^2$, the resistivity without the magnetic interactions. This model successfully accounts for the increase of resistivity but also predicts a divergence of the resistivity at low temperature. In fact in his article Kondo already mentioned that taking higher order terms and contributions, he obtains a saturation below a temperature T_0. We can define a characteristic temperature for the divergence, known as the Kondo temperature:

$$T_K = D e^{\frac{-1}{N_0 J}} \tag{1.2.3}$$

Experimentally this temperature is difficult to define and is sometimes taken as the temperature at which the minimum in resistivity occurs. It is of the order of 10 K in heavy fermion system.

As we discussed previously, in heavy fermion systems, f-orbital electrons are rather "localized" around their atoms (not at the Fermi energy). These "localized" f-electrons act as magnetic impurities and can be described by the Kondo physics. The temperature dependence of the magnetic in-plane resistivity of $Ce_xLa_{1-x}CoIn_5$ for small concentration of Ce magnetic impurities and low temperature follows perfectly these predictions. The magnetic resistivity is defined as: $\rho_M(T) = \rho_{(Ce,La)CoIn_5}(T) - \rho_{LaCoIn_5}(T)$. $LaCoIn_5$ is the non-magnetic compound of the series $Ce_xLa_{1-x}CoIn_5$. A logarithmic divergence of the resistivity that saturates bellow $\sim$ 100mK is observed in figure 1.2 for high La doping as predicted from the theory.

But when more Ce atoms (the magnetic impurities) are present in the compound, a different behaviour is observed at low temperature. For doping below $x = 0.5$ in $Ce_xLa_{1-x}CoIn_5$, figure 1.2, a decrease of the resistance is observed at low temperature and superconductivity appears at even lower doping. Two reasons can be invoked for the failure of the Kondo model for these concentrations:

- The exhaustion principle stands that there is not enough conduction electrons to screen every magnetic moments when their density is too high.

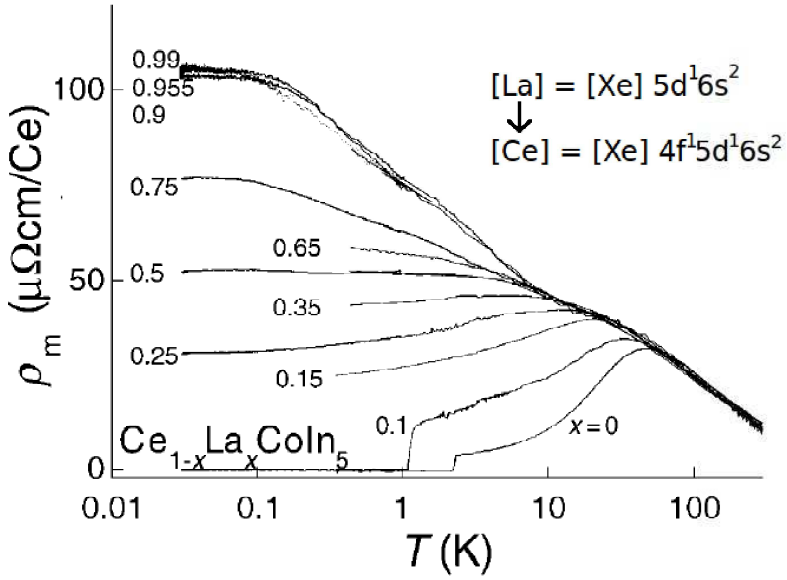

Figure 1.2: Magnetic in-plane resistivity of $Ce_xLa_{1-x}CoIn_5$. Figure from [Nakatsuji 02]

- Spin-spin interactions between localized moment may create a magnetic order with a lower energy than the Kondo state.

For compounds with a high density of localized moments, a new regime appears at temperature $T^\star$ below the Kondo one T_K, called the Kondo lattice regime. A remarkable feature is that below this temperature, the localized f electrons cannot be represented as impurities anymore and seems for example to participate in the electrical conduction. The exact physics of this state is still not completely understood.

So in heavy fermion physics there are two characteristic energies, on lowering the temperature. Below the T_K, the f shell electrons start to be screened by the Kondo effect which leads to strong correlations in the compound. Below $T^\star$, often called the "coherence temperature", the impurity picture breaks down, lattice properties are recovered but with heavy quasiparticles.

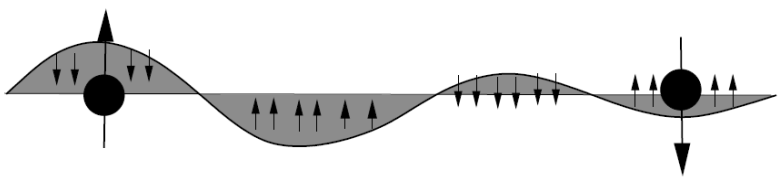

Figure 1.3: Schematic view of the RKKY interaction. Figure from [Coleman 07]

This Kondo physics is competing with the Ruderman-Kittel-Kasuya-Yosida (RKKY) interaction, sketched in figure 1.3. This interaction accounts for the coupling between localized moments and conduction electrons and governs most magnetic properties of metals for example. The nature of the coupling leads to an oscillatory

moment on the conduction electrons that can then interact with other localized moments. The characteristic temperature of this interaction is given by:

$$T_{RKKY} \simeq J^2 N_0 \tag{1.2.4}$$

This brings a third characteristic energy to the heavy fermion physics, the Néel temperature below which the electrons order anti-ferromagnetically (T_N).

An important but somehow confusing concept in the physics of heavy fermion is the one of "localization" of an electron or quasi-particle. A particle is said to be delocalized if it contributes to the Fermi surface, localized otherwise, whatever is it actual geographical distribution in real space.

Hence a usual question in heavy fermion systems is to know if f electrons form bands (delocalized), or if the f character of the quasiparticles at the Fermi level is only coming from the Kondo correlations, leading to an effective hybridization with the f shells (localized for the Kondo effect, delocalized in case of the Kondo lattice).

In most magnetically ordered Cerium based heavy fermions, f electrons are found to be localized. The situation is more complex in uranium based systems.

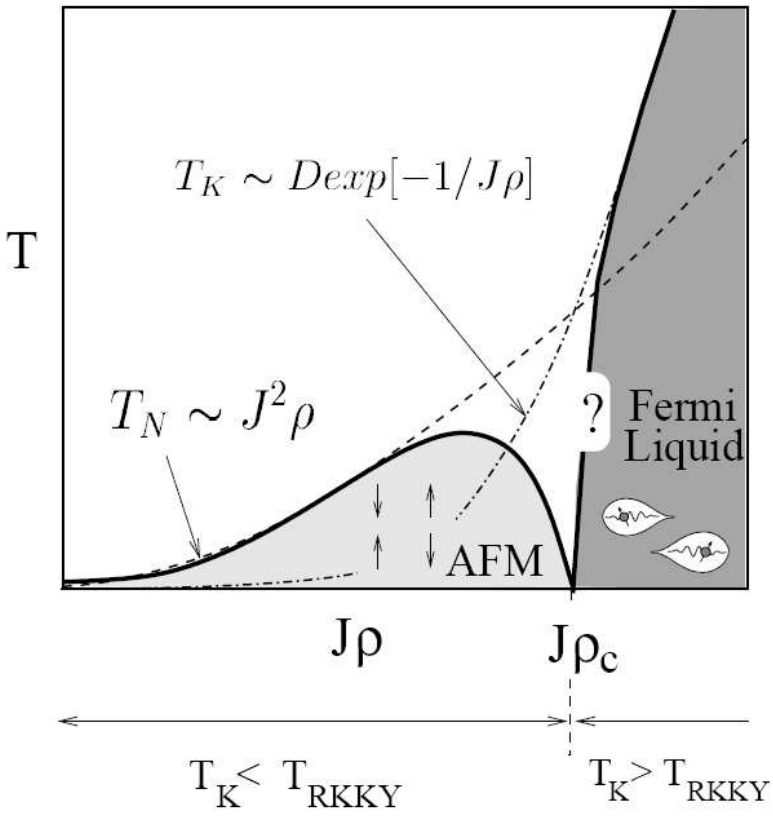

Figure 1.4: Doniach phase diagram. The ground state of the system can be tuned between Kondo and AFM by varying the coupling constant J. Figure from [Coleman 07]

As the dependence of the RKKY and Kondo interactions to the exchange coupling constant J are different, Doniach [Doniach 77] suggested that some compounds can be driven through different ground states by tuning J (figure 1.4). Pressure, magnetic field or doping can be used as tuning parameters in real systems. This description is oversimplified as it does not takes into account the interplay between the Kondo lattice physics or the mixed valence of the f shell electrons and the RKKY interaction as well as crystal field effects but it gives the limit regimes where some of these interactions dominate.

When we study the phase diagram of a heavy fermion, we tune the different energy scales to observe phase transitions and eventually, as suggested in the case of $CeCoIn_5$ we can drive them to quantum critical points.

1.3 Physical properties at low temperature in a Fermi-liquid

In the paramagnetic or magnetically ordered phase of a heavy fermion compound, the physics usually follows the one expected for a Fermi-liquid below some temperature labeled T_{FL}. At a quantum critical point (QCP), this is not the case any more and the characteristic temperature vanishes as one approaches the QCP by tuning a parameter (g): $T_{FL} \to 0$ as $g \to g_c$. This parameter could be pressure, magnetic field or doping. So a convenient way to localize a QCP is to follow the dependence of T_{FL} as a function of a tuning parameter. This is what we will do for $CeCoIn_5$ in a part of this thesis with magnetic field as a tuning parameter. Hence in the following I will briefly review the expected temperature dependence of some physical properties in a Fermi-liquid. The region above the QCP, is called: "Quantum Critical". The expected temperature dependences in this region depend on the theoretical model and have not been calculated systematically. Therefore I will only mention what is usually observed experimentally.

The physical quantities that are probed by transport and thermodynamic measurements in a Fermi-liquid mainly depend on the Fermi surface which can be characterized by two parameters:

- The effective mass tensor given by the slope of the dispersion relation:

$$\frac{1}{m^\star_{ij}} = \frac{1}{\hbar^2}\frac{\partial^2 \epsilon(\vec{k})}{\partial k_i \partial k_j} \tag{1.3.1}$$

- And the Fermi surface volume or Fermi momentum $\vec{k_F}$.

In general these two quantities can be anisotropic. The evolution of these quantities on approaching a QCP depend on the model used for the criticality.

Directional probes are important to differentiate between two different families of scenarios for the Fermi surface evolution through a quantum critical point. In a first scenario a reconstruction of the full Fermi surface is expected whereas in the second only "hot spots" are affected. Similarly the effective mass can diverge in some particular directions or on the entire Fermi surface.

Resistivity

A basic description of the electrical resistivity is given by the Drude formula:

$$\rho = \frac{m}{ne^2\tau} \tag{1.3.2}$$

Where m and e are the mass and charge of the particles, n the density of states, and τ the relaxation time for a particular scattering process.

- lattice imperfection: impurities, grain boundary, dislocation, ... (τ_0)
- thermally excited lattice vibration: phonons, (τ_{ph})
- others conduction electrons (τ_{el}).

The resulting relaxation time can be obtained through the Matthiessens's rule: $1/\tau = 1/\tau_0 + 1/\tau_{el} + 1/\tau_{ph}$. Scattering on lattice imperfections is basically temperature independent so the resistivity can be expressed as:

$$\rho(T) = \rho_0 + \rho_{el}(T) + \rho_{ph}(T), \text{ for } T << \Theta_D. \tag{1.3.3}$$

The part of the resistivity due to electron-phonon interactions is given in the Debye model by $\rho_{ph}(T) \propto \left(\frac{T}{\Theta_D}\right)^5$, with Θ_D the Debye temperature. This contribution is normally quite small at low temperatures ($T < 1K$) as typically $\Theta_D > 100$K.

The electronic part of the resistivity depend on electron-electron scattering events. If we neglect umklapp processes, the momentum is conserved ($\sum_i m_i^\star \vec{v}_i = const.$) in these scattering events. This implies that if the effective mass ($m^\star$) is constant, the electrical current $\vec{j} = \sum_i e\vec{v}_i$ is conserved. The electrical current can only be decreased if the effective masses are different for different velocity directions ($m_i^\star \neq m_j^\star$ for $\vec{v}_i \perp \vec{v}_j$). This decrease will then be proportional to the ratio of effective masses in the different directions.

We can now calculate the probability that an electron excited with energy ϵ above the Fermi level collides with another electron of the system. Due to the Pauli exclusion principle, the collision is only possible if there are two empty states for the two electrons resulting from the collision. Due to momentum conservation, the center of mass of the initial and final electrons has to be conserved, and therefore, the collision can only happen with electrons of energy in the interval $[k_F - \epsilon; k_F]$, as sketched on figure 1.5. The probability of a collision depends on the number of electrons in this interval and the number of final states. In the case of a spherical Fermi surface, with notations of figure 1.5, we have:

$$P(\text{collision}) = \frac{3}{4\pi k_F^3} \int_\epsilon^{k_F} \int_0^\pi 2\pi n_{\text{final states}}(\theta, \epsilon') d\theta d\epsilon' \tag{1.3.4}$$

From figure 1.5 if $k_F >> \epsilon$ we obtain that:

$$1/\tau \propto P(\text{collision}) \propto \frac{\epsilon^2}{k_F^2} \tag{1.3.5}$$

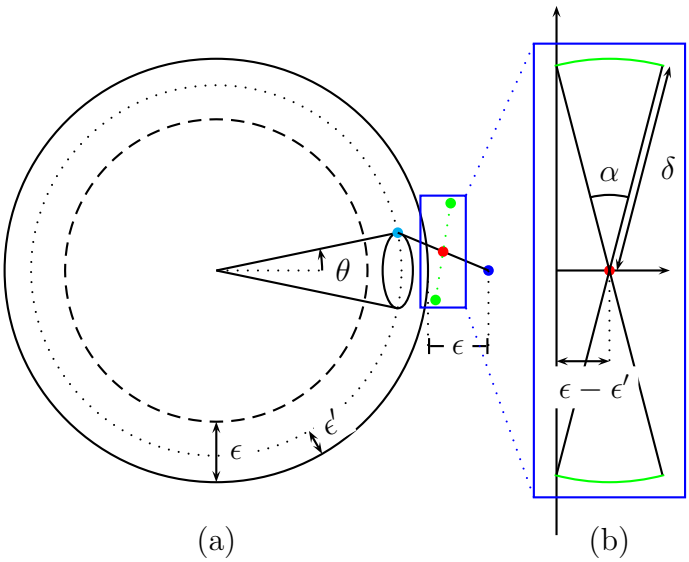

Figure 1.5: (a) Electron-electron contribution to the resistivity. An excited electron with energy ϵ (blue) can only scattered with electrons (light blue) in the momentum range $[k_F - \epsilon, \epsilon]$, so that two empty states exist for the final particles (green) of the scattering event. The probability of a scattering event depend on the number of particles on which the excited particle can scattered (ϵ/k_F) and on the number of final states for that particular collision (b). So the scattering probability is proportional to ϵ^2.

If the excitation is given by the thermal energy: $\hbar\epsilon = k_B T$ we obtain the well known temperature squared dependence of resistivity $\rho_{el}(T) \propto AT^2$. We can also note that $A \propto m^2$, as the mass comes into both the Drude formula 1.3.2 and in the scattering times, through density of final states (Fermi Golden rule) . The A coefficient is a directional measure of the effective mass of the compound as it depends on the electrical current direction.

In the quantum critical region, in the proximity of a QCP, the resistivity is usually observed to be linear in temperature. The origin of this linear temperature dependence remains controversial and triggers many "unconventional" scenarios for a QCP.

Specific heat and Kadowaki-Woods ratio

Specific heat can easily be calculated for an electron gas as [Kittel 96, p. 151]:

$$C_{el} = \frac{1}{3}\pi^2 D(\epsilon_F) k_B^2 T \tag{1.3.6}$$

$D(\epsilon_F) = 3N/2\epsilon_F$ is the density of state as the Fermi level. For a free electron gas $\epsilon_F = \frac{\hbar^2 k_F^2}{2m}$. Then the Sommerfeld coefficient $\gamma = C_{el}/T$ is given by:

$$\gamma = \frac{\pi^2 k_B^2 N m}{\hbar^2 k_F^2} \tag{1.3.7}$$

and depends linearly on the electron effective mass. γ is usually taken as a good measure of the effective mass of a compound, even if the measure is an integral over the full Fermi surface and averages singularities on particular points of the Fermi-surface.

In the Fermi-liquid domain the Sommerfeld coefficient is constant versus temperature. In the quantum critical region it is usually observed to diverge logarithmically as: $\gamma(T) \propto -T\ln(T)$.

The ratio between the A coefficient and the square of the Sommerfeld coefficient is known as the Kadowaki-Woods ratio.

$$\frac{A}{\gamma^2} = \text{const.} \tag{1.3.8}$$

As both quantities depend on the square of the effective mass, this ratio is constant even if the effective mass of the quasi-particles is modified as long as the Fermi surface stays unchanged.

Both resistivity and specific heat can be used to determine the position of a QCP by probing domain in the phase diagram where a Fermi-liquid or quantum critical behaviour are obeyed. The limit of both regimes should extrapolate at zero temperature to the QCP.

Thermal conductivity & Wiedemann-Franz law

The thermal conductivity κ is defined as:

$$\vec{Q} = -\kappa\vec{\nabla}T \tag{1.3.9}$$

Where $\vec{Q}$ is the heat flow across the sample and $\vec{\nabla}T$ the temperature gradient. For a gas of particles with velocity v, specific heat per unit of volume C_v and mean free path l, the thermal conductivity is given by [Kittel 96, p. 166]:

$$\kappa = \frac{1}{3}C_v v l \tag{1.3.10}$$

In a metal, the thermal conductivity depends on different contributions. Indeed, any excitation that propagates through the compound and can be thermally excited contributes: electrons, phonons, magnons, ... The total thermal conductivity can be expressed as the addition of the contributions of parallel channels:

$$\kappa(T) = \kappa_{el}(T) + \kappa_{ph}(T) + \kappa_{magnons}(T) + ... \tag{1.3.11}$$

For the phonon contribution for $T << \Theta_D$, the specific heat is given by the Debye model as: $C_v \propto T^3$, the velocity v is constant for a phonon gas and the mean free path is (from [Kittel 96, p. 123]):

- constant at low temperature when the size of the crystal is the limiting parameter ($l = D$ with D the dimension of the sample),
- inversely proportional to the temperature for electron-phonon scattering ($l \propto 1/T$).

Finally at low temperature the phonon contribution to thermal conductivity is:

$$\kappa_{ph}(T) \propto \begin{cases} T^3 & \text{at very low temperature, usually at } T << T_{SC} \\ & \text{in a superconductor with fully open gap (s-wave),} \\ T^2 & \text{above if electron-phonon scattering processes are important.} \end{cases} \tag{1.3.12}$$

In some models, the magnon contribution to thermal conductivity is $\kappa_{magnons} \propto T^2$ [Ueda 75, Kumar 82]. So in a good metal, at low enough temperature, the electronic contribution should dominate all the others.

In the superconducting phase, the electronic contribution to thermal conductivity is usually decreased as the Cooper pairs do not contribute to thermal conductivity (minimum energy for an excitation 2Δ). In some special cases thermal conductivity can be increased as another effect of superconductivity is the increase of the mean free path of the quasi-particles with the reduction of the number of free quasi-particles. The superconducting transition as measured from thermal conductivity is a bulk measurement. Indeed, if in resistivity a single superconducting path short circuit the measurement, in thermal conductivity a single superconducting path has a negligible effect on κ. The sharpness of the transition (change of slope in $\kappa(T)$) gives an indication of the quality of the crystal. In the superconducting phase, the temperature dependence of the thermal conductivity depends on the nodes of the superconducting gap and can be used to determine the gap symmetry (for example $\kappa(T) \propto T^3$ in the case of a superconducting gap which has lines of nodes). Similarly the thermal conductivity, extrapolated at zero temperature has different field dependence: exponential for "s-wave" superconductivity, sub-linear in the "d-wave" case,... [Shakeripour 09].

In the limit $T \to 0$ the ratio thermal conductivity over temerature (κ/T) of a fully gapped superconductor is zero, as all the quasi-particles have condensed into Cooper pairs that do not carry heat (the first excited state is at an energy 2Δ). The situation is different when the gap has a line of nodes. In this case, the residual value does not vanishes except for the perfectly pure crystal and can even reach the universal limit. It is called universal because it is independent of the purity of the crystal. Indeed, if impurities increase the number of thermal carriers by breaking superconducting Cooper pairs, they also decrease the mean free path which has the opposite effect and the two processes may compensate each other. This works as long as the density of impurities is not too high.

It follows from 1.3.10, 1.3.7 and 1.3.2 that the ratio of the electronic contribution to the thermal conductivity and electrical conductivity is constant. This relation is called the Wiedemann-Franz law:

$$\frac{\kappa_{el}(T)}{\sigma(T)T} = \frac{\pi^2 k_B^2}{3e^2} = L_0 \tag{1.3.13}$$

With $L_0 = 2.44 \cdot 10^{-8} \mathrm{W\Omega K^{-2}}$ the Lorenz number. The Wiedemann-Franz law states that charge and heat are transported by the same carriers, the electrons. This relation is obeyed in the low temperature limit for all metals when the other means of heat transport vanishes. We call $L(T)$ the ratio of conductivities $L(T) = \kappa_{el}(T)/(\sigma(T)T)$. $L(T)/L_0$ is bigger than one if thermal conductivity is bet-

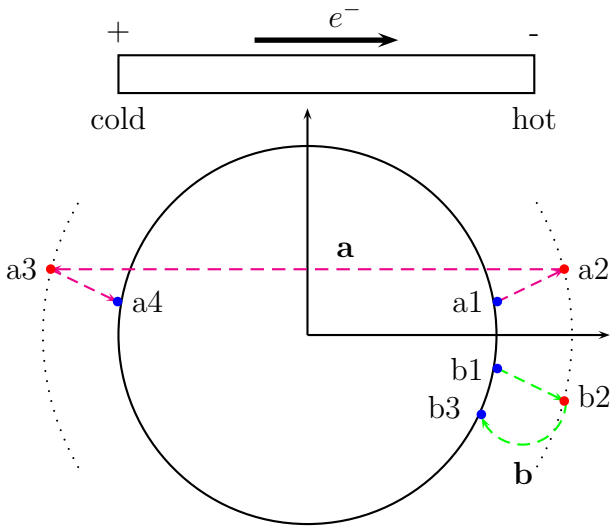

Figure 1.6: Wiedemann-Franz law: We suppose that the charge carriers are electrons. A voltage is applied across the sample. Two processes are possible for heat and charge transport. 1→2 an electron is excited at the cold side (absorption of a phonon for example). On its way to the hot side, two processes can make it relax. (**a**) If there are few elastic scattering, the ones at large $\vec{q}$ are promoted a2→a3 and both electrical and thermal conductivity are affected (change of direction of the charge and thermal excitation). (**b**) In case of a strong elastic scattering, only the thermal conduction is affected, as the velocity of the charge is almost unmodified, but the thermal excitation suppressed.

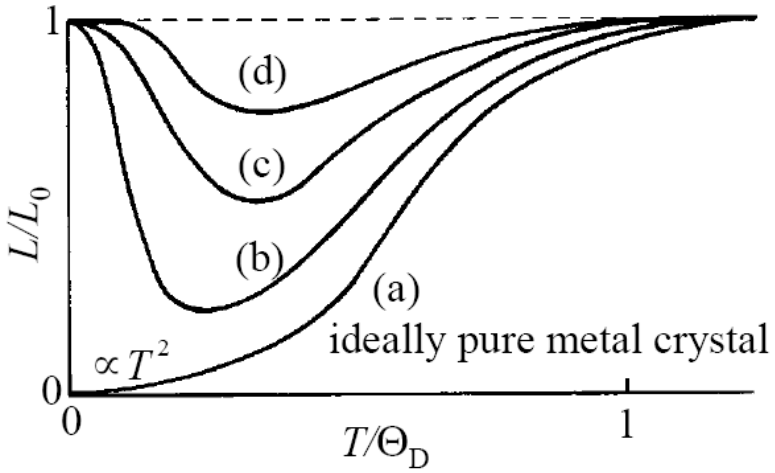

Figure 1.7: Evolution of the ratio L_{el}/L_0 of the electronic contribution to the Lorenz number for different sample purity. From [Mizutani 03, p 302].

ter than electrical conductivity. This happens at high temperature as the phonon contribution increases thermal conductivity. This ratio $L(T)/L_0$ can be smaller than

one when a large amount of inelastic scattering promotes small $\vec{q}$ scattering (figure 1.6). In this case thermal conductivity is smaller than the electrical one. The expected behaviour of the Wiedemann-Franz ratio for the electronic contribution $L_{el}(T)/L_0$ is plotted on figure 1.7.

We used thermal conductivity to gain information about the superconducting state in UCoGe and URhGe both because it is sensitive to the superconducting gap symmetry and because it allows for a bulk determination of T_{SC}.

Thermoelectric power

The thermoelectric power or Seebeck coefficient is obtained from the linearized Boltzmann equation:

$$S(T)/T = \frac{\pi k_B^2}{3e} \frac{\partial \ln(\sigma(E))}{\partial E} \tag{1.3.14}$$

With $\sigma(T)$ the electrical conductivity. As thermopower depends on the derivative of the electrical conductivity versus energy it is very sensitive to a small change of the Fermi surface. This expression is obtained for an isotropic Fermi surface which is certainly not the case in heavy fermion compounds. In the anisotropic case the thermal conductivity is mostly sensitive on the electrical contribution and energy derivative in the direction probed by the current. Behnia and co-workers [Behnia 04] calculate the ratio between thermoelectric power divided by temperature and specific heat.

$$q = \frac{S N_{Av} e}{T\gamma} \tag{1.3.15}$$

with N_{Av} the Avogadro number. They found that, with some approximations, $|q|$ gives the volume per charge and heat carriers in unit cells unities.

Comparison of thermoelectric power and specific heat allowed us to estimate the carrier concentration in UCoGe and URhGe. It is also a way to determine an anomaly on the Fermi surface as expected for example at quantum criticality.

1.4 Quantum critical points

For a classical phase transition, an important tuning parameter is temperature and the state of a system is given by the minimization of its free energy:

$$F(p, T, H) = E(p, H) - TS(p, H) \tag{1.4.1}$$

When a phase transition is tuned at finite temperature by pressure or magnetic field it is because the internal energy and entropy depend on these quantities. For the molecule H_2O, for example, the internal energy E is determined by the interaction between molecules and minimized in the crystalline structure of ice. In contrary, the entropy S gives the amount of randomness of the system and is maximized in water (for the solid liquid phase transition, we do not consider the gas state in this discussion). Hence the free energy is minimized in the ice state at low temperature and in water above $T = 0\,^{\circ}\mathrm{C} = 273.15\mathrm{K}$.

A quantum phase transition happens at zero temperature. The system is driven between two different ground states only by the variation of $E(p, H)$.

We consider a system in which the ground state can be tuned by a parameter g between two different states. Such a system will have a phase transition at zero temperature for a critical value of the tuning parameter $g = g_c$. At this critical value there is a level crossing between two different ground states. For a transition of the second order the energy scale of a fluctuation above the ground state vanishes at g_c. To fix the idea let's consider the case of a ferromagnetic (FM) $g < g_c$ to paramagnetic (PM) $g > g_c$ transition. In a crystal for $g < g_c$ in the ground state the spin of all the quasi-particles point in the same direction, if the system is Ising-like, then a spin flip is the first excitation. Similarly to conventional phase transitions, one can define different critical exponents for a quantum phase transition. On approaching g_c, the characteristic energy D of an excitation of the ground state vanishes as:

$$D \propto J|g - g_c|^{\nu z} \tag{1.4.2}$$

Where J is the characteristic energy coupling and νz a critical exponent independent of the microscopic details of the Hamiltonian of the system.

In addition to a vanishing energy scale, a second order phase transition is characterized by a diverging length scale. This scale can be understood as the characteristic length of critical fluctuations and is also known as the correlation length.

$$\xi^{-1} \propto L|g - g_c|^{\nu} \tag{1.4.3}$$

L is an inverse length scale of the order of the inverse lattice parameters. Combining 1.4.2 and 1.4.3, gives that the characteristic energy scale vanishes to the zth power of the inverse characteristic length. The z exponent is called the dynamic critical exponent or simply dynamical exponent.

$$D \propto \xi^{-z} \tag{1.4.4}$$

The dynamical exponent is the main difference between a classical and a quantum phase transition. It reflects the fact that at a quantum phase transition time fluctuations of the order parameter, in addition to the spacial ones need to be considered leading to an effective dimension of the system: $d_{eff} = d + z$. It can take the values of: $z = 1$ for an AFM insulator or AFM with Q vector Q$> k_F$, $z = 2$ for an itinerant AFM and $z = 3$ for a metamagnetic transition or FM transition [Löhneysen 07]. The exponent of the correlation length is usually taken as $\nu = 1/2$, when above the upper critical dimension, where mean field applies.

Quantum criticality in Heavy fermion

A first consequence for heavy fermion systems is that the Fermi liquid domain should exist only for $T < T_{FL} \propto D$ so we can expect:

$$T_{FL} \propto |g - g_c|^{\nu z} \tag{1.4.5}$$

Going further than the Doniach model, two different classes of models have been proposed for quantum criticality in heavy fermion.

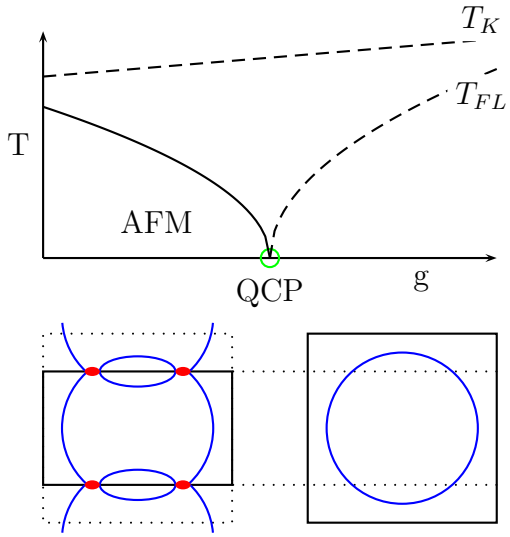

Figure 1.8: Scheme of a spin density wave (SDW) scenario of quantum criticality. At the QCP magnetic order appears, without affecting the Kondo temperature (top panel), the volume of the Fermi surface is unchanged, but due to the folding of the Brillouin zone (dotted lines) hot spot can appears (red region), where a singularity happens in the dispersion relation.

The first class are spin fluctuation scenarios, developed firstly by Hertz Millis and Moriya. In these models, itinerant magnetism appears in the conduction band and triggers quantum criticality. The Kondo temperature stays finite through the transition so that heavy quasi-particles exist on both sides of the transition. The Fermi surface volume stays constant at the transition with a folding of the Brillouin zone due to the appearance of magnetic order. This folding modifies the shape of the Fermi surface with some singularities at the "hot" lines regions. The scheme of the transition is displayed in figure 1.8. The consequences are a divergence of the A coefficient of resistivity at the QCP and an increase without divergence of the Sommerfeld coefficient γ [Moriya 95]. One of the problems of these model is that they can account for the temperature dependences of resistivity and specific heat usually observed in heavy fermion $\rho(T) \propto T \quad \gamma(T) \propto -T\ln(T)$ only if the system is considered to be two-dimensional.

Rosch [Rosch 00] has shown that disorder induces another energy scale which vanishes at the QCP. This has strong effects on the critical exponents of the self-consistent renormalization theory of spin fluctuations.

The second class of scenarios, said to be "unconventional" is sketched in figure 1.9. In this case again nothing particular is observed on the Kondo temperature at the QCP, but another energy scale $T^\star$ vanishes. Some scenarios predict the appearance of a magnetic phase at the QCP, whereas other scenarios even decouple the two effects. But the common point of these scenarios is the reduction and sudden reconstruction of the Fermi surface at the QCP. This reconstruction implies

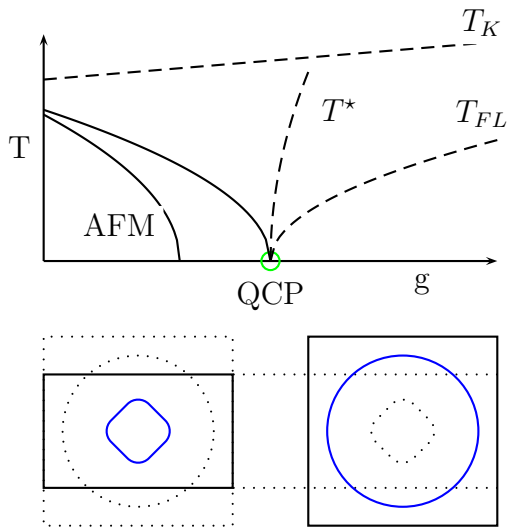

Figure 1.9: Scheme of an "unconventional" scenario for quantum criticality or Kondo breakdown. In this scenario again the Kondo energy is unchanged at the transition, but the Kondo lattice is and a characteristic energy scale of this domain vanishes. A magnetic order may or may not appears at this QCP depending on the model. The Fermi surface volume changes from small to large at the transition.

a divergence of the effective mass $m^\star$ at the QCP.

The magnetism in these cases is usually localized. For example, in a local scenario, the interaction between localized f shell electrons is tuned at the transition so that the system becomes magnetic. At the appearance of the magnetism, a part of the localized moments is taken out of the Fermi surface volume.

In contrary to the spin density wave scenarios, the temperature dependence of resistivity and quantum criticality reproduces the ones observed experimentally. This is even the main reason why these scenarios were developed.

The different scenarios are well described in the thesis of Benlagra [Benlagra 09].

In reality, the character of the f shell electrons is neither purely localized nor delocalized, and probably so is the associated magnetism, implying the need of a model mixing the two classes.

In this work, with the measurements of resistivity and determination of the Fermi-liquid domain, we obtained under some assumption the dynamical exponent z for $CeCoIn_5$. We discuss our results in the framework of these two scenarios.

1.5 Unconventional superconductivity

The general mechanism for the pairing interaction is that an attractive force between quasi-particles can be generated by their interactions. The interaction occurs as the medium (charges, spin orientation, ...) can be polarized by the quasi-particles. Distortion of the ions lattice or magnetic background is sketched in figure 1.10.

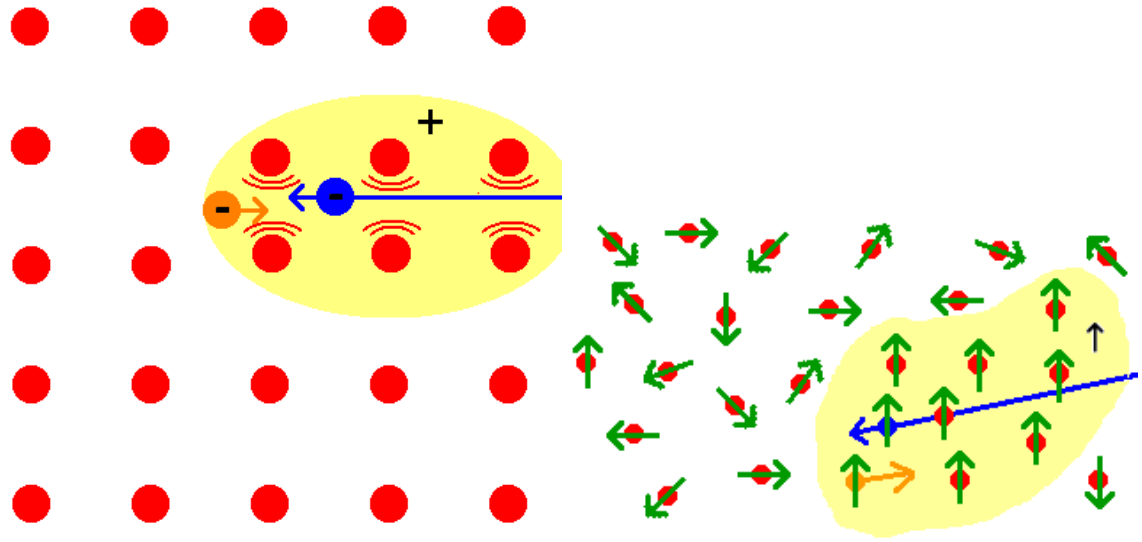

(a) (b)

Figure 1.10: (a) Electron-phonon coupling: a first electron the polariser (blue) distorted the lattice creating a positively charged region, that can attract other electrons. The attraction is maximum for an electron with opposite momentum (orange). (b) Magnetically mediated coupling for equal spin pairing (ferromagnetic interactions): As in the phonon case, the first electron (blue) polarized the medium with a certain spin orientation. Then a second electron (orange) with same spin orientation will be attracted in the opposite direction. Opposite spin pairing is possible in the case of anti-ferromagnetic interaction between the polarizer quasi-particle spin and the medium.

For spin mediated superconductivity, a peculiarity is that the medium is the same electrons which become superconducting. Figure 1.10b sketch the situation for ferromagnetic interactions between the spin of conduction electrons.

The polarization of the medium for the two channels (charge and spin) may depend:

- on the charge (or spin) of the quasi-particle,
- on the coupling between the charge and the medium g_i
- and on the susceptibility of the medium χ_i,

where $i = c, n$ for the charge or spin chanel. It is also well known that pairing is a retarded interaction, so what matters is $\chi_i(r,t)$, the retarded susceptibility, giving the response after a time t following the excitation. The effective excitation can be expressed as [Monthoux 07]:

$$V_{int} = -e'eg_c^2\chi_c(r,t) - \overrightarrow{s}' \cdot \overrightarrow{s}\, g_s^2\chi_s(r,t) \tag{1.5.1}$$

Where e and e' are the particles charges, s and s' the particles spins. The magnetic interactions would then depend on the amplitude of the retarded susceptibility,

a quantity that varies spatially, as sketched in figure 1.11. Hence for a given system, the spin-spin interaction may be attractive or repulsive depending on the relative position of the two quasi-particles

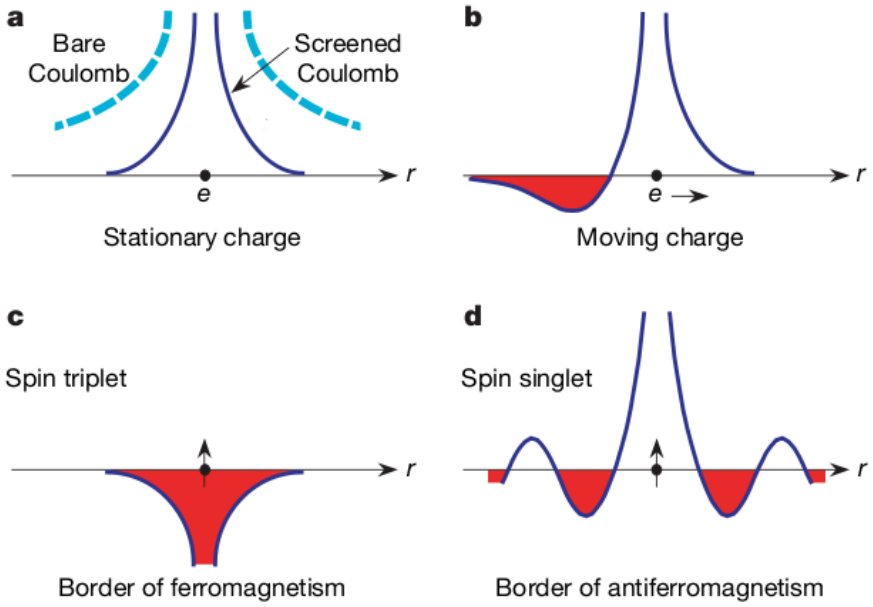

Figure 1.11: Charge and spin interaction versus distance. **a** and **b** charge-charge interaction, no-interactions when the electron is at rest as the charge is balanced between ions and the electron cloud. **b** An interaction is created by a moving charge. **c** and **d** spin-spin interaction. **c** equal spin, triplet pairing for ferromagnetic coupling, **d** opposite spin pairing AFM. From [Monthoux 07].

It was demonstrated that the interaction between spins of equal directions is disadvantageous compared to opposite spin coupling as the inner product of the two quasi-particle spins is a factor three smaller [Monthoux 99]. Anisotropy and Ising systems with uniaxial fluctuations were, on the other hand, suggested to enhance this interaction [Monthoux 01].

Superconductivity in a ferromagnet

Superconductivity and magnetism are often believed to be antagonist phases. Indeed, one property of the superconducting state is the Meissner effect, namely the expulsion of field from the inner volume of the superconductors. However, two mechanisms allow the coexistence of the two orders. First, it is well known that a static magnetic field is expelled from a superconductor on the characteristic length λ: the penetration depth. In a type two superconductor, if the distance between vortices (due to the magnetic field) is smaller than this length $d_{\text{between vortices}} << \lambda$, a static magnetic order can coexist with superconductivity.

A well studied example of a compound with ferromagnetic and superconducting orders is $ErRh_4B_4$, displayed in figure 1.12a. This compound first becomes a super-

conductor when the temperature is lowered below ≈ 8.7K, but then at ≈ 0.9K a long range ferromagnetic order develops and superconductivity is rapidly suppressed.

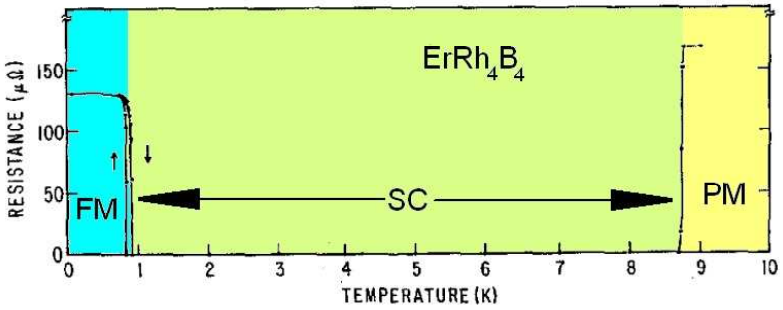

(a)

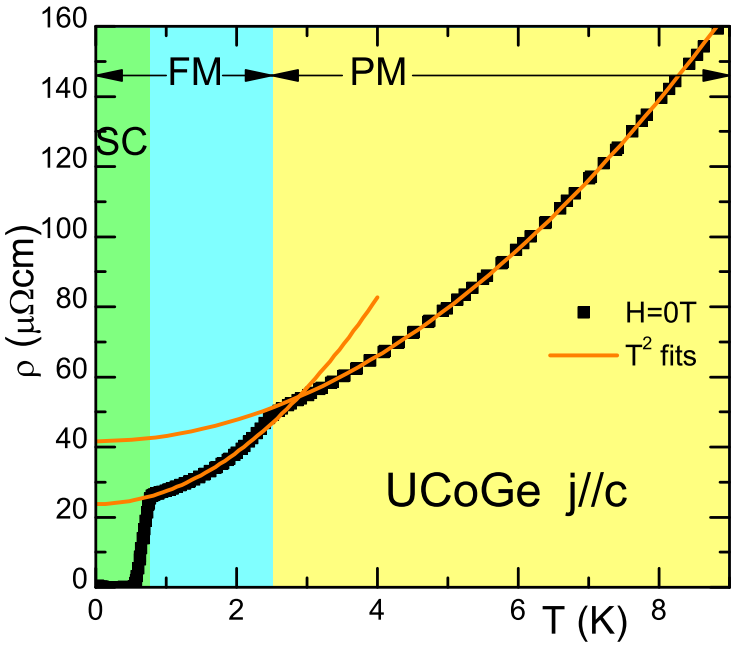

(b)

Figure 1.12: Two compounds that display both ferromagnetic and superconducting orders: (a) $ErRh_4B_4$ the compound becomes first a superconductor when temperature is lowered, but then superconductivity is suppressed with the appearance of a ferromagnetic order. Figure from [Fertig 77]. (b) In UCoGe the ferromagnetic order appears at higher temperature (~ 2.4K) and then coexists with superconductivity below about 700mK [Aoki 01].

A second possibility for the coexistence is if the magnetic order has a zero net moment on the size of the cooper pairs, because it is rapidly spatially modulated. This allows the coexistence of anti-ferromagnetism and superconductivity, or the appearance of superconductivity in a compound with ferromagnetic domains alternating with a period $a << \xi$ than the coherence length. Type one superconductivity coexisting with a magnetic order is even possible in this case.

Such a coexistence is observed in $ErRh_4B_4$, in a small temperature range when the temperature is cooled down: appearance of ferromagnetic domains is forced by superconductivity, in order to satisfied this condition below T_{Curie}. However, the domain of coexistence of superconductivity with the magnetic order is very small in this case, and superconductivity is suppressed when the ferromagnetic order is established.

In a BCS superconductor, the Cooper pairs are made of electrons of opposite momentum and opposite spin ($k\uparrow, -k\downarrow$). Upon applying a magnetic field, two mechanisms will increase the energy of the pairs and therefore act as pair breakers:

- Due to Zeeman splitting, the energy of spin up will be decrease and the one of spin down increased (if spin up are the majority spin) by an amount $g\mu_B H$. This effect is known as the Pauli (or parramagnetic) limitation, and superconductivity is suppressed when the energy gap $\Delta \cong g\mu_B H$.

- The interaction between the momentum of each electrons of the pair and the magnetic field give rise to the orbital limitation. It is controlled by the term $\frac{1}{2m}(p - e\vec{A})^2$ of the Hamiltonian and goes like $\left(\frac{T_{SC}}{v_F}\right)^2$.

In the first case discussed, when long range magnetic order coexists with superconductivity, these two effects will limit the superconducting domain.

Let us examine the situation in the ferromagnetic superconductors studied in this work: UCoGe and URhGe.

- Both states are bulk as observed from specific heat transition for example. Moreover, magnetic imaging in the case of UCoGe demonstrates that at least at the surface, the ferromagnetism coexists with superconductivity (the ferromagnetic domain are unmodified by the appearance of superconductivity) [Hykel 10]. Finally, NMR measurements, also show that no paramagnetic phase persists below T_{SC}, which implies true bulk coexistence of superconductivity and ferromagnetism [Ohta 10]. Furthermore, in these compounds, the same f electrons are responsible for both states.

- In the two cases, $H_{c2}(0)$ is very large for some field orientation $H_{c2} > 20$T for field parallel a-axis in the cases of UCoGe and URhGe (In the latter case in the "re-entrant" phase so with an additional magnetic field of 12T along the c-axis direction).

- internal field due to finite magnetization is negligible of the order of 20-100mT.

We can estimate the paramagnetic limitation in a superconductor as $H^P \cong \frac{\Delta}{g\mu_B}$ and for a BCS superconductor $\frac{\Delta(0)}{k_B T_{SC}} = 1.76$ which implies $H^P(\mathrm{T}) \cong \frac{1.76}{k_B T_{SC} g\mu_B} \cong 1.31 T_{SC}(\mathrm{K})$. This is orders of magnitude smaller than what is observed in the compounds studied in this thesis, for example in UCoGe: $T_{SC} \cong 0.6$K and $H_{c2}(H \parallel a, b\text{-axis}) > 20$T which cannot be explained even in a strong coupling scenario with singlet pairing.

A possibility to overcome this limitation is triplet pairing which can completely suppress the difference of Zeeman energy between superconductivity and the normal

state and hence the paramagnetic limitation. So that the associated pair breaking effect of the ferromagnetic exchange field is suppressed. In such a case, superconductivity and ferromagnetism can fully coexist. This paramagnetic limit suppression is complete when the external applied field is collinear to the internal one. When the external field and the magnetic moments are perpendicular, the paramagnetic limitation is weakened and is of the order of the exchange field [Mineev 10b]. In both cases, the paramagnetic limit becomes negligible compared to the orbital limitation.

We should note that there is another possibility to increase the paramagnetic limitation which is to allow the Cooper pairs to form with a non zero momentum $(\vec{k}\uparrow, -\vec{k}-\vec{q})$. Such a superconducting phase is called an FFLO state and has a spatially modulated amplitude. Such a phase was observed in superconductor-ferromagnet junction [Zdravkov 10] and is claimed to exist close to the upper critical field in $CeCoIn_5$ [Bianchi 03a]. But such effect cannot increase $H_{c2}(0)$ enough to explain the phase diagram of UCoGe or URhGe.

The orbital limitation depends on the velocity of the quasi-particles forming the Cooper pairs. As this velocity is small in the case in heavy fermion, owing to their large masses, this limit can be quite high. In the compounds studied in this thesis (URhGe an UCoGe) this limit can be higher than 20 Tesla and therefore the field induced by the ferromagnetism of only about 20mT has negligible pair-breaking effects due to this limitation.

Finally, two superconducting states with equal spin pairing are possible for a ferromagnetic superconductor as UCoGe or URhGe: $|\uparrow\uparrow>$ and $|\downarrow\downarrow>$.

2 Experimental Setup & methods

In this chapter I will briefly introduce, the experimental setups and the methods used. For both setups, the part of the sample holder in the magnetic field is almost entirely made out of silver instead of cooper. Cooper is commonly used in dilution refrigerators, but the specific heat hyperfine contribution of silver is much smaller than that of copper which allows for faster changes in temperature under magnetic fields of 8 Tesla (particularly below 50mK). Both setups used an Attocube® piezo-rotator, which allows precise rotation of the sample under magnetic field (step size of about 0.0006 ° [Giesbers 09]). The position of the sample holder in magnetic field is controlled with a Toshiba Hall sensor THS118.

2.1 resistivity setup

The setup presented here was used for the measurement of 3 samples of $CeCoIn_5$. Two of them are relatively small with lengths less than a millimeter. We want to fit the obtained resistivity with power laws to determine the different temperature regimes of the compound. For example in a Fermi-liquid case $\rho(T) = \rho_0 + AT^2$. One of the difficulty is that in the temperature range where this law is valid, the AT^2 term can be much smaller than ρ_0. The aim is to define precisely which law follow $\rho(T)$ ($\rho(T) \propto T^2$ or T) and in which temperature range. The changes of temperature dependence are not abrupt but crossovers. Thus we need both high precision on the resistivity and temperature and a well defined criterion to separate the different regimes. Temperature measurement is discussed in section 2.3. Here I will present our resistivity setup.

Resistivity is measured by the standard four wires AC technique. Four contacts are made on the sample aligned along the longest direction. Current is applied between the two external contact and voltage measured between the two internal ones. Then the resistance of the sample is simply obtained with Ohm's law:

$$R = U/I \tag{2.1.1}$$

The precision of the measurements depends on the signal to noise ratio.

The main sources of noise are:

- inductive pick-up

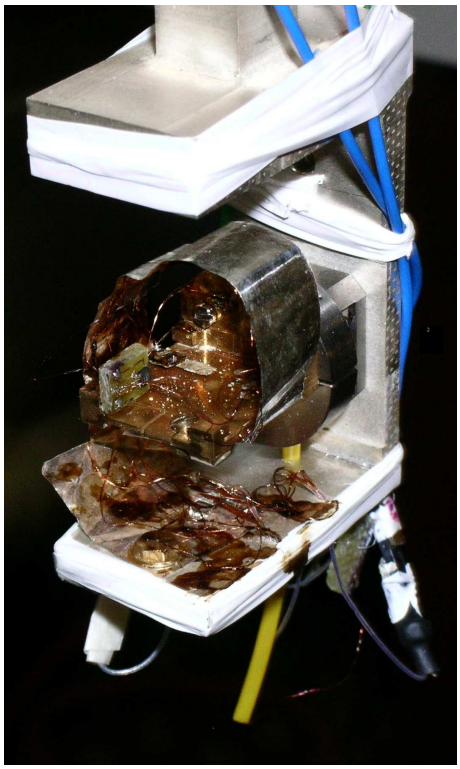

Figure 2.2: Resistivity setup on the dilution fridge. Sample holder is made of silver. Attocube® piezo-rotator on the right, with the rotating stage in silver that is gold coated. The Hall probe and thermometer can be seen on the left of the gold coated plate.

  - Wire loops that can pick-up external oscillating magnetic field (50Hz, ...).
  - vibrating wires, for measurement under magnetic field.

- 300K noise (Instruments, radiation)

Inside the dilution, the setup is well insulated from the external electromagnetic noise. The wires are always fixed to minimize vibration, and we put filters at 300K on each wire to cut high frequencies. Because we wanted to rotate the sample in field, minimization of wires vibrations was obtained by fixing the wires on a silver foil (see figure 2.2) which can be wrapped around the setup with a minimum torque on the piezo rotator. Then, to get a high precision on the measurement of $\rho(T)$, we need to have the biggest signal possible and to amplify it as soon as possible, preferably inside the dilution. We can use four techniques to maximize the signal:

- use the maximum excitation current,
- get a sample with a high geometrical factor l/S,
- use a low temperature transformers,
- use a room temperature preamplifier.

The limiting excitation current is the one that generates a power heating the sample above a maximum allowed threshold to be defined (see figure 2.3). The power generated is proportional to the resistance of the system:

$$P_{heating} = RI^2 \tag{2.1.2}$$

Where R is the addition of the sample and contact resistances, but is dominated by the latter. Heating of the sample is controlled by $P_{heating}$ and the thermal resistance to the fridge: R_{th}.

$$P_{heating} = \Delta T / R_{Th.} \tag{2.1.3}$$

For a constant value of $(\Delta T/T)$, the maximum current is given by:

$$I^2 \propto \left(\frac{\Delta T}{T}\right)\left(\frac{T}{RR_{th}}\right) \tag{2.1.4}$$

Hence, to be able to apply a large current, we need to minimize both the current wire contact resistance (R) and the thermal resistance between sample and sample stage $(R_{Th.})$. The samples to sample stage contacts where done with the minimum amount of G.E. (General Electric) varnish for the contact to be electrically insulating. The thermal contact is due both to the phonon transport through the G.E. varnish and the electrical one through the current wires connected to the sample holder (grounded).

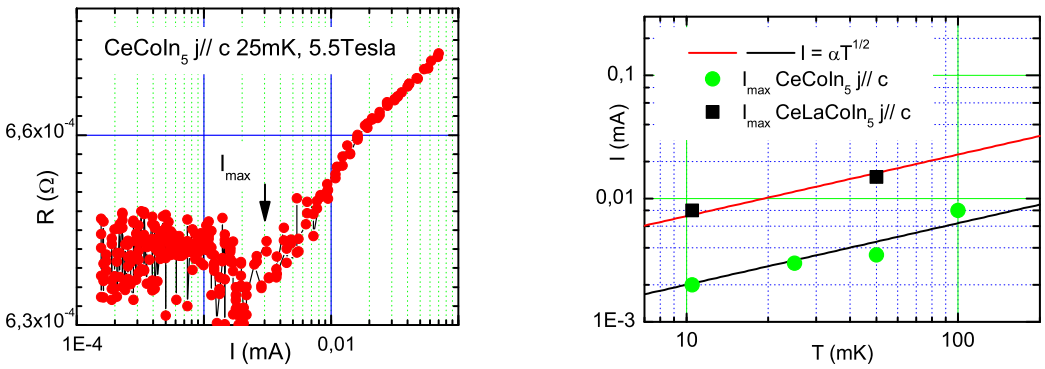

(a) (b)

Figure 2.3: (a) Current dependence of the resistivity of sample B at 25 mK and 5.5 Tesla. Below $I_{max} = 3\mu$A, the temperature of the sample is constant and so is the resistance for larger current we clearly observe an increase of the resistance due to the heating of the sample. (b) Plot of I_{max} versus temperature for samples A and B.

Practically, we used the largest current possible, limited by the detection of a heating above the noise level, as shown on figure 2.3. For the three samples we used currents between 1.5 μA and 1 mA rising as the square root of the temperature (meaning that the thermal contact of the sample is constant). The amplitude of the current used for each sample was determined independently from curves as shown on figure 2.3.

The geometrical factor is mostly given by the size of the crystals that can be grown. $CeCoIn_5$ grows in plate-like crystals with the c-axis being the short axis. The maximum thickness obtained is about 600 μm. To take the best advantage of

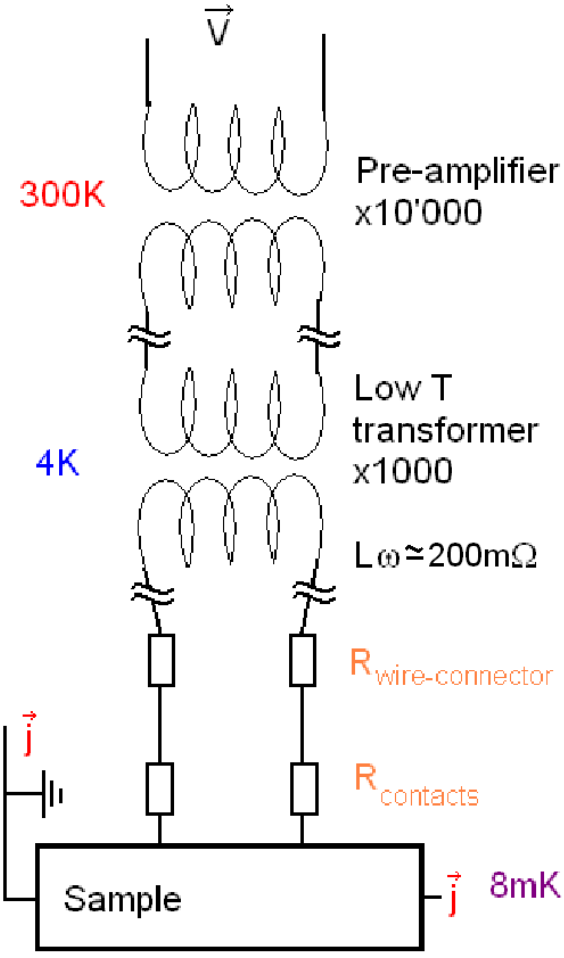

Figure 2.5: Electrical scheme of the resistive setup. Low temperature transformer are placed at 4K. The high gain of the transformer implies that the primary coil contains only few loop (3 for gain 1000). Therefore the impedance of the primary coil is low at the frequencies used for the measurement. For the transformer to amplifies the sample voltage, it is required that $L\omega >> R_{tot}$, where R_{tot} is the total resistance of the sample and wires.

the sample shape and improve the current distribution homogeneity, we solder the current wires at the extremities of the crystal while the two voltage contacts are made on the top side.

The difficulty of using low temperature transformers is that the impedance of the primary coil is low, as the coil is made of only a few loops (3 for gain 1000). For the circuit to work, the impedance of the transformer has to be larger than the total resistance of the circuit $L\omega >> R_{tot}$ (figure 2.5). We used CMR Low Temperature Transformer that have an impedance at 50Hz $L\omega \simeq 200m\Omega$. At low temperature, the wires between the transformer and samples have a resistance of about $5m\Omega$ per wire, mainly due to the use of micro-connectors, which make the sample mounting easier ($R_{Wires-connectors}$ in figure 2.5). The other contribution comes from the contact on the sample and the gold wires used to make these contacts (Fig 2.8). We used 38μm gold wire as they have the better residual ratio and therefore for a wire of 5mm its resistivity is about 2mΩ at low temperature.

Finally the contact resistance between the gold wires and the sample has to be very small, both to be able to use low temperature transformers and in order to minimize the limitation of the current that can be used for the measurements due to Joule heating. Contacts of diameter bigger than the mean free path of the material are limited by the constriction resistance and follow the expression:

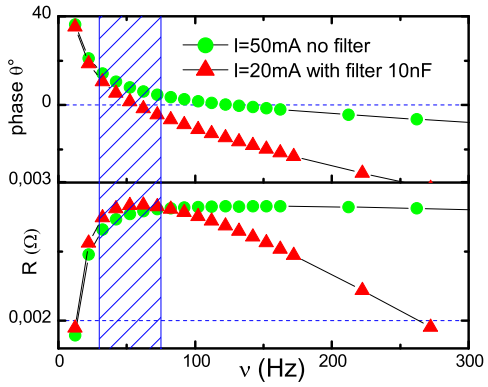

(a)

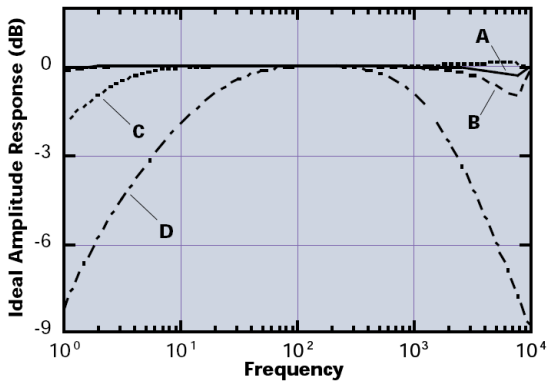

(b)

Figure 2.6: (a) Response of the transformer at different frequency. The frequency must be high enough for the circuit to work $L\omega >> R_{tot}$. The long wires and 300K filters add capacitances between the wires and the ground that dephases the signal at high frequency. For the experiment we use frequencies in the range 30-75Hz (hatched blue region). (b) Ideal response of the transformers for different matching impedances C=10mΩ, D=100mΩ [Ltd. 10]. The response observed in (a) correspond to a circuit impedance between 10 and 100mΩ as expected.

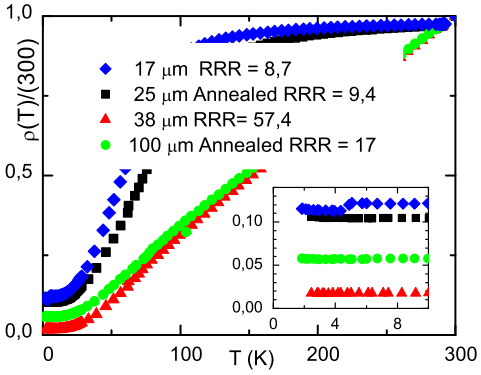

Figure 2.8: Resistivity of several Gold wires. The two different behaviours correspond to different techniques for the production of the wires. The wires are either hard for small diameter or annealed for bigger ones. Further annealing was not successful in improving the wire quality.

$R_{contact} = \frac{\rho_1(T)+\rho_2(T)}{2d}$ where $\rho_i(T)$ $i = 1, 2$ are the resistivity of the two materials in contact and d the diameter of the contact. After ion gun etching we deposited Au stripes (with Ti underlayer) on each samples. Then the gold wires were spot welded. We achieved contact resistances $< 1m\Omega$. This corresponds to a contact diameter bigger than 30μm and emphasizes the importance of the use of large diameter gold wires. The drawback of the use of large diameter gold wires, is that the strain on the spot welded contacts is increased, as the wires are less easy to bend. We add silver paint on each contact to improve it mechanical strength (Fig 2.10).

The use of transformers reduces the range of frequency that can be used for the measurement. The frequency must be high enough for the circuit to work

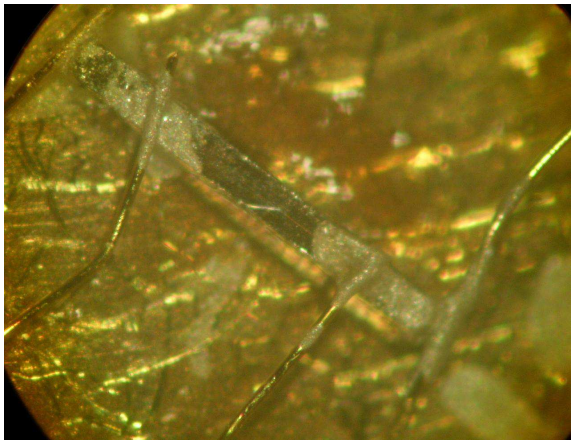

Figure 2.10: Samples of $CeCoIn_5$ (A) the long direction is the crystallographic a-axis. 38 μm wires are used for the voltage and current contacts. Contacts are made by spot welding covered with silver paint for electrical and mechanical efficiency

$L\omega >> R_{tot}$. But also not to high, as the long wires in the dilution, and 300K filters add capacitances between the wires and the ground that dephases the signal at high frequency. We use frequencies in the range 30-75Hz as this corresponds to the best response of the transformer at 4K (figure 2.6).

2.2 Thermal conductivity setup

principle and realization

The principle for the measurement of thermal conductivity is simple. One side of the sample to be measured is cooled by the dilution and we applied some heat power (P) on the other side. A thermal gradient (ΔT) is thus created in the sample and measured by two thermometers. The thermal conductivity is then given by:

$$\kappa = \frac{P}{\Delta T}\frac{l}{S} \tag{2.2.1}$$

Where l/S is the geometrical factor with l the length between the two thermometers contacts on the sample, and S the cross section of the sample.

Figure 2.11 displays two pictures of our setup. The sample stage consists of a 2cm squared silver frame screwed on the piezo-rotator. The frame has a finger on one side that allows to fix the cold end of the bar shape sample. The two *Matshushita* carbon resistance thermometers are glued on a small silver foil that is then fixed to the silver frame with kevlar wires. Similarly the heater, a 10kΩ metallic film resistance, is also glued on a silver foil and fixed to the silver frame with kevlar wires. Then 25μm gold wires are used to connect the sample to the thermometer and heater. Spot welding and silver paint is used at the sample side, silver paint only at the silver foil side to make the contact. Silver foil and gold wires are bent to avoid mechanical stress on the contacts if the thermometers or the heater vibrates. Vibrations are likely when the dilution refrigerator is inserted inside the dewar.

Electrical connections are then made with pure NbTi superconducting wires of diameter 25 μm (35 μm with insulation) and length of about 10cm. The resistance of 1 wire at 10K (above T_{SC}) is about 150Ω. The thermometers are measured with 4 wires; two more wires are connected to the two thermometer's silver foil for voltage

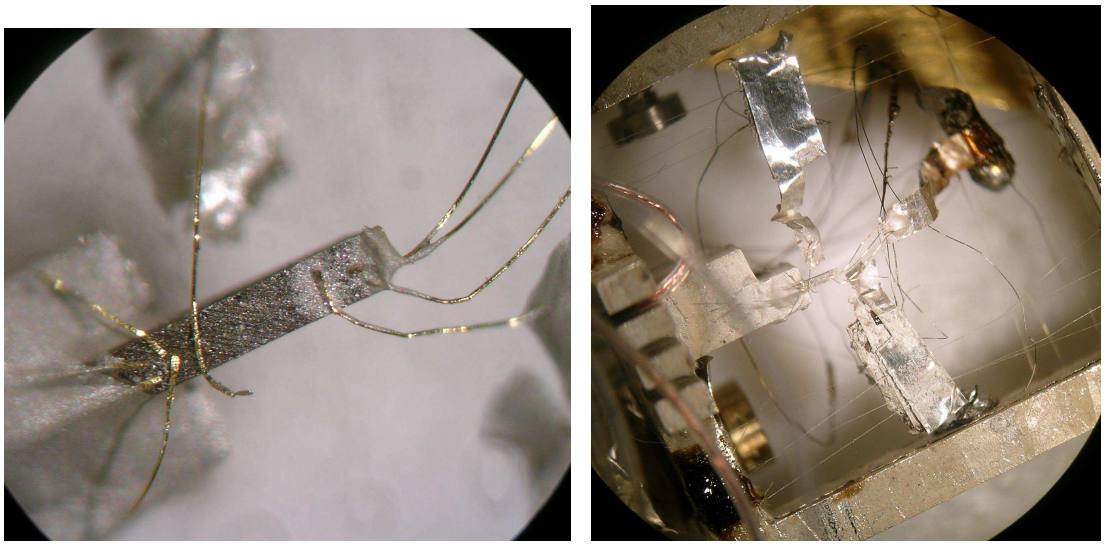

(a) (b)

Figure 2.11: (a) UCoGe sample with 25 μm diameter gold wires. The wires are soldered with spot welding to minimize contact resistivity. (b) Thermal conductivity setup, the sample (a) is mounted on a silver sample holder on the cold side. Two gold wires connect to the two thermometers, and the three last gold wires on the hot side of the sample are used to connect the heater.

measurement. The heater is connected with 2 wires plus one wire on the silver foil to apply current. This allows measurements of thermal conductivity even above the superconducting transition of the NbTi wires. At the superconducting transition of the wires the resistance of the heater is increased by 1.5% (150Ω/10kΩ).

In the same setup we can also measure thermoelectric power. For this matter, continuous copper wires connect the voltage from 4K up to the nano-voltmeter at 300K. Superconducting wires are used between 4K and the sample stage. Finally our setup also allows resistivity measurements in the standard 4 contacts configuration. As the same contacts are used for thermal conductivity and resistivity, the two measurements have the same geometrical factor. This allows an easy check of the setup with the Wiedemann-Franz law.

Sources of errors

The first difficulty for the measurement of thermal conductivity is that the thermometers used to measure the heat gradient are never perfectly calibrated. Hence, the real thermal gradient is the temperature difference of the two thermometers with, and without, heat flow. The thermal conductivity is calculated from:

$$\kappa = \frac{P}{(T_{hot} - T_{cold})_{P\neq 0} - (T_{hot} - T_{cold})_{P=0}} \frac{l}{S} \tag{2.2.2}$$

A scheme of the actual setup is represented in figure 2.13. Another difficulty

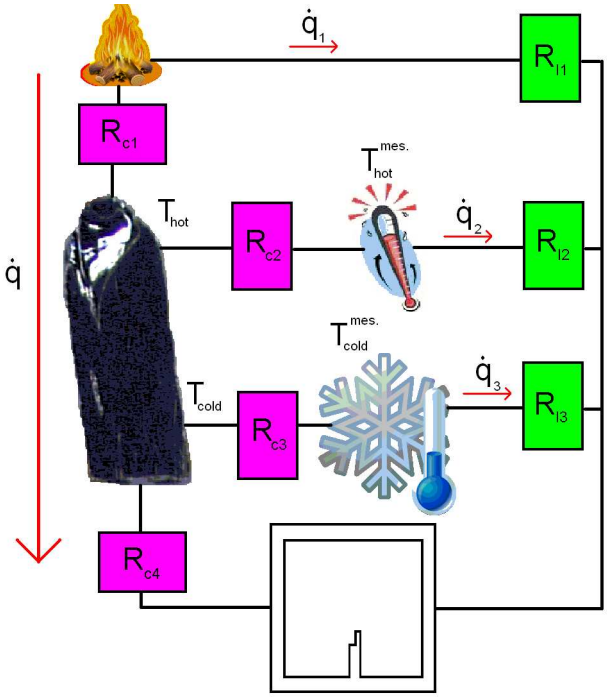

Figure 2.13: Scheme of the thermal conductivity setup. The difficulties of the setup are: First to have the heat current flowing only through the crystal, second to have a good thermalisation of the thermometers on the sample ($T_i^{mes} = T_i$), and third, for a given heat gradient in the sample, to have a not too big one between the sample stage and the sample. To meet these requirements, the four contact thermal resistances on the sample (pink R_{ci}) have to be as small as possible and the thermal contact of the measuring wires (3 leak resistance R_{li} green) as large as possible.

comes from the fact that the thermometers and the heater of the real setup are not perfectly insulated from the environment. Hence we may have two error sources:

- The power dissipated from the resistance will not entirely flow through the sample,
- The temperature of the thermometers is different from the one at the contacts on the sample.

Heat flow is analogous to current flow and from figure 2.13, we can make the analogy of a voltage divider to find the real heat flow through the sample and temperature gradient between the sample and thermometers. The sample thermal resistance is neglected as its contribution is very small. With definitions of figure 2.13, we can calculate the difference between:

- the power generated by the heater P_{heater} and the one applied through the sample P_{sample},
- and the temperature of the thermometer T_i^{mes} and the one on the sample T_i, $i = hot, cold$.

We call the difference between the thermometers temperature and the fridge temperature: $\bar{T}_j^i = T_j^i - T_{\text{fridge}}$ with $i =$ "" or mes, $j = hot$ or $cold$ and we obtain:

$$\begin{aligned} P_{sample} &= P_{heater}\frac{R_{l1}}{R_{l1}+R_{c1}+R_{c4}}\frac{R_{l2}+R_{c2}}{R_{l2}+R_{c2}+R_{c4}} \\ T_{hot}^{\bar{}mes} &= T_{hot}^{\bar{}}\frac{R_{l2}}{R_{l2}+R_{c2}} \cong T_{hot}^{\bar{}}(1-\frac{R_{c2}}{R_{l2}}) \\ T_{cold}^{\bar{}mes} &= T_{cold}^{\bar{}}\frac{R_{l3}}{R_{l3}+R_{c3}} \cong T_{cold}^{\bar{}}(1-\frac{R_{c3}}{R_{l3}}) \end{aligned} \tag{2.2.3}$$

The temperature gradient in the sample (ΔT^{sample}) is usually much smaller than the temperature gradient between the sample and fridge ($T_{cold}^{\bar{}}$) and we can write: $T_{hot}^{\bar{}} = T_{cold}^{\bar{}} + \Delta T^{sample}$. The error on the temperature gradient due to these differences can then be calculated:

$$\Delta T^{mes} = (T_{hot}^{\bar{}mes} - T_{cold}^{\bar{}mes})_{P\neq 0} - \Delta T_0 = \underbrace{\Delta T_{P\neq 0} - \Delta T_0}_{\Delta T^{sample}} + \underbrace{\left(\underbrace{T_{cold}^{\bar{}}\left(\frac{R_{c3}}{R_{l3}} - \frac{R_{c2}}{R_{l2}}\right)}_{1} - \underbrace{\Delta T^{sample}\frac{R_{c2}}{R_{l2}}}_{2} \right)}_{\text{unwanted contribution}} \tag{2.2.4}$$

The unwanted contribution can be important if the two contact resistances R_{c2} and R_{c3} are different and not too small compared to the leak resistances R_{l2} andR_{l3} and as R_{c4} is usually larger than the sample resistance: $T_{cold}^{\bar{}} > \Delta T^{sample}$. Note that depending on the relative contact quality of the cold and hot thermometers, correction may change sign!

In our setup, we try to maximize the leak resistance (R_{li}), and for this reason, we use pur NbTi wires and very thin supporting kevlar wires. We also try to minimize the contact resistances (R_{ci}). We can estimate the precision of the setup from equation 2.2.3 and 2.2.4.

The leak resistances are composed of two contributions. We convert thermal resistance in units of Ω using the Wiedemann-Franz law: $R_{th}(\mathrm{KW}^{-1})\cdot TL_0 = R_{th}(\Omega)$ with $L_0 = 2.44\cdot 10^{-8}\mathrm{W}\Omega\mathrm{K}^{-2}$, for comparison with electronic contribution. First the thermal resistance of the Kevlar wires:

$$R_{Th\,Kevlar\,wires} = \frac{TL_0}{\kappa_{Kevlar\,wires}}\frac{l}{S} \cong 550\Omega/\mathrm{K} \tag{2.2.5}$$

for $\kappa_{Kevlar\,wires}/T^2 \cong 3\cdot 10^{-3} W m^{-1} K^{-3}$[Ventura 09], l=5mm, $\Phi = 17\mu m$. There are 12 kevlar wires per thermometer and for the heater. The second contribution is from the superconducting NbTi wires, with 5 wires in parallel for the two thermometers and 3 wires for the heater all of them having an electrical resistance of about 150Ω in the normal state. In the superconducting state, the thermal resistance is increased due to the gap opening, but then the contribution of phonons should also be taken into account. Thus the leak thermal resistance at 1K are in the worst scenario about:

$$R_{l1} \cong 25\Omega \quad (1/(3/150{+}12/550)) \quad R_{l2} \cong R_{l3} \cong 20\Omega \quad (1/(5/150{+}12/550)) \tag{2.2.6}$$

larger at lower temperature and smaller at higher temperature ($\cong 5\Omega$ at 10K).

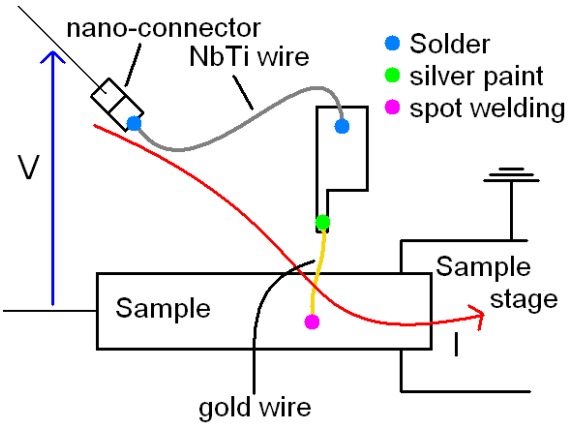

Figure 2.14: Scheme for the measure of the electrical contact resistance. Current is applied through a voltage contact and the sample holder (cold end). The four contacts plus the NbTi wire plus the gold wire are measured. The value of the spot welding contact can be singled out at the superconducting transition of the sample (height of the transition).

The contact resistances are more complicated to measure. We measured the electrical resistance using a setup as sketch on figure 2.14, with the electrical current flowing through one voltage wire, and hence, we measure the resistance of: 1 nano-connector, two solder contacts of the superconducting wire, the superconducting wire, the silver foil, the silver paste contact between the silver foil and the gold wire, the gold wire, and its contact on the sample. Doing so for the UCoGe sample, we found that the resistance of the two voltages contacts was very different 40mΩ and 400mΩ respectively. We believe this difference comes mainly from the difficulties to solder the NbTi superconducting wires and not from the gold wire contact. Indeed, at the superconducting transition of the sample, the drop in resistance was of a few mΩ. This value is characteristic of the gold wire-sample contact. The contact between the gold wire and the silver foil with silver paint is easy to do and hence normally good. In a different way we can measure the fridge-sample contact thermal resistance, measuring its thermal conductivity $\kappa_{fridge-sample} = P/(T_{cold} - T_{fridge})$. We obtained a thermal contact of a few mΩ (figure 2.15). Hence, we can estimate all the contact resistances as:

$$R_{c1} \cong R_{c4} \cong 4m\Omega \quad R_{c2} \cong R_{c3} \cong 15m\Omega \tag{2.2.7}$$

as the contact on the thermometer are made of only 1 gold wire instead of 3 for the heater or fridge-sample contact.

Precision of the measurements

Finally from equation 2.2.3 we deduce that more that 99.9% of the power crosses the sample. Similarly from equation 2.2.4 the error on the temperature gradient can be in the worst case (1 thermometer contact resistance is 0 and the other 20mΩ) about 0.1% of the sample temperature (T_{fridge}). However, if we measure thermal

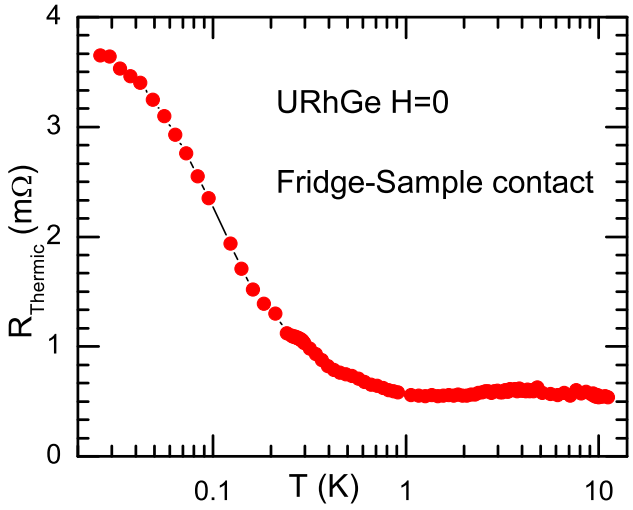

Figure 2.15: Fridge-sample thermal contact obtained from thermal conductivity data

conductivity with a heat gradient of $1\%T_{fridge}$, this can lead to an error of 10% on ΔT and thus on $\kappa(T)$. We checked our measurements in two differents ways: measuring the same sample in the identicual conditions with differents heat gradients, typically $\Delta T \in [0.5, 5]\%$. The differences lies in the noise value of the measurement ($\sim 1\%$). This insures that the "unwanted contribution 2" is small. The second technique is to check the Wiedemann-Franz law $L_0 = \kappa/\sigma T$ that is always obeyed for $T \to 0$ (see for example [Ashcroft 76, p. 322]). In all our measurement we found that the Wiedemann-Franz law was obeyed within a few percent, which allows us to say that the unwanted contribution is of this order. The reason is certainly that the two thermometers contacts resistance have a similar value and it insures that the "unwanted contribution 1" is also small.

Another reason why we need low contact resistances between the fridge and the sample is that this determines the lowest temperature to which we can measure thermal conductivity. Indeed, as the samples measured are good metals, their thermal resistivity even with a good geometrical factor is only about $0.2m\Omega$. This is about 20 times less than the thermal contact measured between the sample and fridge (see figure 2.15). Hence the thermal gradient between the fridge and sample is about 20 times the thermal gradient in the sample. This makes low temperature measurements time consuming as for each point of thermal conductivity, the fridge has to be regulated at two temperatures: at the base temperature with heat flow through the sample $\Delta T_{P\neq 0}$ (**a** on figure 2.17), and at the sample temperature with no power $\Delta T_{P=0}$ (**b** on figure 2.17). For a $\Delta T = 3\%$ these two temperatures are separated by 60% and the fridge has to be cooled down for the next point if we want

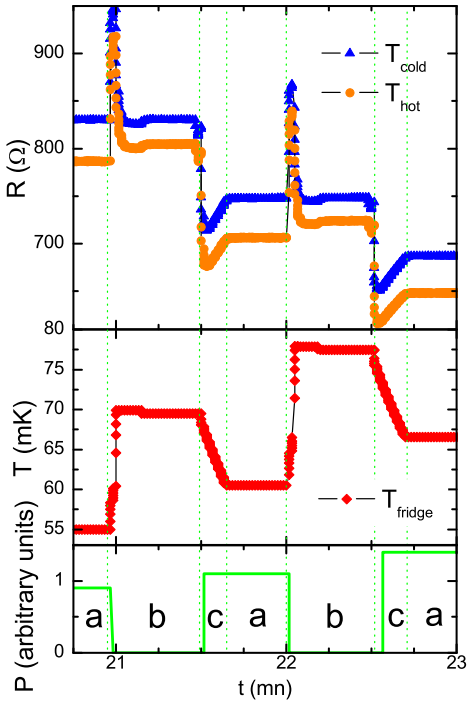

Figure 2.17: Evolution of the temperatures and power for one point of thermal conductivity. Top: resistance of the two samples thermometers, middle: temperature of the fridge and bottom: power applied on the sample (to create or not a heat gradient). The different steps for a thermal conductivity measurement are: **a** At base temperature, with a heat gradient in the sample we measure the $\Delta T(P \neq 0)$. **b** The heat power is switched off and the program regulates the fridge temperature such that the cold thermometer has the same value as in **a**. Then we measure $\Delta T(P = 0)$. **c** The fridge is cooled down for the next point.

data spacing of less than 60% (c on figure 2.17). This last step can take quite long time at low temperature (< 50mK).

2.3 Temperature measurements

Temperature measurement at very low temperature is not the easiest task. I will briefly describe how we do it on the fridge used during my thesis.

The main thermometers are located below the mixing chamber in a compensated field region. They are used for the calibration of other thermometers and regulation of the fridge temperature. For the range 30K-100mK we used two Ge thermometers (doped semiconductor resistance thermometers). The resistance of these thermometers is highly reproducible with thermal cycling. For the lowest temperatures (100mK-6mK), we used a carbon resistance thermometer. The resistance of this thermometer is not reproducible with thermal cycle and has to be calibrated each time the cryostat is cooled down. For this calibration, we use a CMN (cerous magnesium nitrate) paramagnetic salt. The temperature is obtained by fitting the susceptibility (measured with a mutual inductance bridge) of the CMN with a Curie-Weiss law:

$$\chi_{CMN} = \frac{C}{T_{CMN} + \theta}, \quad M = M_0(1 + \alpha\chi_{CMN}) \tag{2.3.1}$$

Where M_0 and αC are constants to be determined and θ is related to the Néel temperature of the salt, which also depends on its geometrical factor through de-

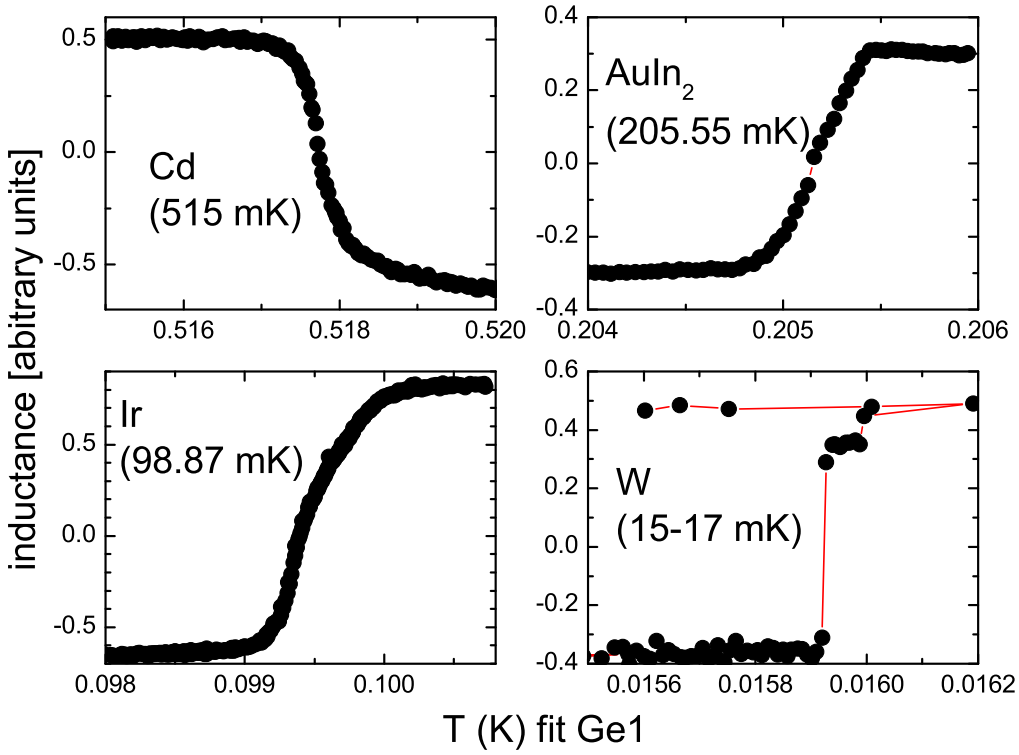

Figure 2.18: Susceptibility measurements of the fixed points, plotted versus the temperature of fridge as given by the resistive thermometers (named Ge1). Values in brackets give the tabulated value.

magnetization effects. For our device $\theta \cong$1mK and is reproducible with thermal cycling. M_0 and αC depend also of the environment and are determined from a high temperature fit to the Ge thermometer. The CMN is very sensitive to magnetic field and can only be used when its surrounding has been properly demagnetized. The dilution fridge is equipped with 10 fixed points (temperature tabulated superconducting phase transitions) from the National Bureau of Standard (series 767 and 768) covering the range 15mK-7K. We used them to check the calibration of the thermometers at the beginning of my thesis, figure 2.18. They also allow to precisely determine the value of θ. A complete and absolute calibration at higher temperature is also possible with a He^3 pot (0.5K$< T <$3.5K), to calibrate the Ge thermometers. Gas pressure of the liquid-gas coexistence of He^3 is used in this case to obtain the temperature. As these processes take a lot of time we limited ourself to:

- calibration of the CMN just after the fridge is cooled down (We demagnetize the lower part of the dilution at 300K before cooling)
- followed by a calibration of the carbon thermometer with the CMN thermometer.

- once in a while (every 3-5 years) check of the full calibration with the fixed points and determination of θ for the Curie-Weiss law.

We estimate that the precision on the absolute temperature we get this way is of about 3% at 15mK, to a maximum of a few mK at 1K.

The second type of thermometers are used at the sample stage under magnetic field. They are the thermometers used to measure the heat gradient for thermal conductivity or the temperature of the sample in the case of resistivity measurements. These thermometers need to be recalibrated at each different magnetic field. Calibration is done with the main thermometer located in a compensated field region.

For thermal conductivity measurements or to fit with a power law the resistivity data, it is important to have a high relative precision in our thermometry. This is possible as the variation of resistance of the thermometer with temperature is smooth. It requires a good fitting technique. Indeed, the temperature dependence of the resistance of the thermometers with temperature is complicated and cannot be fitted with a single function deduced from a physical law in its full temperature range. Hence we used an approximated function for example for the *Matshushita* carbon resistance thermometers we have:

$$(T_{Matshushita})^{0.5} = F(ln(R_{Matshushita})) \tag{2.3.2}$$

where $F(x)$ is approximately a linear function. $F(x)$ is precisely a polynomial best fit on a smaller interval, typically the equivalent in resistance of 100mK, centered on the resistance value for which we want to calculate the temperature (spline interpolation). The interval is hence sliding with x on the calibration points. To avoid any abrupt change when a new point is added to the interval, the calibration points are weighted: 1 if they are part of the interval and smoothly (exponentially) decreasing when outside of the interval. The weight is then used for the interpolation. The different parameters are adjusted to get the best compromise for the function to be accurate and vary smoothly. We obtain this way a relative precision of about 0.5% over the full temperature range (8mK-10K), and of about 0.05% on a range of 5% of the temperature. A heat gradient less than 5% is typically used for thermal conductivity.

Coulomb Blocade Thermometer

Working principle

The technique described above only works because our dilution has a field compensated region. Magnets with field compensated region are only available for relatively low field. We could go up to 8.5 Tesla. Thermometers that have no or a weak field dependence are therefore very important if one wants to make higher field measurements. Coulomb Blocade Thermometers (CBT) have such properties in addition to being primary thermometers and hence are, theoretically, the perfect thermometer desired by an experimentalist. We tested a CBT versus our thermometry. If our measurement technique is not yet fully satisfactory, the device itself shows promising response.

A Coulomb Blocade Thermometer (CBT) may replace paramagnetic salts and fixed points, as secondary or even primary thermometers under magnetic field. The thermometer is made of small islands of aluminum (μm sized) deposited on a SiO_2 substrate. Al islands are insulated one from another with AlO_2 layers placed in series. Details about the fabrication can be found in [Kauppinen 98, Farhangfar 97]. A bias voltage is applied across the array of islands and we measure the current tunneling through the array. The conductance of the system will have a minimum at 0 bias voltage, and a constant value for high bias voltages. The width of the dip in conductance is proportional to the temperature.

The range of temperature in which the CBT can be used is limited at low temperature by the electron-phonon decoupling around 20mK that prevent the device to be cooled further down. At high temperature, the finite height of the barriers between the islands modifies the CBT response to the bias voltage.

It was demonstrated by Pekola et al[Pekola 94], that the shape of the dip is given by:

$$\begin{aligned} G(V)/G_T &= 1 - u_N g(v_N) \\ \text{with} \quad g(x) &= [xsinh(x) - 4sinh^2(x/2)]/[8sinh^4(x/2)], \\ v_N &= eV/[Nk_BT] \\ \text{and} \quad u_N &\propto 1/T \end{aligned} \tag{2.3.3}$$

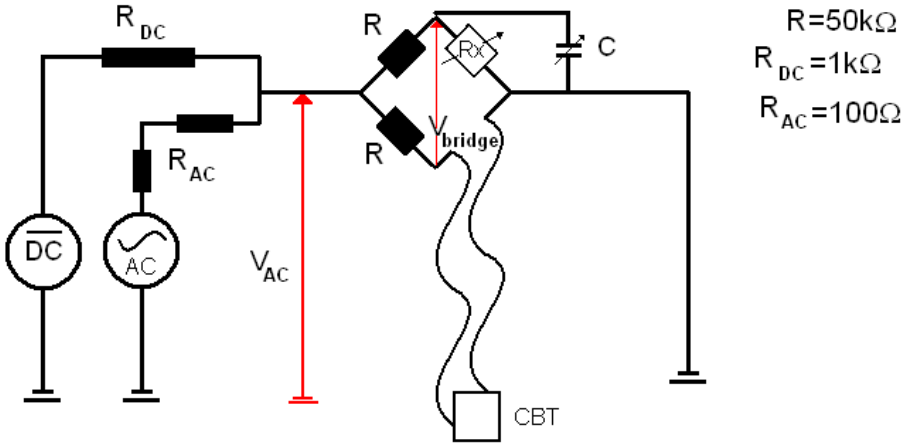

Figure 2.19: Scheme of the electronic used to measured the CBT device.

G_T is the conductance for high bias voltage, $G(V)$ the conductance at a given voltage and u_N depends on the charging energy of the system and is inversely proportional to temperature. We measure the resistance of the CBT, with a home made resistance bridge (scheme on figure 2.19). As resistance is one over conductance we have:

$$G/G_T = R/R_{max}. \tag{2.3.4}$$

Pekola et al. show that from 2.3.3, one can obtain that the full width at half maximum is:

$$V_{1/2} \cong 5.439 N k_B T/e \tag{2.3.5}$$

Depending only on the number of junctions (N=100 in our case), fundamental constants and the temperature: this is why a CBT can be considered as a **primary** thermometer. At low temperature, the applied voltage warms up the CBT if the bias voltage is too large. Below about 100mK the critical voltage, above which the CBT heats up, is lower than the value where the resistance is constant ($V_{\text{critical}<V(R_T)}$) and broaden the pick. Equation 2.3.5 can be corrected for these overheating effects and calculated to higher order[Pekola 10]:

$$V_{1/2} = (1 + 0.53022(\Delta R/R_{max}) - 3.64193(\Delta R/R_{max})^2)5.439Nk_BT/e \tag{2.3.6}$$

To get the full width at half maximum, the CBT has to be measured for various bias voltage which makes it a slow thermometer (typically several minutes are necessary to obtain 1 temperature). The CBT can however also be used as a secondary thermometer as the height of the resistance pick depends on the temperature as:

$$\Delta R/R_{max} = 1/6u_N - 1/60u_N^2 + 1/630u_N^3 \tag{2.3.7}$$

Measurement technique and precision

In our setup, we obtain the resistance of the CBT through a resistance bridge. If we call $u = V_{bridge}/V_e$ the ratio between the AC voltage of the bridge and the applied AC voltage, we get from the scheme on figure 2.19:

$$u = \left(\frac{R_{CBT}}{R_2 + R_{CBT}} - \frac{R_x}{R_1 + R_x}\right) \tag{2.3.8}$$

With R_i and R_x the bridge resistance and R_{CBT} the CBT resistance. We set $a = R_1/R_x$ and obtain:

$$R_{CBT} = R_2\frac{1 - u(1 + a)}{a + u(1 + a)} \tag{2.3.9}$$

Then we can calculate the error that our measurement technique implies on the value of the resistance of the CBT:

$$\frac{\partial R_{CBT}}{\partial a} = R_2\frac{u - a - 1}{(a + u(1 + a))^2}$$
$$\partial R_{CBT} \cong 2R_2\partial a$$

$\partial a < 1 \cdot 10^{-6}$ for the accuracy of the resistances. The temperature drift is compensated between the two resistances. This contribution is small $dR < 1\Omega$. The contribution of ∂R_2 is small if the bridge is well balanced:

$$\frac{\partial R_{CBT}}{\partial R_2} = \frac{1 - u(1 + a)}{a + u(1 + a)}\partial R_2 \cong \partial R_2 \tag{2.3.10}$$

$\partial R_2 \cong 5{\cdot}10^{-6}$ for a temperature variation of 1°C of the bridge as we use 5ppm/ °C resistances. Which implies $dR \cong 0.25\Omega$

$$\frac{\partial R_{CBT}}{\partial u} = R_2 \frac{(1+a)^2}{(a+u(1+a))^2}$$
$$\partial R_{CBT} \cong 4R_2 \partial u$$

$\partial u = \frac{\partial V_{bridge}}{V_{AC}}$. In the first experiment we measured $\partial V_{bridge} \cong 1 \cdot 10^{-6}$V that is the variation observed when measuring a constant resistance over 24 hours. The voltage applied on the bridge (V_{AC}) vary between $6 \cdot 10^{-3}$ and 10^{-5}V, as the signal as to be small compared to the size of the peak in resistance we want to measure. This create a large error of $\partial R_{CBT} = (10\% - 2\%)$

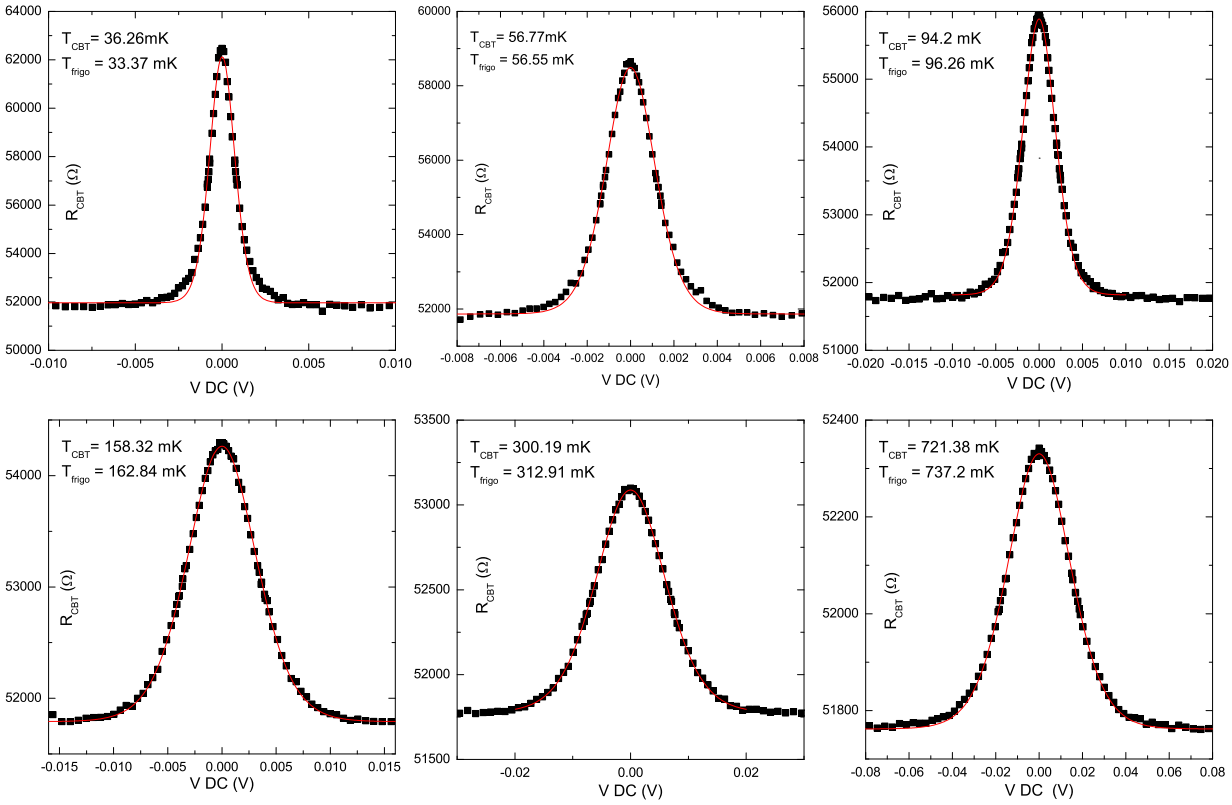

Figure 2.20: R-V curves of the CBT at different temperature. Red curves are fits from equation 2.3.3 and 2.3.4. One can clearly see the effect of DC current heating at low temperature. For this reason, the measured tail of the resistance pick are bigger than the simulation.

In that setup, we found that the precision was limited by the accuracy of the addition of the AC and DC signal. Accuracy on the addition of the two signals was limited by the precision of the output resistance of the reference channel of the lock-in. Therefore we built an additional electronic device and added a transformer at the output AC source to cut the ground loops generated through the lock-in.

Doing so, we were able to reduce considerably the level of noise on the signal but we then we still had a drift of the signal with time, due to a bad connector that added a fluctuating resistance in parallel of the CBT. In the latest setup, all of these issues are solved with no more time drift and a much lower noise level. The device in this configuration is now tested.

Nevertheless, in the first experiment we could obtained full conductance curves (figures 2.20) of the CBT. Fit from equation 2.3.4 give temperatures that are in very good agreement with the thermometry of the fridge.

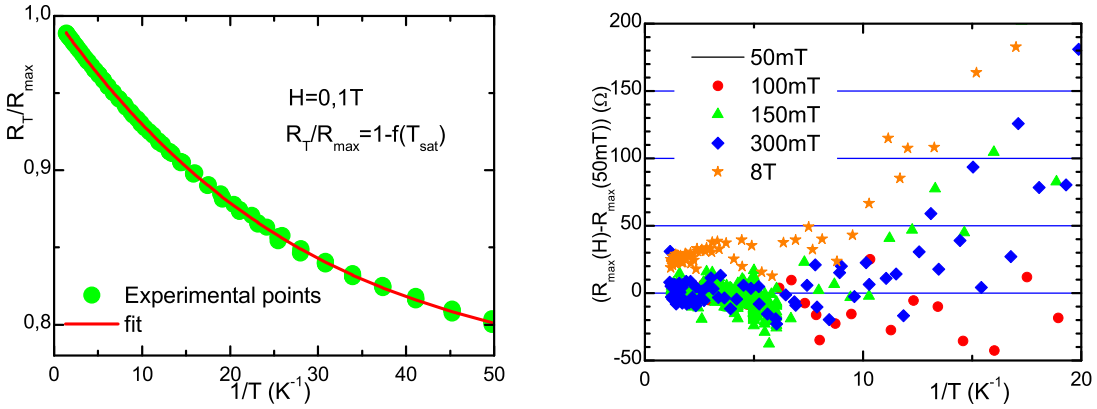

(a) (b)

Figure 2.21: (a) show the temperature dependence of R_T/R_{max}. As excpected from equation 2.3.7, R_T/R_{max} is almost linear versus $1/T$. (b) Field dependence of R_{max}, the variation of the resistance under magnetic field is quite small especially above 100mK.

In the last experiment we could look at the field dependence of R_{max}. Figure 2.21b, show the deviation under magnetic field with the curve taken at 50mT. Above 100mK the variation is less than 50Ω and lies in the noise of the measurement except for the curve at 8T where a constant offset of about 25Ω is found. At 100mK a variation of 50Ω correspond to a ΔT of 1mK. Figure 2.21a show the temperature dependence of the maximum of resistivity. From 2.3.7 and 2.3.4, R_{max} should follow the relations:

$$\begin{aligned} T_{\text{sat}} &= \frac{1}{(T_{frigo}^n + T_0^n)^{1/n}} \\ f(T_{\text{sat}}) &= 1/6 \cdot u_N \cdot T_{\text{sat}} + b2 \cdot (u_N \cdot T_{\text{sat}})^2 + b3 \cdot (u_N \cdot T_{\text{sat}})^3 \\ \frac{R_T}{R_{max}} &= 1 - f(T_{\text{sat}}) \end{aligned} \tag{2.3.11}$$

With $b2 = 1/60$ and $b3 = 1/630$. Fit of our data with 2.3.11 can be very accurate (within 0.1% for $T \in [100mK, 800mK]$) if we modifie the value of the coefficients to $b2 = 0.0483$ and $b3 = 0.0058$. The value of these coefficients may hence be dependent of the microscopic details of each device. However it is remarkable that

such a simple law can describe the physics of the CBT in a very large temperature range. The power of the saturation in the temperature of the CBT n is not well defined in our fit but could take the value $n = 5$ excpected for the electron-phonon decoupling. Then we obtain a saturation $T_0 \cong 16$mK.

Finally, we confirm that the CBT thermometers have a very small field dependence and are hence suitable for measurements under magnetic field. The laws for the temperature dependence of R_{max} and $V_{1/2}$ and also probably our measurement technique still need some improvements for a use of these devices as primary thermometers, but are promising as we are able to measure them with a high signal to noise ratio.

3 $CeCoIn_5$

3.1 Background

"115" Family

$CeCoIn_5$ is the Ce based heavy fermion compound which displays superconductivity at the highest critical temperature discovered up to date. It is part of a family of compounds called "115" for their chemical composition XMT_5 with X=(Ce,Pu), M=(Co,Rh,Ir) and T=(In,Ga), that crystallize in a tetragonal crystal structure. The parent compound of this family is $CeIn_3$ in which superconductivity was discovered in 1998 by Mathur et al. [Mathur 98], during the search for a magnetically mediated superconductor. Indeed, superconductivity can be induced in this ambient pressure anti-ferromagnet by applying pressure. Applying pressure also drives the system paramagnetic and the superconducting pocket is located at the quantum phase transition. The "115" family can be viewed as a more two dimensional version of the same material with a MT_2 layer introduced in the original cubic compound. The first material is $CeRhIn_5$, with as for $CeIn_3$, an anti-ferromagnetic ground state and pressure induced superconductivity [Hegger 00]. Four compounds in this family display ambient pressure superconductivity: $PuRhGa_5$, $PuCoGa_5$, $CeIrIn_5$ and $CeCoIn_5$, with T_{SC} respectively of 8.7, 18.5, 0.4 and 2.3K. At least, the following properties can be inferred from this series of compounds on the appearance of superconductivity:

- Two dimensionality has increased T_{SC}.
- 5f systems have much higher T_{SC} than 4f ones (Pu→Ce). Delocalization of magnetism seems to be favourable for superconductivity.
- Two systems with identical electronic structure $CeIrIn_5$ and $CeCoIn_5$ display rather different superconducting properties which suggest an important role of the crystal field for superconductivity[Maehira 03]. Indeed, the gap between the two first doublets of the 4f, $J = -5/2$ manifold increases from 6.9 to 8.6 meV (25%) but the other parameters undergoe little change [Pfleiderer 09]. Band structure calculations of the two compounds suggest very similar Fermi-surfaces. Which could imply that magnetic anisotropy plays an important role for superconductivity.

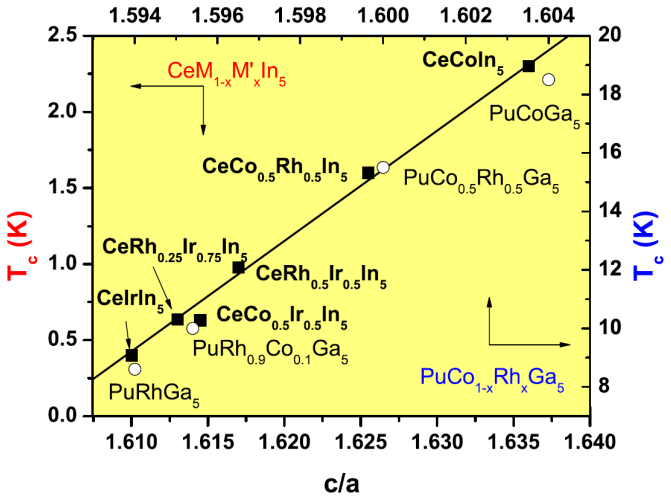

Figure 3.2: Evolution of the crystal axis ratio c/a with superconducting temperature T_{SC}. The linear scaling suggest that crystaline anisotropy is important for superconductivity [Sarrao 07].

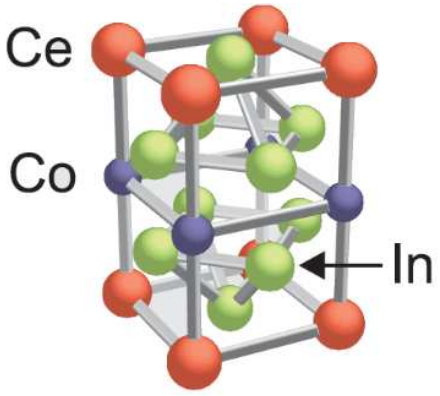

Figure 3.4: $CeCoIn_5$, has a tetragonal crystallographic structure. The inclusion of $CoIn_2$ planes make it more two-dimensional than its parent compound $CeIn_3$. Two-dimensionality is favourable for superconducting paring [Monthoux 01].

- Similarly the ratio of the crystallographic axis c/a has been found to change continuously with T_{SC} in either the Ce or the Pu family as shown in figure 3.2 from [Sarrao 07].

General physical properties of $CeCoIn_5$

The unit cell of $CeCoIn_5$ (Figure3.4) is composed of layers of $CeIn_3$ and $CoIn_2$ and band structure calculation show some two-dimensional properties, with some cylindrical Fermi surface sheets [Maehira 03]. On this matter, $CeCoIn_5$ is similar to the high-T_c cuprates even if for $CeCoIn_5$ the electronic properties are only weakly anisotropic.

The compound $CeCoIn_5$ contains several challenging problems for the understanding of heavy fermions and more generally the interactions between superconductivity and magnetism. In the following I will present some of the important experiments on this compound on four different subjects:

- The detection/position of a field induced quantum critical point (QCP).
- The coexistence of anti-ferromagnetism within the superconducting phase.
- The existence of a FFLO phase at high field and low temperature.

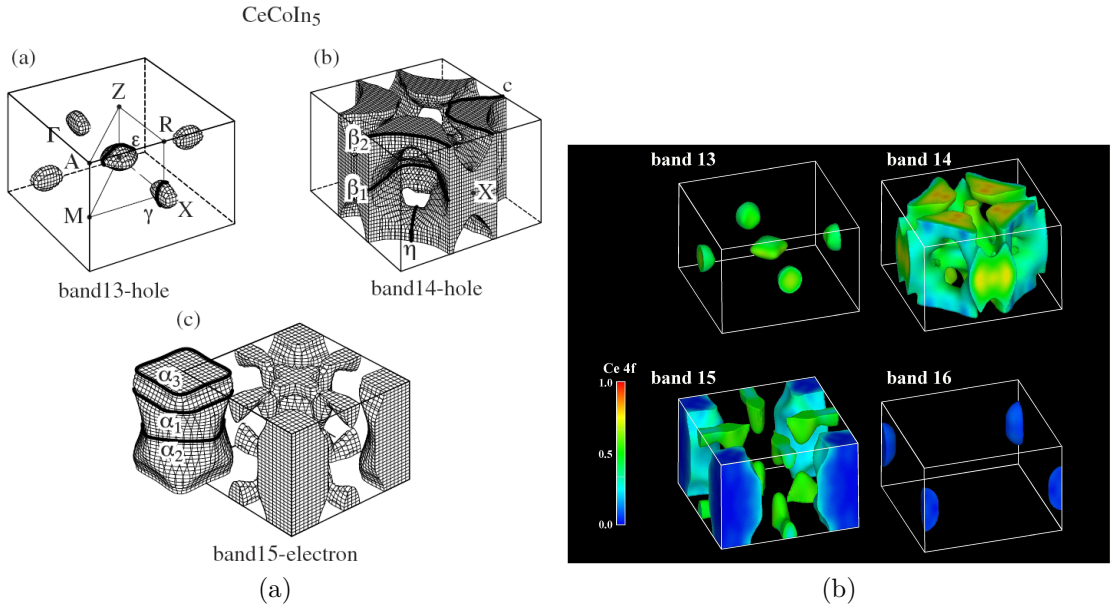

Figure 3.5: Fermi surface simulation from band structure calculation (a) from [Settai 01], (b) from [Maehira 03]

- The unusual pressure, field, temperature phase diagram for superconductivity (and magnetism?)

The aim of these experiments is the understanding of the link between superconductivity and magnetism.

Field induced QCP

A long list of experiments have reported non-Fermi liquid behaviour and a possible field induced QCP at $H_{c2}(0)$ for the field applied in the [001] direction and possibly also in the basal plane. The first measurements of charge transport by Paglione et al.[Paglione 03] have located a QCP exactly at $H_{c2}(0)$ (Figure 3.6a). This has then been confirmed by Tanatar et al [Tanatar 07] and Bianchi et al. [Bianchi 03b] combining measurements of resistivity and specific heat (Figure 3.6b). Specific heat (C_p) is in principle an ideal thermodynamic indicator of non Fermi liquid behaviour. However, the difficulty is that in $CeCoIn_5$ no saturation of C_p/T is observed close to H_{c2}, that would reflect Fermi-liquid properties, even when a T^2 regime is still measured in resistivity. This may be due to the fact that this observed T^2 regime exists below the minimum temperature of specific heat measurements. Indeed, at 100mK at least 70% of the bare signal is coming from the hyperfine contribution which severely limits the precise determination of the Fermi liquid border and no data are shown below 80mK. Nevertheless, analysis by spin fluctuation theories point to the proximity of the QCP to $H_{c2}(0)$, with a continuously increasing logarithmic divergence on approaching the upper critical field [Bianchi 03b, Bauer 05]. Deviation from this logarithmic law was also used as a mark from a "cross-over regime" (Figures 3.6b and 3.6d).

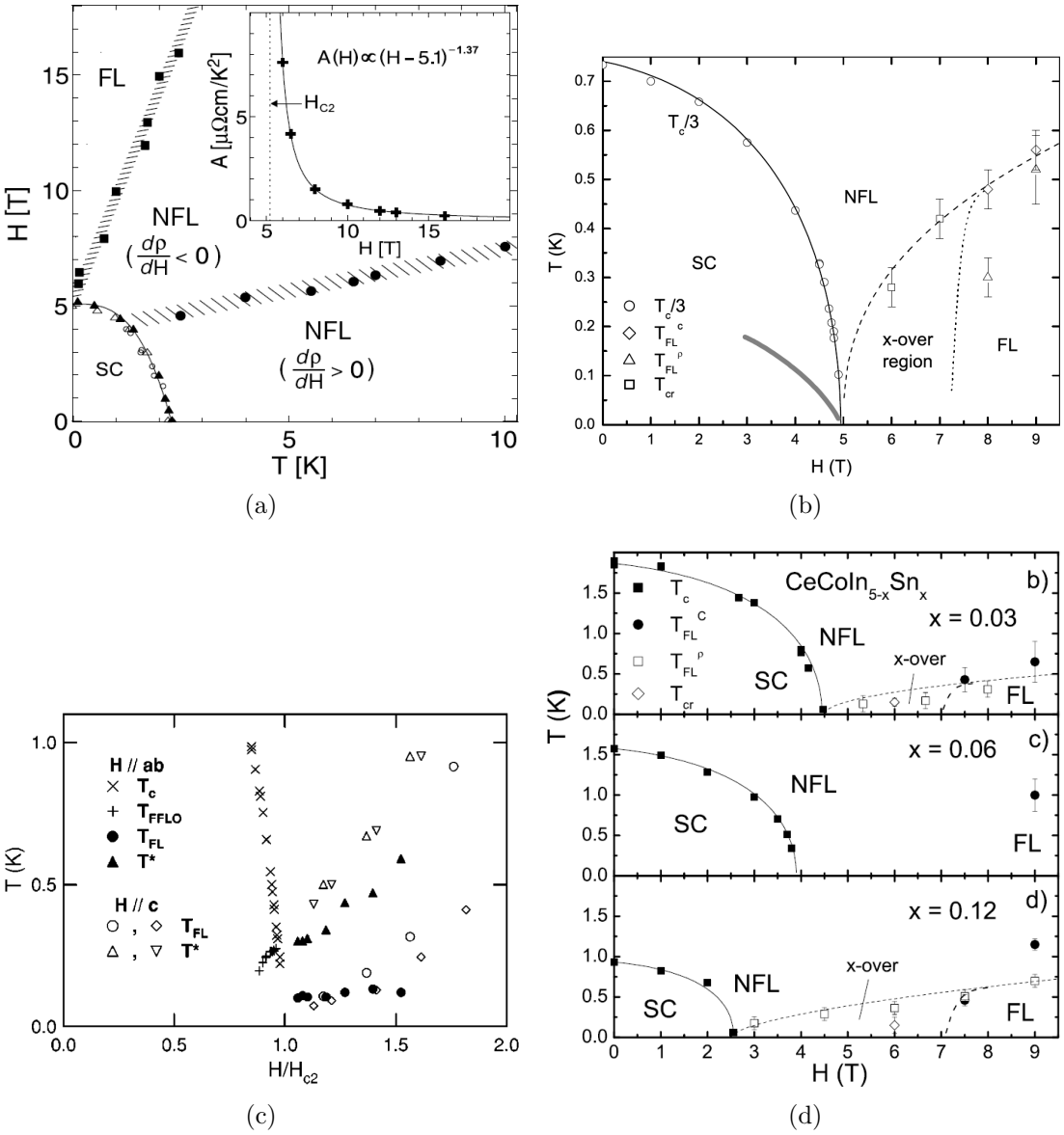

Figure 3.6: Previous experiments strongly suggest that the field induced QCP is located exactly at $H_{c2}(0)$ [Paglione 03, Bianchi 03b, Ronning 05, Bauer 05].(a) and (c) FL domain determine by mean of resistivity. (b) FL domain determined by combination of methods, $T_{FL\,\rho}$: resistivity; above T_{cr} specific heat over temperature $C(T)/T \propto -ln(T)$ (Non-Fermi Liquid). Bellow T_{FL} $C(T)/T = const.$ (Fermi-liquid). (d) Same notations, evolution with Sn doping.

Ronning et al [Ronning 05] performed resistivity measurements for the two fields directions (H//[001] & H//[100]) (Figure 3.6c). Their measurements point to a QCP at a lower field than $H_{c2}(0)$ but the coincidence of the two points was still within experimental error. The fact that both fields directions point to a QCP close to $H_{c2}(0)$ reinforced the previous statement of a coincidence of $H_{c2}(0)$ and the QCP. Later the same authors show that upon applying pressure the QCP is clearly moved inside the superconducting domain and the divergence of the A coefficient of resistivity gets

weaker [Ronning 06]. Malinowski et al. located the QCP well inside the superconducting domain at ambient pressure using transport measurements[Malinowski 05] along the c-axis.

Other probes also reflect the non Fermi-liquid behaviour in proximity to $H_{c2}(0)$ without being able to precisely locate the QCP. This is the case from thermal conductivity measurements, where the Wiedermann-Franz ratio (heat over charge conductance) is found to have a value well below the Lorentz number down to 50mK, when the current is parallel to the c-axis [Tanatar 07]. The authors claim that it indicates a collapse of the quasi-particle concept with a singularity along the c-axis. Indeed, such a deviation is not observed in the basal plane [Tanatar 07, Seyfarth 08]. A large increase in the Seebeck coefficient (Thermoelectric power) is also found in the vicinity of $H_{c2}(0)$ [Izawa 07a] and is comparable to the increase of $A^{1/2}$ and γ. In this experiment, the current was applied parallel to the a-axis. Another probe that can be used is the Hall effect [Singh 07]. This probe does not directly give a criterion for the determination of the Fermi-liquid boundary but it allows to single out a characteristic field, function of temperature which happens to coincide with the line drawn from resistivity data. The interest in the Hall determination is that it is less prone to magnetoresistance effects which affect resistivity at the lowest temperatures (or the highest field), allowing for a more precise determination of the border of the Fermi-liquid domain close to $H_{c2}(0)$. Hall effect would clearly locate the putative QCP below $H_{c2}(0)$. Finally, doping the In site with Sn, suppress T_{SC}. The Fermi-liquid domain and associated QCP have been measured to follow the position of $H_{c2}(0)$ as it decreases through the doping (Figure 3.6d)[Bauer 05], which is another reason to believe that the QCP is pinned at $H_{c2}(0)$.

	Technique	T_{SC}	$H_{c2}(0)$
[Paglione 03]	ρ	2.3K	5.1±0.2T
[Tanatar 07]	ρ κ		5.0±0.1T
[Bianchi 03b, Ronning 05]	ρ C_p	2.3K	4.95T
[Malinowski 05]	ρ		5T
[Seyfarth 08]	κ	2.25K	5.1T
[Izawa 07a]	κ		5.4T
[Singh 07]	ρ_{xy}		5T

Table 3.1: Superconducting transition temperature reported from different authors with different experimental techniques: ρ resistivity, κ thermal conductivity and ρ_{xy} Hall effect

Although their is a good agreement between the different experiments for the presence of a field induced QCP in $CeCoIn_5$, the actual coincidence of the QCP and $H_{c2}(0)$ is a matter of debate. The variation between different experiments is probably not linked to sample quality; reported values for T_{SC} and $H_{c2}(0)$ are similar and are mainly dependent on the measurement technique: table 3.1. The difficulties arise from the temperature below which a Fermi-liquid regime is obtained (T_{FL}) and its weak field dependence. Then the precision of the points T_{FL} and the extrapolation to $T = 0$ needed to obtain the field value of the QCP can explain the

variability of results. In that sense, quantities sensitive to the crossover or quantum critical region such as magnetoresistance [Paglione 03], may give a more accurate position of the QCP as the field dependence of T_{FL} is stronger. Nevertheless, a precise determination of the position of the QCP from the Fermi-liquid domain was missing and is one of the subjects of this thesis.

Suborders and possible origin of the QCP

Several hypothesis have been made for the origin of the QCP:

- Superconductivity; this would explain the apparent coincidence.
- The FFLO phase.
- Anti-ferromagnetic fluctuations that would coexist with superconductivity as in $CeRhIn_5$.
- A valence phase transition [Watanabe 09, Miyake 07] (not discussed here).

The superconducting transition is first order at low temperature and high field [Bianchi 02], which excludes the possibility of a true superconducting quantum critical point and should further reduce the critical region. Furthermore, the superconducting coherence length in $CeCoIn_5$ is large (> 50Å). This implies that superconducting fluctuations in the paramagnetic phase are expensive in terms of energy and therefore unlikely to be present in a wide region of the phase diagram as necessary to account for the extended non Fermi-liquid region.

The FFLO and magnetic order origin for the QCP are linked together. Indeed, even if no magnetism can be directly observed in the pure compound, it is believed that its ground state is close to anti-ferromagnetism and that this order would develop if there was no superconductivity. There are even several pieces of evidence which point out that superconductivity and anti-ferromagnetism coexist in a small part of the phase diagram: ambient pressure for magnetic fields applied in the [100] direction, close to the upper critical field. But it is also in this part of the phase diagram that the FFLO phase is predicted to exist.

Therefore experiments with two types of interpretations have been reported:

- In the first type, an anti-ferromagnetic phase has been observed. This observation was made by NMR and Neutron scattering experiments, under high magnetic fields in the basal plane, but only inside the superconducting mixed state. Neutron diffraction measurements have revealed a competition of two ground states, in this region, one being magnetic and the other superconducting [Kenzelmann 08]. Similarly, NMR data can be explained by an incommensurate anti-ferromagnetic order [Young 07, Sakai 10, Koutroulakis 10]. Anti-ferromagnetic ordering favored by the superconducting paramagnetic limitation was proposed for this region[Ikeda 10] and strong anti-ferromagnetic spin fluctuations are observed in the normal state close to the superconducting domain for magnetic field applied in both [100] and [001] direction [Kohori 01, Kawasaki 03, Sakai 10]. These experiments do not show evidence for an FFLO phase, even if they are generally compatible with such a phase.

- The upper critical field in $CeCoIn_5$ is known to be strongly controlled by the paramagnetic (also called Pauli) limit. The value of the upper critical field ($H_{c2}(0)$) given by the orbital limit can be estimated as 39T (and 17T) from the initial slope $H_{orbital} = 0.7T_c dH_{c2}/dT(T_c)$, as the observed limitation is 11.8T (and 5T) for the [100] (respectively [001]) field orientation. Hence, the Maki parameter can be estimated to be $\alpha = \sqrt{2}H_{orbital}/H_{Pauli} \cong 4.7$ [Matsuda 07]. Together with a large value of mean free path, this makes $CeCoIn_5$ one of the most suitable candidates for the observation of the predicted Fulde-Ferrel-Larkin-Ovchinnikov state (FFLO). In fact several experiments already suggest the observation of such a state with a phase transition detected from torque, specific heat and NMR measurements [Radovan 03, Bianchi 03b, Mitrović 06].

Doping experiments also support the proximity of $CeCoIn_5$ to an anti-ferromagnetic order. Doping the In site with Cd or Hg reveals AFM order and suppresses the high field, low temperature domain (putative FFLO phase). Coexistence of superconductivity and anti-ferromagentism is clearly observed with 7.5% Cd doping at ambient pressure and zero field [Pham 06, Tokiwa 08]. Doping the Co site with Rh tuned the system from a superconducting ground state to a coexistence of superconductivity and commensurate AFM and then finally through a reconstruction of the Fermi-surface to an incommensurate AFM ground state [Goh 08]. In this last experiment, the question as to the type of AFM that would coexist with superconductivity: commensurate as suggested or incommensurate as suggested from NMR and observed in $CeRhIn_5$?

Superconducting phase diagram

The superconducting phase diagram (temperature, pressure, magnetic field) of $CeCoIn_5$ is quite unusual among heavy fermions superconductors. Indeed, it is usually acknowledged that in heavy fermions superconductors the coupling strength reaches its maximum at a quantum critical point (or line in a 3D phase diagram). Such a scenario is well documented; for example in the case of $CeRhIn_5$, all the parameters that can be linked to the presence of a QCP: effective mass determined from de Haas van Alphen measurements, slope of the upper critical field, A coefficient of resistivity, specific heat jump at the superconducting transition and residual resistivity point to a single pressure p_c=2.5GPa. At this critical pressure (p_c), the maximum of T_{SC} and $H_{c2}(0)$ is also observed. The observed phase transition inside the superconducting dome $p_c^\star$ is located at a lower pressure. The shift is due to the appearance of superconductivity that modifies the phase diagram expected otherwise. p_c is the pressure at which the transition AFM-PM would happen in the absence of superconductivity. Data and graphs are from [Knebel 08, Knebel 10].

In contrast, applying pressure to $CeCoIn_5$ increases the T_{SC} from $T_{SC} = 2.3K$ at $P = 0$, to $T_{SC} = 2.6K$ at $P = 1.3GPa$ and then decreases it above $P = 1.3GPa$. At the same time the slope dH_{c2}/dT and the upper critical field $H_{c2}(0)$ continuously decrease with pressure [Knebel 04, Miclea 06]. The upper critical field in this compound is Pauli limited $H^P(0) \cong \frac{\Delta}{g\mu_B}$. The ratio $\Delta/T_{SC} = 1.76$ in the BCS theory and is larger in the case of strong coupling. An increase of the coupling

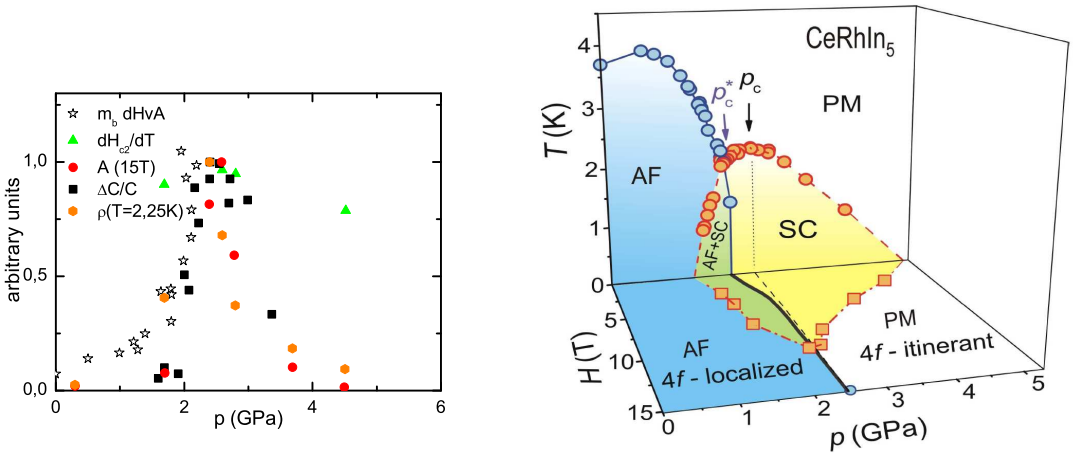

(a) (b)

Figure 3.7: Parameters and superconducting phase diagram of $CeRhIn_5$. All the measurements display an anomaly at a single pressure p_c associated with the QCP (details in the text). Data and graphs from [Knebel 08, Knebel 09].

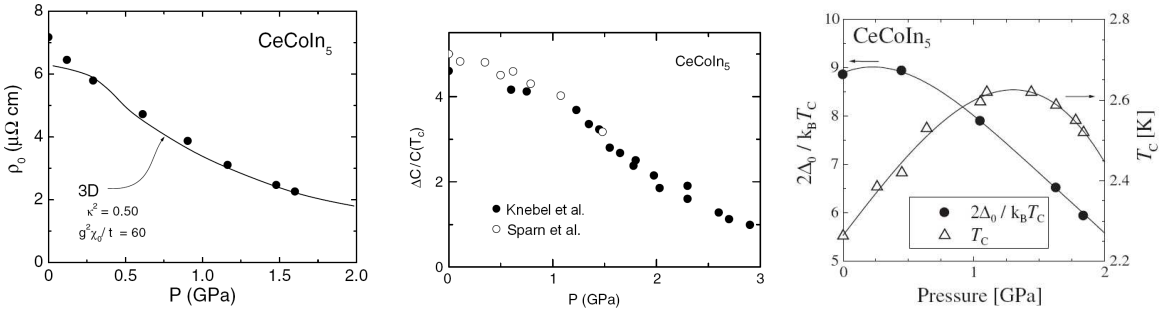

(a) (b) (c)

Figure 3.8: Evolution of different physical properties of $CeCoIn_5$ with pressure: (a) residual term of resistivity ρ_0, (b) specific heat jump $\Delta C/C$, (c) ratio Δ/k_BT_{SC} obtained from NQR. Each of this measurements indicates that the system is moving away from quantum criticality with pressure. Data from from [Nicklas 01, Knebel 04, Sparn 02, Yashima 04]

constant λ at low pressure is expected to account for the increase of T_{SC} and is in contradiction with the decrease of $H^P(0)$. Similarly the slope of the upper critical field depends on the coupling constant as: $dH_{c2}/dT \propto 1/(1+\lambda)$ also in contradiction with the evolution of T_{SC}.

Figure 3.8 displays the evolution with pressure of the residual resistivity, specific heat jump at T_{SC} and ratio of the superconducting gap to k_BT_{SC} with pressure. Each of these measurements suggests that the maximum of anti-ferromagnetic fluctuations associated with the QCP is not located at 1.3GPa, where T_{SC} is maximum but at lower field. The maximum of each of these values is obtained at pressures between negative (no maximum observed) and 0.5GPa. We can note that in the precision

of the measurements, an anomaly at 0.4GPa is certainly compatible with the three experiments.

Hence we observe two and not one characteristic pressures in the phase diagram of $CeCoIn_5$ at about 0.4GPa and 1.3GPa. In the second part of this chapter we will discuss this anomaly and present a model for the QCP and superconducting domain in this compound.

Finally, a short summary of what is known in $CeCoIn_5$ is that:

- the ground state of the system is close to anti-ferromagnetism, and anti-ferromagnetic fluctuations are present in the paramagnetic phase of the compound.
- It has a field induced QCP located close to $H_{c2}(0)$, with some debate on the actual coincidence. The first aim of the work presented here is to clarify this point, notably because the pressure dependence of $H_{c2}(0)$ is also very unusual.
- Under pressure, the maximum of T_{SC} does not correspond to a maximum in $H_{c2}(0)$, neither does it correspond to the maximum of the slope of the upper critical field dH_{c2}/dT. This is unusual for heavy fermion systems and seems at odds with the scheme of T_{SC} controlled by a QCP.

3.2 Aim and interest of this study

One of the important, open questions in Heavy Fermion systems is the interplay between superconductivity and quantum criticality. In $CeCoIn_5$ precise determination of the position of the QCP relative to superconductivity is of special interest. Indeed if the QCP is pinned at $H_{c2}(0)$, a special mechanism should be introduced which could control the unusual pressure phase diagram and in particular this coincidence. A second problem that can be partially addressed within our experiment is the type of criticality that is present in this compound. Indeed it is a matter of debate whether conventional criticality, that is triggered by a second order phase transition to an anti-ferromagnetic state, or "unconventional criticality" exists in $CeCoIn_5$.

The difficulty to address this question experimentally is the need to probe the physics in the immediate proximity of the QCP, that is at very low temperature. As described in the previous section, few probes can be used at very low temperatures (below 100mK). In this study we used resistivity as it is possible to perform measurements down to 8mK at very low noise level. Several experiments point to a QCP right at $H_{c2}(0)$ even though contradictions remain and the precision of all measurements seems insufficient to give a clear cut answer on the boundary of the Fermi-liquid regime. In the first part of this study, we endeavoured to improve on the resistivity measurements utilizing:

- low temperature transformers (gain 1000) and extended temperature measurement (down to 8mK), in order to reduce the noise and work at low enough currents to prevent heating down to the lowest temperature measured.

- c-axis transport, which has been pointed out as the most sensitive to Fermi-liquid regime breakdown [Tanatar 07], and has the advantage of strongly limiting magnetoresistance effects (configuration of field parallel to the current), together with the more usual [Paglione 03, Bianchi 03b, Bauer 05] a-axis transport for detailed comparison to previous work.

- a slightly La doped sample (about 1% doping), also measured along the c-axis, to further damp magnetoresistance effects, strongly limited by impurity scattering. It was shown that La doping has little effect on the superconducting properties of $CeCoIn_5$, it moderately decreases T_{SC} and the anisotropy of the upper critical field H_{c2} is constant [Petrovic 02].

- two different field orientations (parallel to c-axis or at 45 ° from c-axis), to check the coincidence of the QCP and $H_{c2}(0)$ on the same samples, during the same experiment.

3.3 Resistivity measurement on $CeCoIn_5$

Samples

Samples were grown by flux method with a large excess of In in the starting composition by Gerard Lapertot or Dai Aoki. Figure 3.9 shows resistivity and AC susceptibility measurements for various samples grown with different starting compositions. We checked them for good homogeneity: sharp transitions and coincidence of resistivity and AC susceptibility transitions. The samples B and C used in this experiment were grown with the same parameters as samples LAP385A-B in figure 3.9. Sample A is the one used for thermal conductivity measurements by G. Seyfarth [Seyfarth 08].

Experimental details

We have measured the resistivity with a standard 4 wire technique down to 8 mK and in magnetic fields up to 8.5 Tesla on three different samples. The setup is described in more detail in section 2.1. In all measurements we used a low temperature transformer with gain of 1000 and a low noise preamplifier (built in the CNRS-Néel Institute) to amplify the signal. The current at the lowest temperatures was carefully adjusted to avoid heating of the samples. Samples A and B have pure $CeCoIn_5$ composition, sample C is 1% doped with Lanthanum on the Cerium site ($Ce_{0.99}La_{0.01}CoIn_5$). The samples were cut in bar shapes of size $\sim 0.2 \times 0.2 \times 0.5$ mm^3 for samples B and C and $\sim 1.2 \times 0.2 \times 0.2$ mm^3 for sample A. Resistivity was measured with current applied in the basal plane (a-axis) for sample A and along the c-axis for the samples B and C. Contact resistances smaller than $1m\Omega$ are necessary at the voltage leads to take full advantage of the low temperature transformer. To achieve such small contact resistances, gold stripes (with Ti underlayer) were deposited under vacuum, after ion gun etching of the surface. $38\mu m$ gold wires are fixed by spot welding to these stripes. The three samples were glued with a small

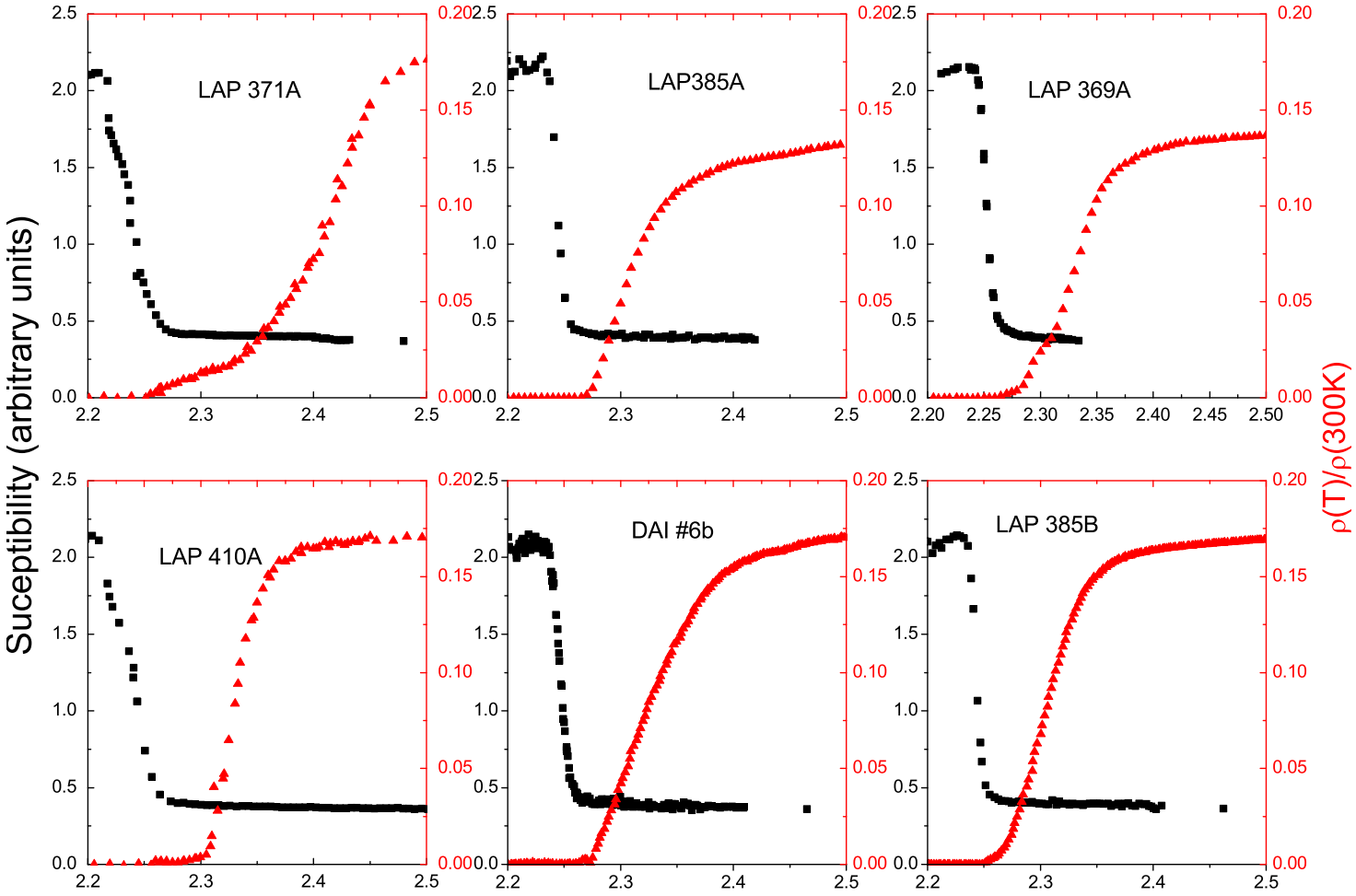

Figure 3.9: Resistivity and AC susceptibility curves for samples of $CeCoIn_5$ from various batch. We used samples grown in the conditions of batch LAP385.

amount of G.E. varnish (enough to prevent grounds) directly on a silver plateau which is screwed on an Attocube® piezo-rotator. This allows in-situ change of field orientation. The angle is determined by a Hall probe.

Figure 3.10a shows a typical measurement of $\rho(T)$ for $H = 7$ T applied along the [001] direction for the three samples. In sample A we see a clear upturn at low temperature. This upturn increases with magnetic field which is an indication that the behaviour of the quasi-particles is dominated by magneto-resistance effects when entering the quantum regime $\omega_c\tau >> 1$. Therefore, as in previous works, we have to discard the lowest temperatures data and we can fit the resistivity with a Fermi-liquid law ($\rho = \rho_0 + AT^2$) only above about ∼80mK in this sample. This is not the case for samples B and C for which magnetic field and current are parallel (H‖c‖I). In sample C, La impurities further decreases the mean free path τ and

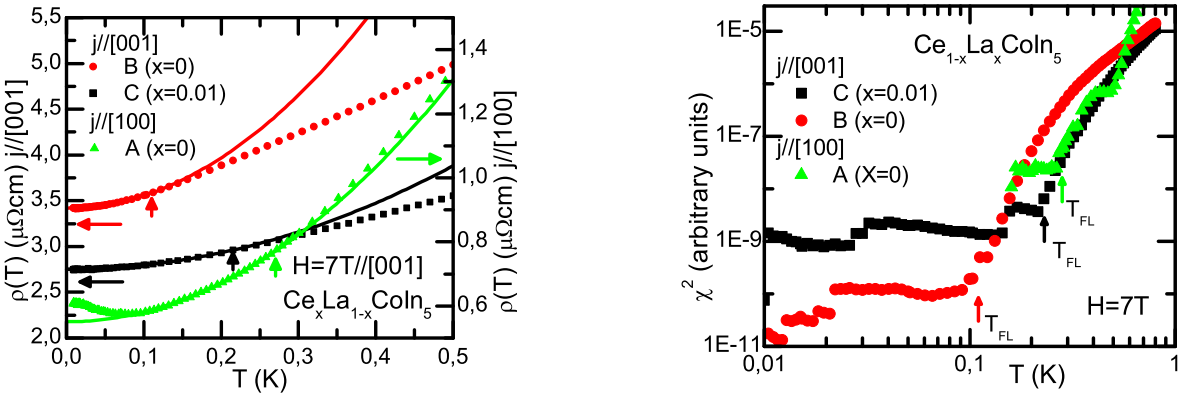

(a) (b)

Figure 3.10: (a) Typical resistivity curves for the three samples. When magnetic field and current are applied perpendicular to each other, magneto-resistance effects are very strong at low temperature ($\omega_c\tau >> 1$, sample A). In sample B these effects are strongly reduced because the magnetic field and current are parallel. The same is true for sample C in which $\omega_c\tau$ has been further decreased through a light (1%) La doping. (b) To determine the region in which the data can be fitted with a Fermi-liquid law $\rho(T) = AT^2+\rho_0$, we determine the mean "chi-square" term χ^2, normalized by the number of points. For $T < T_{FL}$ the value is constant and corresponds to the noise of the measurement; at higher temperature, the mean square term increases exponentially due to systematic deviations. Data are shown for the three samples at $H = 7$ T $H \parallel [001]$. The small steps, at very low temperature, correspond to change of gain or sensibility in the lock-in amplifier used for the measurement, not perfectly calibrated. The fits and T_{FL} as deduced from the χ^2 criterium are displayed on (a).

therefore the magneto-resistance effects. The residual resistivity (figure 3.11) shows a weak field dependence with two different slopes: positive on sample B and negative on sample C. At H=0, we can extrapolate the residual ratio of the three samples $RRR = \rho(300K)/\rho(T \to 0)$: RRR(Sample A) $\simeq$ 335, RRR(Sample B) $\simeq$ 24 and RRR(Sample C) $\simeq$ 20. Variation between samples B and C reflect the presence of La impurities. The high RRR value of sample A demonstrates the high quality of our samples (ρ_0 almost 10 times smaller than in the samples of refs.: [Bianchi 03b, Paglione 03] and 20 times smaller than in the sample of ref: [Nicklas 01]). The factor $\sim$ 15 between RRR of sample A and the one of sample B or C is due to the difference in current directions.

Figure 3.10b, shows how we determine the upper boundary of the Fermi-liquid regime T_{FL}. The curves are the "chi-square" values $\chi^2(T)$ between the data point and a fit of these points ($\rho(T) = AT^2 + \rho_0$), from the lowest temperature up to temperature T. The $\chi^2(T)$ function is normalized by the number of points in the fitted interval. For Sample A the lowest value taken into account is 80mK due to low temperature magneto-resistance effects mentioned previously, whereas we could go down to 8mK for the other two samples. At low temperature, χ^2 is roughly

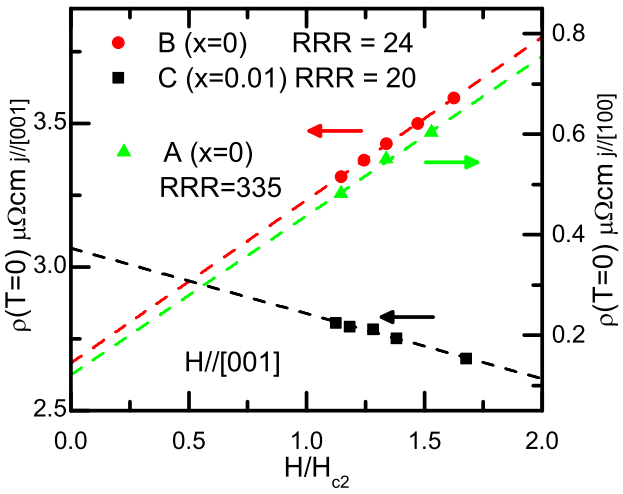

Figure 3.11: Value of the residual resistivity ρ_0, for the three samples obtained from a fit on the data ($\rho(T) = \rho_0 + AT^2$). In the range of our measurements, the residual value of sample A ($\vec{j} \perp$ H geometry) varies more than 50%, compared with variation of less than 20% for the two other samples B and C (($\vec{j} \parallel$ H geometry)). The different slopes between sample B and C indicate that two different effects dominate the field dependence: either magneto-resistance (B) or Kondo effect (C). RRR is taken from values extrapolated at H=0.

constant and its value reflects white noise on the data points. Above T_{FL}, χ^2 increases logarithmically due to systematic deviations.

Results

Sample A compared with previous experiments

Figure 3.12 shows fits for the various samples and magnetic fields. The previous studies [Bianchi 03b, Paglione 03] were done with the geometry of sample A (magnetic field [001] applied perpendicular to the current [100]). Our measurements of sample A agree with the previous reports (figure 3.13), but the deduced value of T_{FL} has a large error owing to the restricted temperature range imposed by the low temperature magneto-resistance effects (between 80 mK and T_{FL}). Moreover, T_{FL} is strongly dependent on the lowest temperature used for the fit. We note that to obtain the T_{FL} shown in figure 3.13, Paglione et al. used different temperature ranges for low fields ($T < 0.1K$ at 6.5T) and high fields ($T > 0.2K$ at 10T). In our measurements, we believe that the resulting T_{FL} temperature obtained in this configuration is slightly overestimated.

Position of the QCP

Figures 3.14b and 3.15b shows the field dependence of the A coefficient of resistivity ($\rho(T) = \rho_0 + AT^2$) for samples B and C. The strong increase of the A coefficient

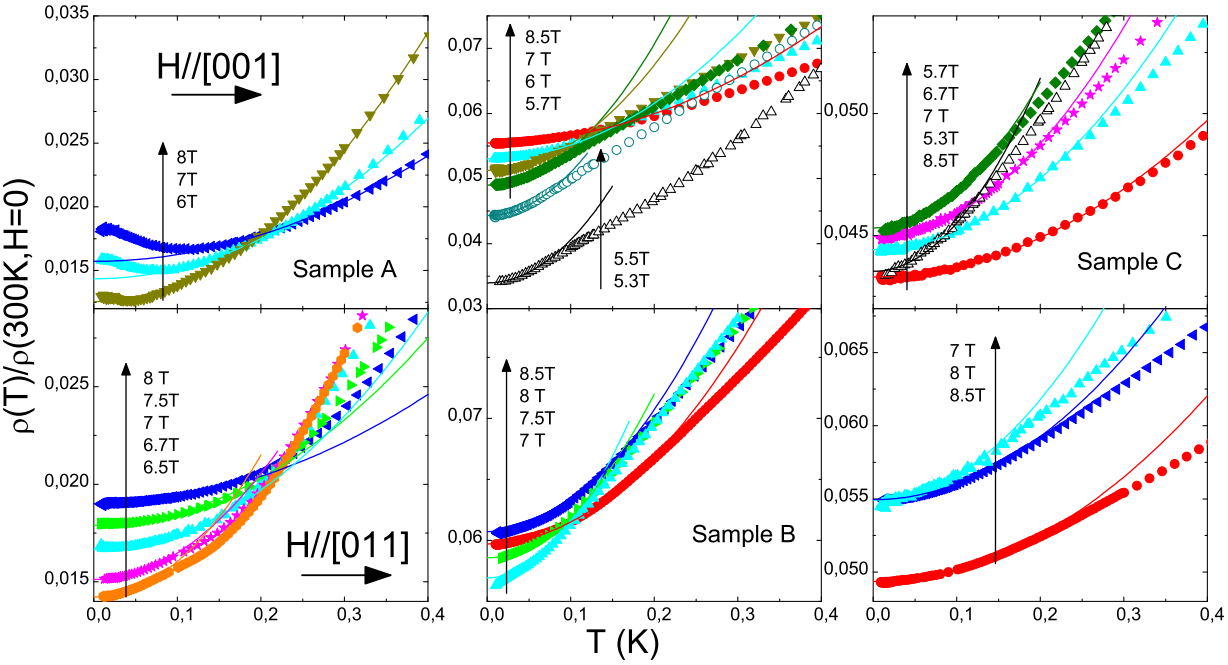

Figure 3.12: Various measurements of $\rho(T)$ at a constant magnetic field (raw data). Each column is dedicated to one sample, each row, to a given field orientation (upper row, $H \parallel [001]$, lower $H \parallel [011]$). The same colours and symbols are used for each field value on all graphs. Current direction: $\vec{j} \parallel [100]$ for sample A, $\vec{j} \parallel [001]$ for sample B and C.

reported on figures 3.14b and 3.15b is commonly found on approaching a QCP, and we used it's divergence to define a critical field H_{QCP} by fitting A as proportional to $(H - H_{QCP})^{-\alpha}$. This reflects the strong increase of the quasi-particles effective mass on approaching a QCP [Gegenwart 08] as from the Kadowaki-Woods relation, the A coefficient is proportional to the square of the effective mass ($A \propto \gamma^2 \propto m^{\star 2}$). We should note that this relation is probably not valid in the direct vicinity of the QCP (for example not valid in the spin density waves scenario A diverges and γ is finite [Moriya 95]).

The power of the divergence α can be obtained by fitting the 5 sets of A values simultaneously: we measured 3 samples in 2 field orientations, but we discarded the data of sample A - H||[001] for the above mentioned reasons. More precisely, we have allowed for a regular contribution $(A0)$ to the A coefficient: $A_i^\theta = (A0)_i^\theta + (A1)_i^\theta((H - H_{QCP})/H_{QCP})^{-\alpha}$, $i = [A, B, C]$, $\theta = [0\,°, 45\,°]$ with the same exponent α for all fits and H_{QCP} depending only on sample composition and field orientation (same H_{QCP} for samples A and B). $(A0)_i^\theta$ have the constraint to be positive as they are the values of A far from criticality and they are found to be very small (could even be forced to 0) except for sample C. The fitted exponent is very close to one ($\alpha = 1.08 \pm 0.6$).

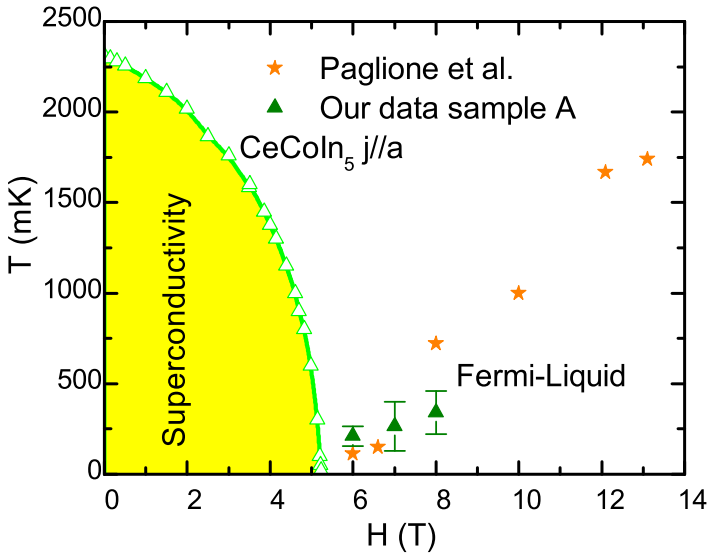

Figure 3.13: Sample A with magnetic field and current perpendicular, the Fermi-liquid domain is identical to the one obtained by Paglione et al. [Paglione 03], but due to large magnetoresistance effect at low temperature T_{FL} is over estimated and has less precision.

We can use the divergence of A to extrapolate the location of the QCP on the magnetic field axis. Such a divergence is expected for example in the spin fluctuation scenario [Moriya 95]. In case A only reaches a maximum at the QCP, the divergence of the fit gives the lower bound ($H_{QCP} \geq H_{\text{divergence of } A}$) of the magnetic field value for the position of the QCP. Figure 3.16 shows the confidence region boundary (one standard deviation) between the exponent α and each H_{QCP} for the three different geometries. In the three cases, the divergence of A locates the QCP at fields below $H_{c2}(0)$. Also, at $H_{c2}(0)$ we can still fit resistivity with a T^2 law up to about 50mK in the pure sample (B), and up to about 100mK for the doped one (C): figures 3.14a and 3.15a. These two observations clearly indicate that resistivity does not point to a field induced QCP precisely at $H_{c2}(0)$, as previously stated for this compound [Bianchi 03b, Paglione 03]. Instead, they confirm the phase diagram for Fermi-liquid domain suggested from Hall effect measurements[Singh 07]. This is also confirmed with the data analysis of sample C (figure 3.15a) which has more disorder and is therefore less prone to magnetoresistance effects at low temperature/high fields: if a QCP should exist at ambient pressure in this compound, it is hidden by the superconducting phase.

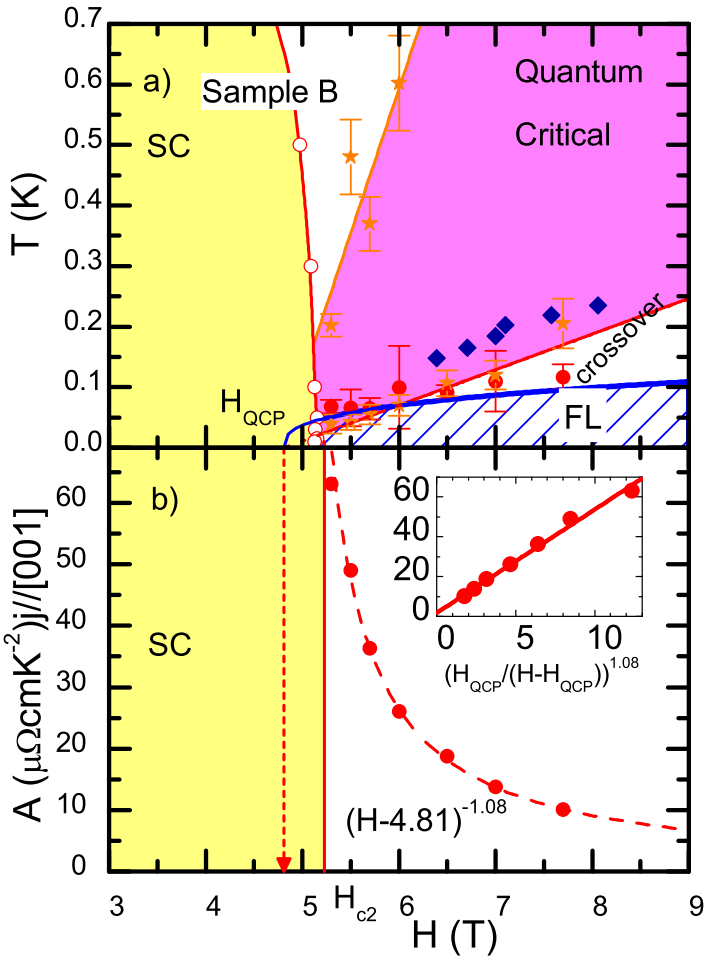

Figure 3.14: (a): Phase diagrams for sample B of $CeCoIn_5$, $H \parallel [001] \parallel \vec{i}$. Yellow: superconducting phase, dashed blue: Fermi-liquid domain from "chi-square" analysis. Red vertical doted lines, position of the QCP, deduced from the divergence of the A coefficient of resistivity. The quantum critical region, where resistivity is linear in temperature, (same "chi-square" analysis) points to the same field. To vanish at the same value, the T_{FL} line must follow $T_{FL} \propto (H - H_{QCP})^{z/2}$ with $z < 2$. Blue diamonds are the values obtained from the anomaly in Hall effect measurements [Singh 07]. (b) Divergence of the A coefficient, fitted with a law $A \propto \frac{1}{(H-H_{QCP})^{-\alpha}}$, $\alpha = 1.08$: it points to a value $H_{QCP} < H_{c2}$. Inset shows the validity of the law.

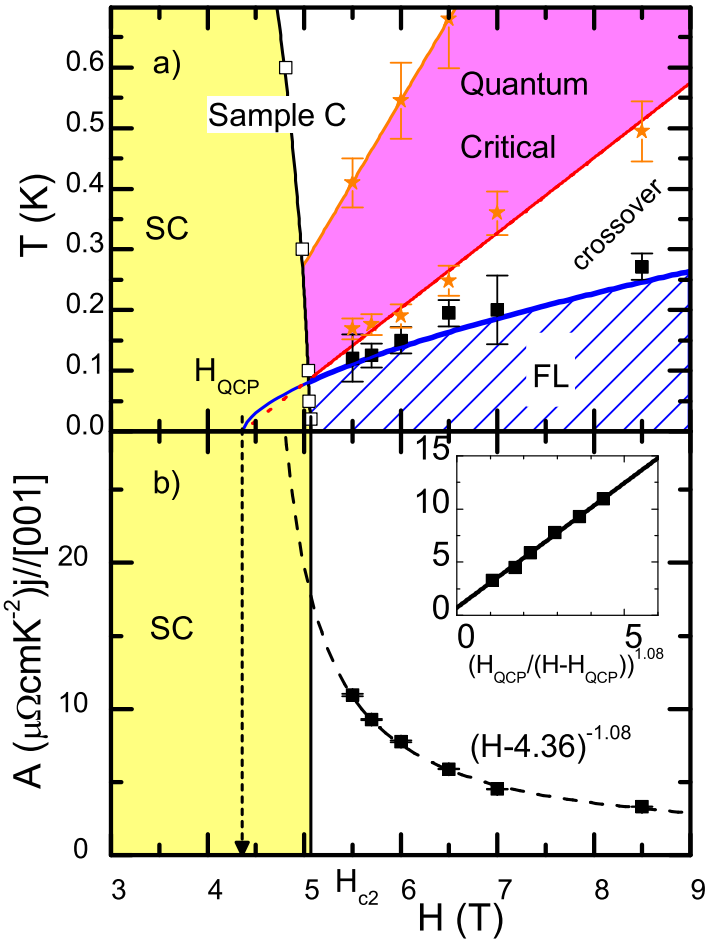

Figure 3.15: (a) Phase diagrams for sample C of $Ce_{0.99}La_{0.01}CoIn_5$, $H \parallel [001] \parallel \vec{i}$. Yellow: superconducting phase, dashed blue: Fermi-liquid domain from "chi-square" analysis. Black vertical doted lines, positions of the QCP, deduced from the divergence of the A coefficient of resistivity. The quantum critical region, where resistivity is linear in temperature, (same "chi-square" analysis) point to the same field. To vanish at the same value, the T_{FL} line must follow $T_{FL} \propto (H - H_{QCP})^{z/2}$ with $z < 2$. (b) Divergence of the A coefficient, fitted with a law $A \propto \frac{1}{(H-H_{QCP})^{-\alpha}}$, $\alpha = 1.08$: it points to a value $H_{QCP} < H_{c2}$. Inset shows the validity of the law.

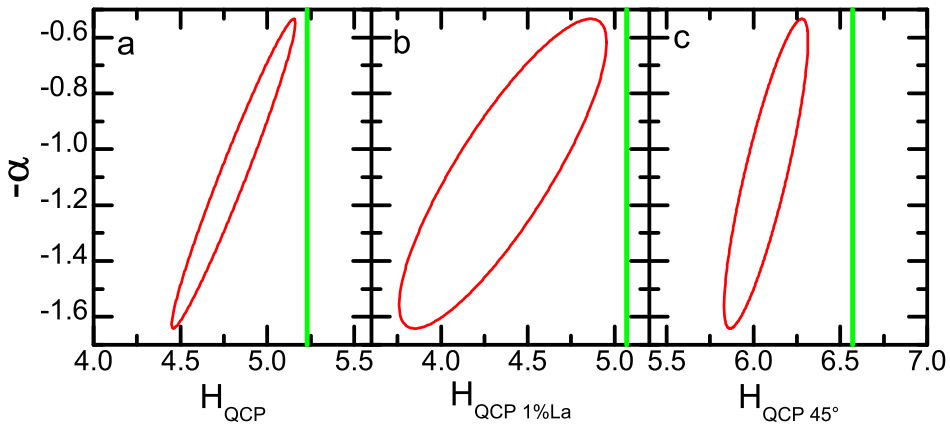

Figure 3.16: Confidence region boundary (one standard deviation) from the fit of the divergence on the A coefficient of resistivity, of the two parameters α and H_{QCP}: a) for sample B with H‖c-axis, b) for sample C with H‖c-axis and c) for samples A and B with field applied at 45,° to the c-axis. In the three cases, the divergence of A locate H_{QCP} below $H_{c2}(0)$ (green vertical line).

Field dependence of T_{FL}

We can also compare the value of the field for which we extrapolate a divergence of the A coefficient with the value of the field for which we extrapolate that the upper bound of the Fermi-liquid regime (T_{FL}) goes to zero. In the Hertz-Millis scenario [Millis 93], the Fermi-liquid border is linear in the parameter controlling the approach of an anti-ferromagnetic QCP. If we identify this parameter with the magnetic field, we expect: $T_{FL} \propto (H - H_{QCP})^{z/2}$, with $z = 2$ the dynamical exponent. A simple examination of figures 3.14a, 3.15a and 3.18a shows that linear extrapolation of T_{FL} always yield a value for H_{QCP} much lower than that extrapolated from the divergence of A. It further confirms that if there is a QCP in $CeCoIn_5$, it has to be located below $H_{c2}(0)$. However, the discrepancy of H_{QCP} as deduced from the divergence of A or the linear extrapolation $T_{FL}(H) = 0$ is problematic.

Another point of view would be to fix the value of H_{QCP} from the divergence of A, and then consider z as an adjustable free parameter: for example, for $H_{QCP} = 4.81$ Tesla (sample B), obtained with $\alpha = 1.08$, we then obtain $z = 0.7 \pm 0.14$. Similarly, we get $z = 1.24 \pm 0.12$ for the doped sample C, however, in the latter case extrapolation of H_{QCP} from the field divergence of A is very hazardous as the increase of A down to $H_{c2}(0)$ remains very modest. When magnetic field is applied at 45 ° from the c-axis, we get $z = 1.22 \pm 0.08$ for samples A and B. Note that even if we let the value of H_{QCP} vary in the full confidence interval obtained from the divergence of the A coefficient we cannot obtain $z = 2$ for the dynamical exponent. We found $z \in [0.4; 0.9], [0.9, 1.6], [0.5; 1.4]$ respectively for the three cases discussed

previously. If the value of the dynamical exponent is set to be constant for all the configurations, we obtain: $z = 1.16 \pm 0.14$. Conversely, a value of $z = 1$ is expected in a scenario where the f-electrons do not form bands [Reyes 09]. However, a main difficulty might be that the standard scenarios, which do not consider polarisation of the bands under field, are simply not applicable to a field induced QCP. Experimentally, the mechanism driving the destruction of the AFM order under field, without any kind of metamagnetic transition is also unclear. For $CeCoIn_5$, one might argue that the jump of magnetization observed at $H_{c2}(0)$ [Tayama 02] is not only a diamagnetic jump but has also a paramagnetic origin [Kos 03], which could reflect such a metamagnetic transition. In any case, quantitative theoretical prediction is missing for such a field induced QCP. Let us note however that the factor two we find between the power law for the divergence of the A coefficient and the field dependence of T_{FL}, is what is simply expected from a dimensional point of view, if the approach of the QCP is governed by the collapse of a single energy scale "T_0". If $\rho \propto (T/T_0)^2 \Longrightarrow A \propto (1/T_0)^2$, and $T_{FL} \approx T_0$, then independently of the identification of T_0 with a Kondo temperature, spin fluctuation temperature..., we obtain $\frac{\alpha}{2} = \frac{z}{\nu}$.

Quantum critical region

Another way to defined the Fermi-liquid regime is to observe the growth of the non Fermi-liquid behaviour: a T-linear regime is often observed above the T^2 regime and has been reported in the first studies of $CeCoIn_5$. With the same technique than for the Fermi-liquid region, we determine the T-linear domain (purple region in figure 3.14a and 3.15a). The resistive data in this temperature range are shown on figure 3.17 for sample B and C. The lower bound of the T-linear domain matches that of the observed dip in differential Hall coefficient associated with a departure from the Fermi-liquid regime[Singh 07]. The onset temperature of this T-linear regime of the resistivity is extrapolated to vanish at the same magnetic field value (H_{QCP}) than the divergence of the A coefficient (see Figures 3.14a,3.15a. and 3.18a). This is consistent with a linear behaviour of the resistivity down to $T = 0$ if it could be measured at H_{QCP}. Surprisingly, we do not observe a linear dependence of resistivity up to the higher temperatures in low fields as usually excpected. However, the upper limit of the Quantum critical region cannot be precisely defined in our experiment as the increase of mean square term χ^2 is much weaker for this limit than for the others. The temperature range in which resistivity is found to be linear is also quite small (typically less than half of a decade) compare to the one used to determined the Fermi-iquid region (more than a decade except for sample B at the lowest fields).

Field applied along [011] direction

Figure 3.18 shows the same analysis when the magnetic field is applied in the direction [011]. In this case, the magneto-resistance effects are weak enough whatever the direction of the applied current and therefore we can compare the two pure samples A ($j \parallel [100]$) and B ($j \parallel [001]$). As in the previous case, both the divergence of the A coefficient of resistivity and the collapse of the Fermi-liquid domain happen

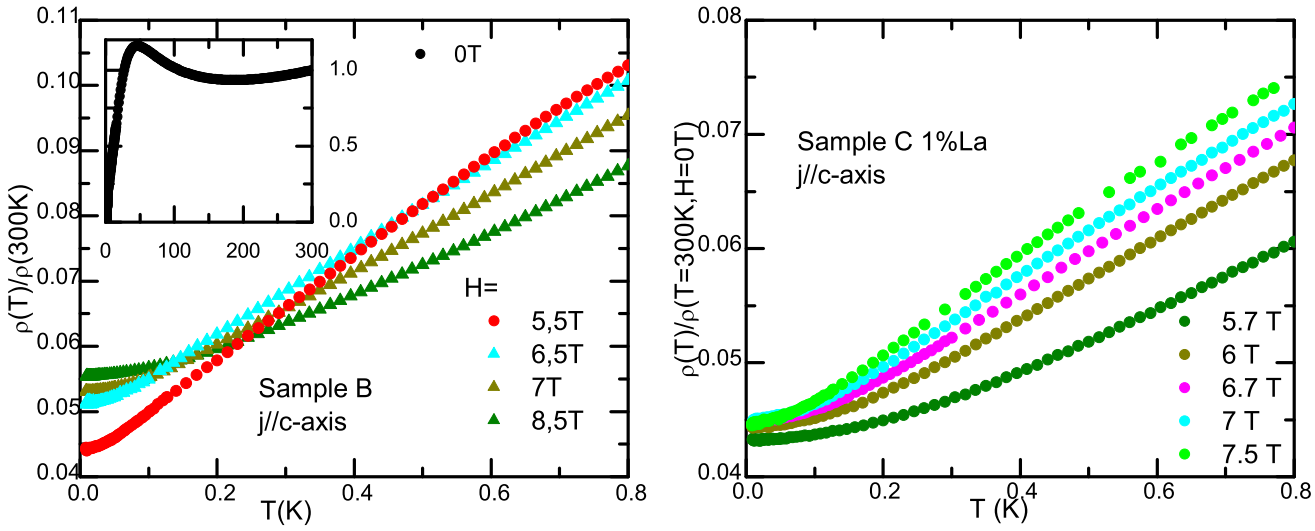

(a) (b)

Figure 3.17: Resistivity curves up to 800mK linear temperature dependence of resistivity is clearly observable at high temperatures, high fields. At low field the temperature dependence of the resistivity curves is sublinear. (a) Resitivity data for sample B at various fields $\vec{j} \parallel$ H $\parallel$ [001]. Inset show a curve from 300K taken on a similar sample without magnetic field. (b) Resitivity data for sample C (1%La) at various fields $\vec{j} \parallel$ H $\parallel$ [001].

inside the superconducting phase. It is interesting to point out, that even if the absolute values of resistivity are very different, the two Fermi-liquid borders T_{FL} and divergences of A coefficient coincide for both samples. This is a good indication of the validity of our analysis. However, the T-linear domains have different borders depending on the current direction. This underlines an intrinsic difficulty of discussing Ferm-liquid borders from transport measurements. Indeed, the Fermi-liquid domain is inherently an isotropic property of the system which should not depend on the current direction. But if the breakdown of the Fermi-liquid regime is associated with singularities located on some peculiar regions of the reciprocal space (it has been suggested that for $CeCoIn_5$ quasi-particles disappear along the c-axis [Tanatar 07]), it will differently affect transport depending on the current direction, which can easily lead to different determinations of "non Fermi-liquid" behaviour. In the present case, these measurement for $H \parallel [011]$ confirm that the c-axis is much closer to "criticality" than the a-axis when using a criterion of T-linear behaviour.

Order of the transition

Finally from our measurements of the upper critical field by means of resistivity we can easily find the change from a second order to first order transition. Figure 3.19 shows the raw resistive data. When the transition is second order, one clearly sees a large "foot" of the transition before the regime $\rho = 0$ is reached. This may arise from flux flow effects, which are suppressed when the transition becomes first order.

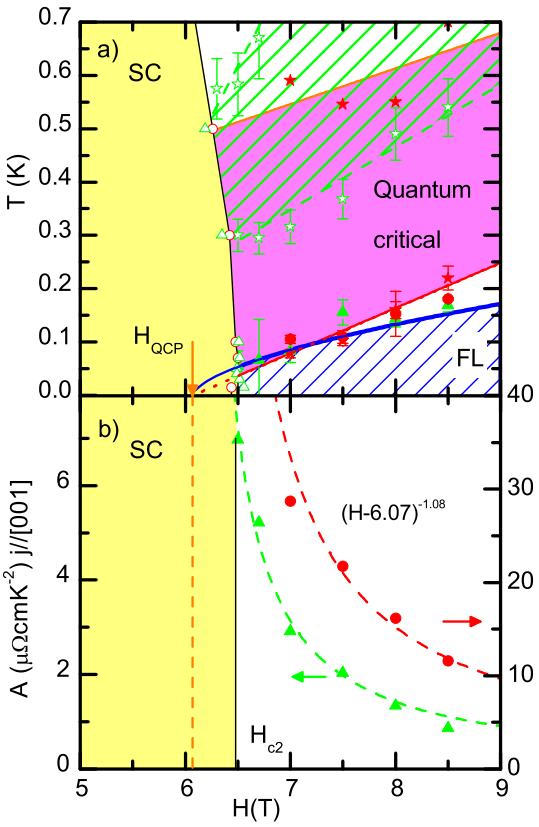

Figure 3.18: When the magnetic field is applied along $H \parallel [011]$ direction, the magneto-resistance effects are weak for all the samples. Sample A (j//a-axis) full green triangles: Fermi-liquid and A term, open green triangles: H_{c2} and open green stars: T-linear (quantum critical) regime. Idem for sample B (j//c-axis) with red circles and full red stars. :(a) Fermi-Liquid domain: as expected, it is the same for samples A, and B. The two T-linear regions (stars) have different borders, this can be understood as the T-linear region depends on the nature of the QCP fluctuations (see text). (b) Divergence of the A coefficient ($A \propto \frac{1}{(H-H_{QCP})^{-\alpha}}$, $\alpha = 1.08$) for both samples, pointing to the same H_{QCP} despite their different amplitudes.

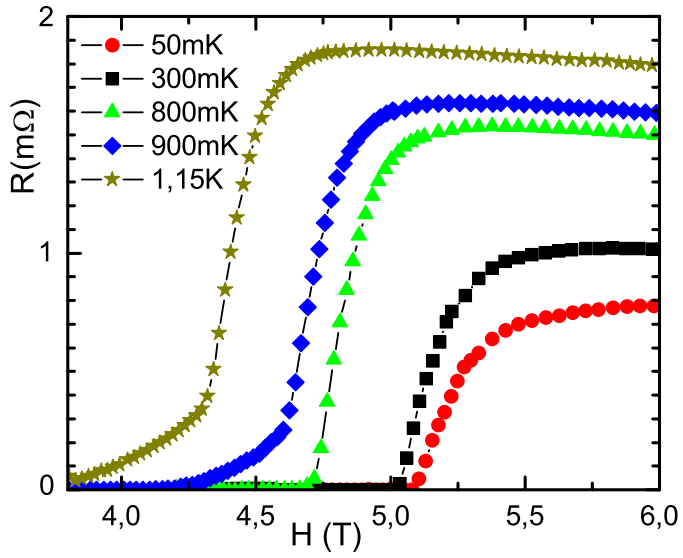

Figure 3.19: The upper critical field (H_{c2}) is a second order phase transition at high temperature and becomes first order below about 800mK. An effect of this order change can be seen on flux flow as measured from resistivity. Flux flow effects are clearly visible when the transition is second order and are suppressed when the transition is first order.

Discussion

Our analysis of the temperature dependence of the resistivity converges to a QCP located clearly below H_{c2}. This is in good agreement with previous measurements of specific heat, Hall effect and thermal expansion of other authors [Singh 07, Bianchi 03b, Donath 08] that point to a QCP located inside the superconducting dome.

Nevertheless, as for other heavy fermions systems, it is difficult to go beyond this qualitative analysis and deduce more quantitative information on the nature of the QCP from the precise laws and exponents of the divergence of A or field variation of T_{FL}. Spin fluctuation models do not predict a divergence of the specific heat for anti-ferromagnetic fluctuations (at $T \to 0$), whereas they predict a divergence of the A coefficient of resistivity. Experimentally, a diverging behaviour of both quantities is observed in the measured temperature range. However, specific heat measurements stop below 80mK, so they remain compatible with any scenario. Scaling even matches predictions of spin fluctuation models, as saturation of specific heat is only expected at very low temperature close to a QCP. A problem with the spin fluctuation model is that it does not predict the T-linear regime observed in resistivity. This has triggered the theoretical development of so called "unconventional models" of criticality where a breakdown of the Kondo effect could generate

a divergence of the specific heat and predict the T-linear dependence of resistivity at the expense of a change of the Fermi surface. Presently, such a Fermi surface change has not been observed in $CeCoIn_5$ despite the rare possibility to perform de-Haas-van-Alphen experiments below H_{c2}. In any case, there are still very few quantitative predictions of these new models that we could test with the present experiment.

Curiously, our data match several predictions of the phase diagram proposed by A. Rosch [Rosch 00], for an anti-ferromagnetic induced QCP with magnetic impurities (and for small effect of the magnetic field). For example, the work of Ref. [Rosch 00] predicts two different behaviors : $T_{FL} \propto (H - H_{QCP})^{1/2}$ and $T_{Linear} \propto (H - H_{QCP})$ which are very close to our experimental observations. This may seem at odds with the well known high quality single crystals available for this system, however, from the magnetism point of view, there is a clear "smoking gun" for the presence of unusual magnetic disorder in $CeCoIn_5$. For example, the unusually large specific heat jump at the superconducting transition [Rosch 00, Petrovic 01], and the jump of magnetization observed at H_{c2} even close to T_c [Ikeda 01] can be explained by the presence of magnetic disorder like remaining, fluctuating, paramagnetic centers [Kos 03] (see discussion on page 72). A complete and quite successful model for the appearance of coherence in this system (in the framework of "Kondo-Lattice physics") has also been proposed, which points to residual "uncondensed" Kondo impurity centres in $CeCoIn_5$ down to very low temperatures [Nakatsuji 04].

A possible way to have our data of $T_{FL}(H)$ satisfy the linear behaviour of the Hertz-Millis scenario, could be to claim that no QCP is present in the $(H, T, P = 0)$ phase diagram. If the QCP is located under pressure, then in the plane P=0 of phase space, the Fermi-liquid boundary (T_{FL}(H)) would be an hyperbola. This cannot be excluded by our measurement of T_{FL}, because superconductivity hides the low field regime. However, the apparent divergence of the A coefficient at a finite field seems unlikely in such a scenario.

Comparison to $YbRh_2Si_2$

Another approach would be to compare $CeCoIn_5$ with other prototypes of quantum critical points and particularly of field induced quantum critical points. From this point of view, probably the best documented case is that of $YbRh_2Si_2$: a divergence of the A coefficient and an anomalous T-linear behaviour of the resistivity at H_{QCP} together with a well identified anti-ferromagnetic ordered phase have been reported[Custers 03]. The Grüneisen ratio in the critical region has the same temperature dependence for the two compounds [Donath 08] and has been claimed as a proof of an "unconventional" scenario[Si 01] for the non Fermi-liquid behaviour and QCP in $YbRh_2Si_2$. This is also suggested by Custers et al. [Custers 03], in order to explain the exceptional broad range of a linear in temperature behaviour of the resistivity. It has also been stressed that recent experiments [Friedemann 09] using Ir or Co doping of this system, support such a local scenario because they show that the QCP related to transport anomalies is not pinned to the magnetic phase transition. In any case, even in the pure system, Knebel et al [Knebel 06b]

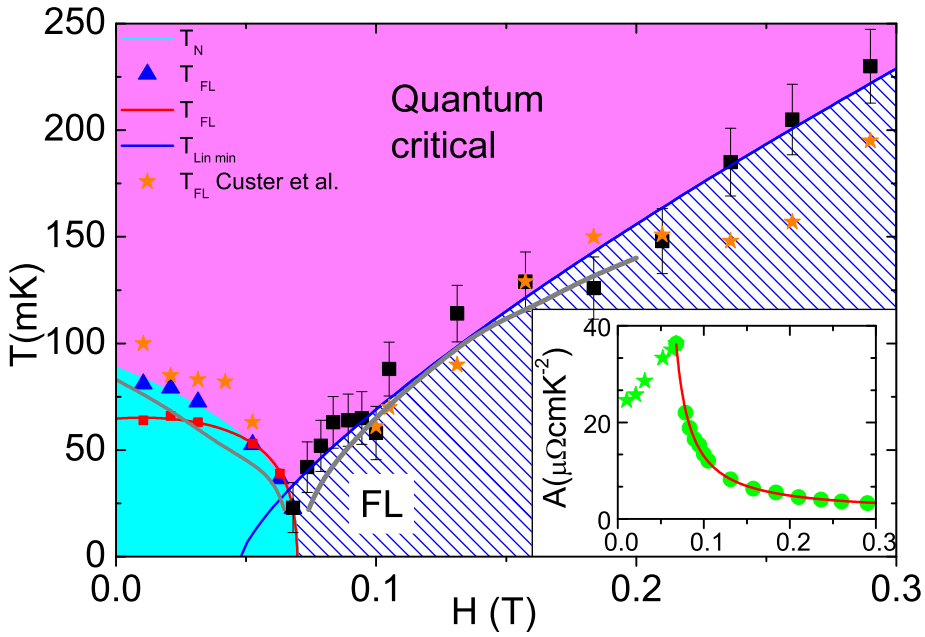

Figure 3.20: Comparison with $YbRh_2Si_2$ another field induced QCP. Black and red squares: T_{FL}, orange stars: minimum of the T-linear domain, blue triangle $T_{\text{Néel}}$. The Fermi-liquid domain has a similar shape as $Ce_{0.01}La_{0.99}CoIn_5$. The lines clearly does not vanish at $H(T_{\text{Néel}} = 0)$. Grey line, from Custers et al. ($\rho \propto T^n$ Line represent maximum of $n = 2$) [Custers 03]. Inset, divergence of the A coefficient for $YbRh_2Si_2$. The coefficient does not diverge at the upper critical magnetic field $H(T_{\text{Néel}} = 0)$ as we would expect for a magnetic QCP. We believe the reason is that the QCP is not directly induced by this transition as it was already previously suggested with the disappearance of magnetism and no change in the QCP with Ir and Co doping on the Rh site [Friedemann 09].

had already shown that no true divergence of the A coefficient was observed at the magnetic "QCP" and that the range of observation of the T^2 law remains finite in the whole temperature-field phase diagram. So, there is a strong similarity between pure $CeCoIn_5$ and pure $YbRh_2Si_2$, where in the first case the superconducting transition would mask the appearance of a field induced QCP, and in the second case the AFM order would mask the appearance of the (possibly local) QCP.

We use the same technique to re-analyze the resistive data of $YbRh_2Si_2$ measured by Knebel et al. [Knebel 06b] (Figure 3.20). It is interesting to note that comparison can be pushed a step further when looking at the "critical exponents" of $YbRh_2Si_2$ (data of Ref.[Knebel 06b]): in both cases, the divergence of the A coefficient can be well fitted by a simple law : $A \propto (H - H_{QCP})^{-\alpha}$, and the dynamical exponent for $T_{FL} \propto (H - H_{QCP})^{z/2}$. The exponents are found to vary in the interval $\alpha \in [0.4; 1.25]$ and $z \in [1.1; 1.6]$ surprisingly similar to the case of the doped $Ce_{0.99}La_{0.01}CoIn_5$ sample, and also in contradiction with the Hertz-Millis scenario.

The case of $YbRh_2Si_2$ has the advantage that one can fit a Fermi-liquid both in the AFM and paramagnetic domain. If on the paramagnetic side, a divergence of A coefficient and collapse of Fermi-liquid temperature is clearly observed, it is clearly not the case in the AFM domain. This indicates that AFM hides quantum criticality and does not induce it.

Whether these similarities originate in a similar mechanism for the QCP remains to be investigated. But a major interest of the case of $CeCoIn_5$ is that it combines the rare advantages of high purity and a field scale ($H_{QCP} \approx 5T$) large enough for Fermi surface studies. Of course, de Haas-van Alphen studies in the superconducting phase are notoriously difficult, but they are possible in this system, meaning that both sides of the putative QCP can be probed [Settai 01]. Up to now, they did not reveal any change as expected in the local scenarios of Kondo breakdown, but $CeCoIn_5$ might be a good candidate to test the most dramatic predictions of this class of QCP models, and so is worth a deeper look.

3.4 Upper Critical Field under pressure

The problem

As explained in the introduction of this chapter, the pressure dependence of H_{c2} in $CeCoIn_5$ is at odds with the conventional coincidence of the QCP and the maximum of T_{SC}. Moreover, having seen that the field-induced QCP is also not coinciding with $H_{c2}(0)$ we endeavoured to have a fresh look at this phase diagram, compiling the recent data of $H_{c2}(P,T)$, determined by thermodynamic specific heat measurements, for both in-plane and out-of-plane directions from measurements ranging from zero pressure up to more than twice p_{max}. The measurements were done by Georg Knebel [Knebel 10], and compared to older ones [Miclea 06]. We realized that $CeCoIn_5$ is probably the first example where the specific behaviour predicted for anti-ferromagnetically mediated superconductivity [Monthoux 01] can be clearly identified, strongly supporting the idea of magnetically mediated superconductivity in this compound. We propose a new phase diagram for this compound, a model of strongly coupled, 2D, anti-ferromagnetically mediated superconductor.

Let us first focus on the raw data of the upper critical field H_{c2} in $CeCoIn_5$, as presented in figures 3.21, 3.22 and 3.23. Full symbols data (except for the curve at $p = 0, H \parallel c$ and one at $p = 0, H \parallel a$) were obtained on the same sample by ac calorimetry in the same diamond-anvil cell, turned 90 degrees in the fridge for $H \parallel a$ (description in reference [Knebel 10]). Data at $p = 0, H \parallel c$ as well as a curve at $p = 0, H \parallel a$ (squares) were obtained from resistivity measurements and are displayed for comparison with specific heat data. Data on figure 3.23 are from [Miclea 06]. A remarkable feature which can be seen on the raw data of figures (3.21-3.23) is that except for the lowest pressure of 0.35GPa, the initial slope of H_{c2} at T_{SC} ($H'_{c2}(T_c)$) is continuously decreasing with increasing pressure. The initial slope of H_{c2} is controlled only by the orbital limitation and, for a superconductor in the clean limit, it is proportional to T_{SC} and to the inverse of the Fermi velocity (v_F). The clean limit is well satisfied for $CeCoIn_5$: mean free path $l > 1300$ Å,

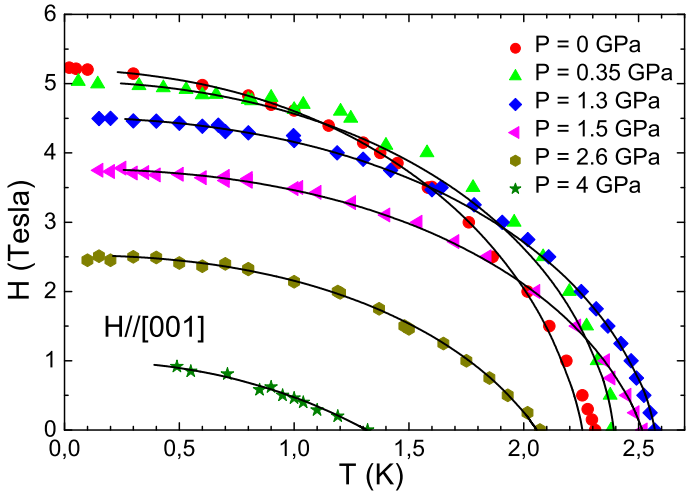

Figure 3.21: Data (points) and fits (full lines) of the upper critical field of $CeCoIn_5$, for $H \parallel [001]$. Fits (full lines) as described in the text.

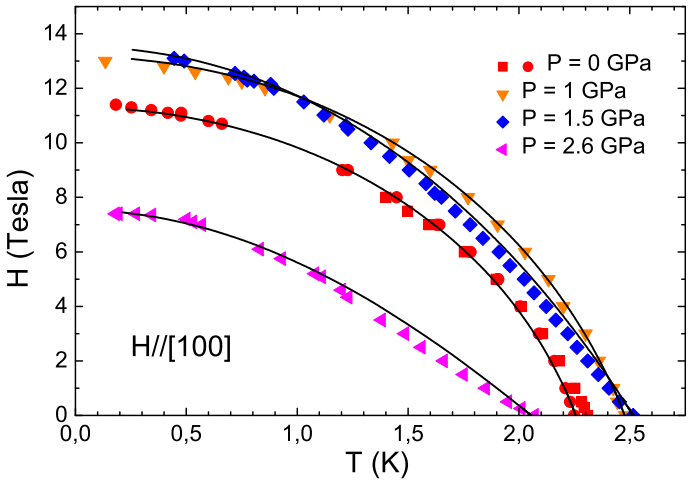

Figure 3.22: Data (points) and fits (full lines) of the upper critical field of $CeCoIn_5$ for $H \parallel [100]$, measured by specific heat and compared with resistivity at ambient pressure (red squares).

coherence length $\xi \cong 100$ Å from specific heat and thermal conductivity measurements [Movshovich 01], also in agreement with the value obtained from Nernst and Seebeck effect at H=0 [Izawa 07b]. On such a small pressure scale (a few GPa), the evolution of T_{SC} is normally governed by that of the coupling strength usually quantified by a parameter labeled λ. The interactions responsible for the pairing also contribute to the renormalization of the Fermi velocity by a factor of precisely

$1/(1+\lambda)$. So if the maximum of T_{SC} in $CeCoIn_5$ is due to a maximum of λ, one expects an increase of $H'_{c2}(T_c)$ between $p = 0$ and p_{max} and both T_{SC} and $1/v_F$ should increase. This is clearly in contradiction with the experimental results for $H \parallel c$.

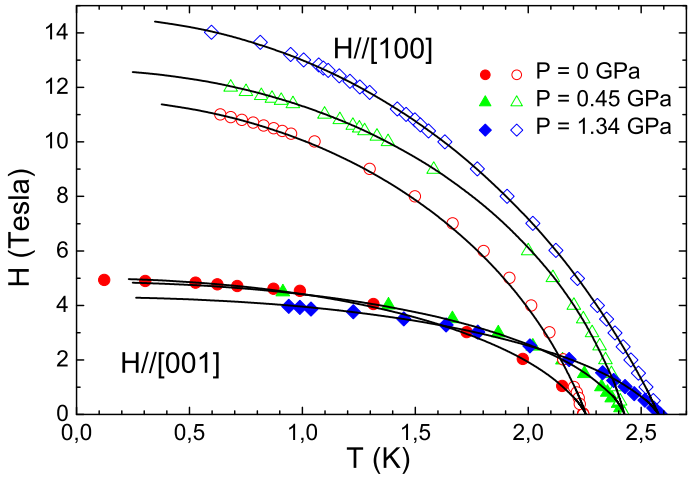

Figure 3.23: Data from [Miclea 06] of the upper critical field of $CeCoIn_5$ for $H \parallel [100]$ and $H \parallel [001]$. Fits (full lines) as described in the text.

A similar problem occurs for the opposite limit of H_{c2}, namely $H_{c2}(0)$. It is well known and, again clearly visible on the raw data, that the saturating behaviour of H_{c2} in $CeCoIn_5$ at low temperature, notably for $H \parallel c$, is due to a dominating paramagnetic limitation (H^P) also called Pauli limitation. However, because $H^P \approx \Delta/g\mu_B$, where Δ is the superconducting gap, g the gyromagnetic factor and μ_B the Bore magneton an increase of T_{SC} due to an increase of λ should enhance H^P beyond the proportionality to T_{SC} as it is also well known that strong coupling effects increase the ratio Δ/T_c. Again, this is in very strong contradiction with the experimental data of figure 3.21. Let us note that these two points were already visible on the first data of H_{c2} under pressure extending up to p_{max} (ref. [Miclea 06], reported on figure 3.23).

Such a contradiction is very unusual among heavy fermions superconductors : most of the time, the pressure variation of T_{SC}, $H'_{c2}(T_c)$, and $H_{c2}(0)$ are fully consistent with the simple expectations given above [Settai 08] and can even be quantitatively fitted with essentially only λ as a pressure dependent parameter [Glémot 99, Knebel 08]. In particular, for the parent compound $CeRhIn_5$, the situation is very well documented with a maximum of T_{SC} at $p \approx 2.4$GPa. This maximum corresponds with a maximum of the effective mass as detected by de-Haas-van-Alphen quantum oscillations or by $H'_{c2}(T_c)$, as well as by the A coefficient of the resistivity (see figure 3.7). A fit of the complete dependence of $H_{c2}(T)$ with pressure does point to a maximum of λ at the maximum of T_{SC}, coinciding with the maximum of the specific heat jump ($\Delta C/C$) at T_{SC} [Knebel 09] which is a

good measure of the strong coupling effects [Knebel 08]. Moreover, in $CeRhIn_5$, it has been shown that when superconductivity is suppressed by a magnetic field, the antiferromagnetic order is restored with a Néel temperature which also vanish at $p_c \approx 2.4GPa$ [Knebel 06a]. Therefore, in this system the coincidence of the critical pressure p_c of the magnetic quantum critical point, p_{max} of the optimum T_{SC} and of the strong coupling effects is well established.

Scenario: QCP as a glue and pair breaker

Clearly, for $CeCoIn_5$, the scenario of $CeRhIn_5$ cannot be applied directly (First compound has two critical pressures, second compound has one). However, if we put aside the pressure dependence of T_{SC}, all other results: $H'_{c2}(T_c)$, $H_{c2}(0)$, but also the coupling strength as measured by the specific heat jump $\Delta C/C$ [Knebel 04] or the gap to T_{SC} ratio obtained from nuclear quadrupole resonance [Yashima 04] are consistent with a decrease of the coupling strength with pressure. They are also consistent with the proposal that under pressure, $CeCoIn_5$ moves away from a quantum critical point. From this standpoint, a natural hypothesis would be that:

- the pairing strength (measured by λ) decreases with pressure,
- T_{SC} is controlled by λ and by an additional (limiting) mechanism, which also decreases under pressure.

The maximum T_{SC} of $CeCoIn_5$ under pressure would then arise "artificially", from the competition between the pressure dependence of both mechanisms. Such a scenario was predicted by Monthoux and Lonzarich, when moving away from a quantum critical point [Monthoux 01]. Hence a natural candidate for this limiting mechanism is magnetic fluctuations associated with quantum criticality. Evidence for coupling between superconductivity and anti-ferromagnetic (AFM) fluctuations is given by inelastic neutron scattering that detected a resonant signal below T_{SC} [Stock 08]. NQR and residual resistivity under pressure demonstrated the strong decrease of these AFM fluctuations under pressure [Yashima 04, Nicklas 01] (see figure 3.8).

Magnetic fluctuations from specific heat

There is also another piece of "evidence" for a peculiar pair breaking mechanism in $CeCoIn_5$ coming from a completely different property, namely the very large specific heat jump $\Delta C/C$ at T_{SC}. Indeed, in $CeCoIn_5$, $\Delta C/C \approx 4.5$ is beyond any expectation even for a strong coupling superconductor. Such a large value could be explained by the coupling of "fluctuating paramagnetic moments" to the superconducting order parameter [Kos 03].

The explanation developed by Kos et al. [Kos 03] is that the superconducting transition $T^\star$ given by the coupling constant would be higher than the one observed. Magnetic fluctuations would then act as pair breakers and reduce T_{SC}. Figure 3.26 gives the ratio $T_{SC}/T^\star$ depending on the amount of magnetic impurities characterized by the temperature τ_M. Such fluctuations could also explain the unusual

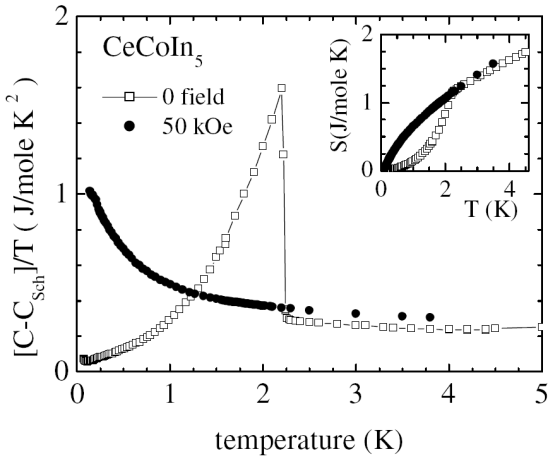

Figure 3.25: Specific heat from [Petrovic 01]. Large transition peak is observed: $\Delta C/C_n(T_{SC}) \cong 4.5$ compared with the BCS value of 1.43. But entropy is conserved ($\int_0^{T^\star} \frac{C}{T} dT = const$) between the superconducting phase H=0 and normal state H=0.5T.

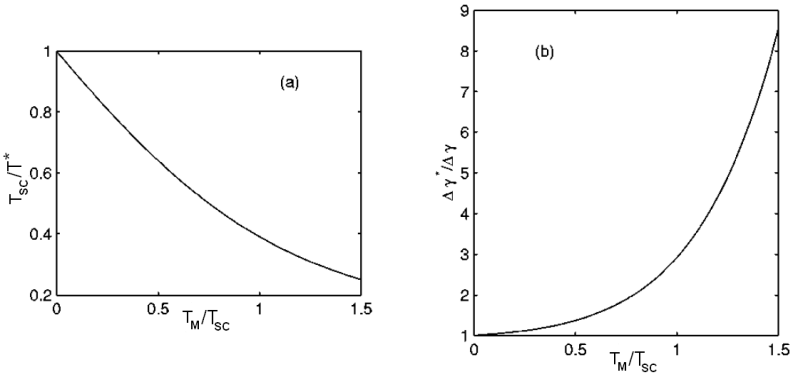

Figure 3.26: Model from [Kos 03]. a) Ratio between the superconducting transition without magnetic pair breaking and the observed one $T_{SC}/T^\star$, versus amplitude of the magnetic fluctuation $\tau_M/T^\star$. b) Idem for the height of the specific heat transition peak. In $CeCoIn_5$ $\Delta\gamma^\star\Delta\gamma \sim 3 \quad \rightarrow \tau_M/T^\star \sim 1 \quad \rightarrow T^\star \sim 6K$. (Notation adapted to the present discussion)

magnetization curves observed in the superconducting phase close to H_{c2}. The field dependence of magnetization is stronger than linear [Tayama 02, Ikeda 01]. A similar spin-fermion model in the proximity of two-dimensional critical magnetic fluctuations can also reproduce the specific heat results[Bang 04] in the proximity of a quantum critical point.

These fluctuations can also explain the magnetization data in the mixed state of $CeCoIn_5$ close to H_{c2}. It is interesting to point out that Kos et al. [Kos 03] could quantify the magnetic fluctuations (at P=0) with the superconducting transition $T^\star$ that the system would have in absence of these fluctuations $T^\star \cong 3 \cdot T_c$.

Model for the fit of H_{c2}

In order to give a quantitative model of the pressure dependence of H_{c2}, we used an Eliashberg strong coupling model for the calculation [Bulaevskii 88] and in the spirit of reference [Kos 03] added magnetic impurities to account for the T_{SC} reduction

induced by strong AFM fluctuations. T_{SC} and H_{c2} are therefore functions of the parameters:

$$T_c/\Omega(p) = \Psi(\lambda, \mu^\star, T_M), \tag{3.4.1}$$

$$H_{c2}(p,T) = \Phi(T, T_c, T^\star, \lambda, \mu^\star, v_F, g), \tag{3.4.2}$$

where Ω is a characteristic temperature of the coupling mechanism (analog to the Debye temperature in the electron-phonon case), λ is the strong coupling constant, $\mu^\star$ is the coulomb pseudo-potential (fixed to a typical value of 0.1), T_M gives the characteristic energy of the pair breaking magnetic impurities ($k_B T_M = \hbar/\tau_M$ where τ_M is the transport relaxation rate), v_F is the Fermi velocity controlling the orbital limitation and g the gyromagnetic ratio controlling the paramagnetic limitation. $\mathrm{T}^\star(\mathrm{p}) = \Omega\Psi(\lambda, \mu^\star, \mathrm{T}_M = 0)$ as in reference [Kos 03], with $\mathrm{T}^\star(\mathrm{p}=0) = 3 \cdot T_c$. The functions Ψ and Φ are calculated numerically as reported in [Glémot 99].

We endeavoured to fit the data with no other hypothesis than the fact that pressure should take away the system from a magnetic quantum critical point and so we imposed the following constraints: we assumed that at the highest pressure, the effects of τ_M should be negligible so that T_M can be turned to zero. We also imposed that the change of slope of H_{c2} for both field orientations should be entirely controlled by the pressure dependence of the strong coupling parameter, in other words that the pressure dependence of the Fermi velocities along the c and a axis follow $v_F^i = v_{F0}^i/(1+\lambda(p))$, $i = a, c$, with v_{F0}^i constant. Because the slope of H_{c2} changes strongly in this narrow pressure range this implies that $\lambda(p)$ is large (at least at low pressure) in order to provide enough dynamics with v_F to fulfil that constraint. Eventually, we adjusted T_M against T_{SC}assuming that Ω has negligible pressure dependence (it was kept constant). So only λ, T_M and g where allowed to vary with pressure and only $g = g^i$, $i = a, c$ was allowed to be different for both directions. All the parameters are constant with magnetic field.

The absence of field dependence of λ, v_{Fi} and T_M is suggested from specific heat measurements [Ikeda 01, Petrovic 01]. Indeed, the entropy is conserved between zero field and $H_{c2}(0)$, the large jump at T_{SC} is compensated in the normal state by a continuous increase of the Sommerfeld coefficient $\gamma = C/T$. This implies that the effective mass of the quasi-particles in this interval is roughly constant ($m^\star = \gamma_N(T \to 0)$). λ, v_{Fi} and T_M are linked to the effective mass and hence also roughly constant.

Resulting parameters and discussion

We could find a set of parameters yielding very satisfactory fits of H_{c2}: the fits are displayed, together with our data points, on figures 3.21, as well as on figure 3.22. Data of reference [Miclea 06] are also displayed in figure 3.23 and equally well fitted. In particular, we can see that the change of slope of H_{c2} at T_{SC} can be well reproduced by only the pressure dependence of a unique parameter λ. The complete pressure dependence of the parameters used for the fit are displayed on figures 3.28. As expected λ is essentially a decreasing function of pressure except at very low pressure where it exhibits a maximum at around 0.4GPa. This is consistent with the NMR data [Yashima 04] which pointed to a maximum of the gap to T_{SC} ratio

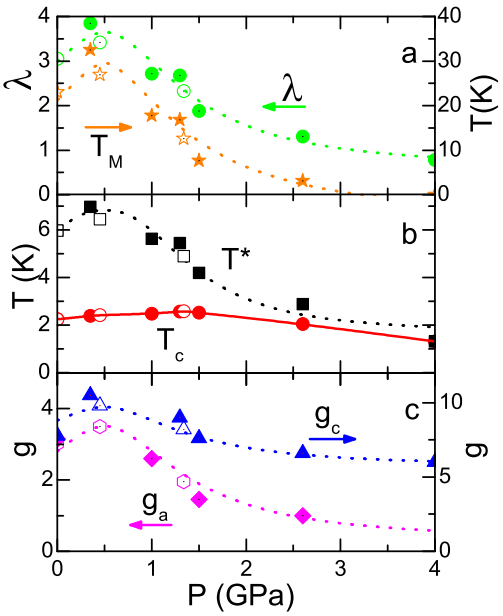

Figure 3.28: a and c, parameters used for the fit of the upper critical field. All parameters have a maximum around 0.4GPa. This points to a quantum critical point at this pressure rather than at the maximum T_{SC}. (a) pressure evolution of the strong coupling constant λ and of the pair breaking strength T_M. The variation from about 3.5 to 1 of λ is controlled by the variation of $\partial H_{c2}(T_c)/\partial T$, for both field directions. (b) Pressure evolution of T_c (and $T^\star$), the superconducting transition at H=0 with (and respectively without) magnetic pair breaking, see text. (c) Pressure evolution of the gyromagnetic ratio. Lines are guide for the eyes.

(or equivalently, to a maximum of the strong coupling regime as measured by λ) in the same pressure range. Therefore, this analysis of H_{c2} as well as the previous NMR work does suggest that the pairing strength is maximum at neither zero pressure nor p_{max}, but rather at $p \approx 0.4$GPa.

If we keep in mind the paradigm of superconductivity in strongly correlated systems, namely the coincidence of QCP and optimum T_{SC} due to optimum pairing strength, this weak maximum of λ suggests a QCP at $\approx$ 0.4GPa, instead of the 1.3GPa [Ronning 06] usually inspired by the maximum of T_{SC}. We should note that the parameter controlling the magnetic pair breaking T_M has a maximum at the same pressure value $\sim$ 0.4GPa which supports the idea that the two mechanisms: interaction strength and magnetic pair breaking reflect a unique coupling mechanism associated with the quantum critical point.

In fact, Monthoux and Lonzarich have calculated the dependence to the distance of a quantum critical point of different parameters for superconductivity induced by anti-ferromagnetic fluctuations. They show that the maximum of the superconducting temperature is not necessarily located at the QCP as AFM fluctuations also act as pair breakers. This is particularly the case when the interaction is strong and the system two-dimensional (figure 3.29a) [Monthoux 01]. Then it is known that the pairing interaction has an effect on quasi-particle renormalization mainly on their effective mass or velocity. They show that in the case of a non-fully symmetric superconducting state, one should distinguish between parameters λ_z for the mass renormalization and λ_d for the coupling. The first one is the average of the pairing interaction over the Fermi surface and the second one is an average over the Fermi surface of the pairing interaction multiplied by the symmetry of the superconducting state. In case of "s-wave" superconductivity, both parameters are the same, but

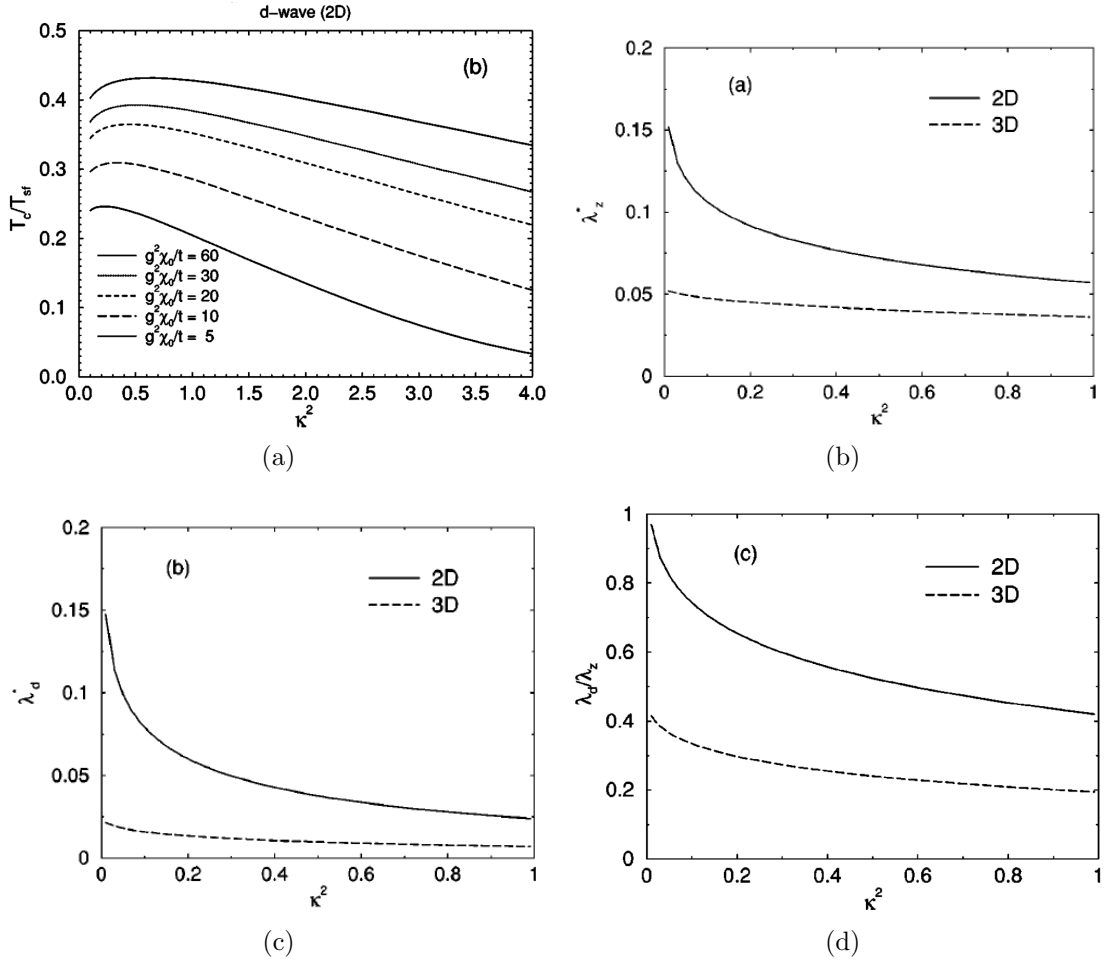

Figure 3.29: Calculation of (a) the superconducting temperature, (b) the strong coupling parameter for mass renormalization λ_z, (c) the strong coupling parameter for "d-wave" pairing λ_d and (d) the ratio λ_z/λ_d as a function of the distance to a QCP and pairing strength for a weak anti-ferromagnet. From Monthoux and Lonzarich [Monthoux 01]. We observe that the maximum of $T_{SC}$is not located at the maximum of the strong coupling constant at the QCP ($\kappa = 0$) due to magnetic pair breaking mechanisms. The pairing coupling constant $\lambda'_d = \lambda_d/g^2\chi_0\kappa_0^2/t$ decrease faster than the mass renormalization coupling constant $\lambda'_z = \lambda_z/g^2\chi_0\kappa_0^2/t$ with distance to the QCP.

the ratio λ_d/λ_z is smaller than one in case of any less symmetric superconducting state. Figure 3.29d show the evolution of this ratio for a "d-wave" superconducting state mediated by weak anti-ferromagnetism. This is important as a quantity as T_{SC} depends on λ_d as v_F does on λ_z.

Our fitting exactly reproduces this effect with T_M accounting for the pair breaking and leading to an effective maximum of the pairing strength λ_d at some distance from the QCP. T_M has no physical meaning in the sense of this model as it is an artificial method to obtain a pairing that intrinsically depends on two mechanisms associated with the proximity to the QCP: the direct increase of the spin suscep-

tibility and a decrease of the retarded susceptibility due to the fluctuations. The model is done for a "s-wave" scenario, but as $CeCoIn_5$ is "d-wave" the distinction between λ_d and λ_z should be done. The implication of this simplification will be discussed later. The value of T_M might seems high. Indeed it gives the mean free path of the quasi-particles $l = \frac{\hbar v_F}{k_B T_M}$ which has to be bigger to the coherence length ($l > \xi_0$) for superconductivity to exist. However the coherence length is short in $CeCoIn_5$ as it has a large gap $\xi_0 = \frac{\hbar v_F}{\pi \Delta}$ with $\Delta \cong 1.76 k_B T^\star$. Hence we have the condition $T_M < 5.53 T^\star$ which is always satisfied in our model.

One parameter of the model is the gyromagnetic factor (g). Because g is most sensitive to the low temperature part of H_{c2} where the transition becomes experimentally first order whereas our calculations are restricted to a second order phase transition, its value could be less significant than that of v_F. Nevertheless, owing to the strong curvature of H_{c2} even close to T_{SC}, g is already well determined within the limit of validity of the model, and the overall behavior with pressure is certainly correct. A striking feature, independent of the model is the strong anisotropy of g which points to a regime strongly different from the free electron case. Another one is the large value we deduce along the c axis, which results from the strong Pauli limitation in that direction, combined with the rather large value of λ we need to fit the pressure variation of $\partial H_{c2}(T_c)/\partial T$. However, theoretical predictions for magnetically mediated superconductivity show that one should distinguish, for non "s-wave" symmetry of the interaction, a strong coupling constant for the mass renormalization and for the pairing strength (respectively λ_Z and λ_Δ in the notations of [Monthoux 01]). Because the absolute value of the g factor is mainly governed by λ_Δ, a more correct treatment of the calculation of H_{c2} for magnetically mediated superconductivity would certainly lead to smaller value of g (λ_Δ is always smaller than λ_Z). It would also implie less magnetic pair breaking (T_{SC} depend on λ_Δ as v_F of λ_Z).

At this point we should remark that if the gyromagnetic ratio has a value of about 2 in the free electron case there are several reasons to believe this value could be different in heavy fermions:

- Due to the exchange coupling between localized moments and the conduction band, the gyromagnetic ratio of the quasi-particles is an effective one, influenced by the susceptibility of the localized moments. Spin-orbit coupling can also modify the value of these g factors and give rise to anisotropy, especially for the localized electrons. In experiments on semi-metals nano-wires of InSb, values of g up to 70 [Nilsson 09] and for pure Ge $g = 7$ [Hensel 68] have been reported and are associated to the orbital momentum contribution ($\vec{J}$ and not $\vec{S}$ is the good quantum number) and spin orbit coupling. Moreover, Fermi-liquid corrections (ie, interaction between quasi-particles) may also change the value of the g-factor.

- At a magnetic quantum critical point, the susceptibility is modified (diverges at $\vec{q} = 0$ for FM and $\vec{q} = \vec{q}_{AFM}$ for AFM), that is why we can expect an increase of the previously discussed effects, and hence an enhancement of the quasi-particle g-factor.

In our model, we could get a lower value of the g factor (4-6 in the c direction and less than 2 in the a direction) than those reported for our fit if we start with a lower value of $\lambda_0 = 2$ (minimum value to obtain the correct T_{SC} evolution). In that case the fits are slightly less good.

The values obtained for the Fermi velocity are $6.2 \cdot 10^3$ m/s for H//[100], and $7-7.5 \cdot 10^3$ m/s for H//[001] (depending on the data set), from which we can extract $v_{Fa} = 7.2 \cdot 10^3$ m/s, $v_{Fc} = 5.3 \cdot 10^3$ m/s. This indicates that the system is only weakly bi-dimensional from the electronic point of view. This was already pointed out as electrical resistivity and magnetic susceptibility are not strongly anisotropic [Settai 01].

3.5 Conclusion

Fitting the resistivity data down to 8mK with $\rho(T) = \rho_0 + AT^2$ allows us to determine the boundary of the Fermi-liquid domain in $CeCoIn_5$ in the neighborhood of $H_{c2}(0)$, for $H \parallel c$ with unprecedented precision. T_{FL} does not vanish at $H_{c2}(0)$ in $CeCoIn_5$, and if a quantum critical point exists in this system, its location is at a lower magnetic field and therefore hidden by the superconducting state. Moreover, no anomaly has been found for transport along the c-axis, meaning that a Fermi-liquid regime is still observed in resistivity down to $H_{c2}(0)$ along this direction, albeit in a very restricted temperature range (below 50mK). This is also confirmed by an accurate determination of the "divergence" of the A coefficient of resistivity. Moreover, the field dependence of A and T_{FL} are compatible with a QCP governed by the collapse of a single energy scale. We can explain the differences with some of the previous works as due to improved precision and/or the use of a more favourable setup geometry which is less prone to low temperature magneto-resistance effects. This may help to clarify the relationship between QCP and superconductivity in this compound, however it also stresses the need for theoretical studies and predictions for a field induced QCP.

We were able, with quite a simple model to fit the upper critical field of $CeCoIn_5$ under applied pressure with only two free parameters. We observed for the first time, the expected decoupling between the optimum T_{SC} and maximum pairing strength, due to dominant pair-breaking effects in the neighbourhood of the QCP. This is probably due to a stronger coupling regime, or stronger 2D character [Monthoux 01] $CeCoIn_5$ is different from its parent $CeRhIn_5$, where the coincidence of the QCP and maximum T_{SC} is well documented. We claim that many peculiar features of $CeCoIn_5$ like the large specific heat jump at T_{SC}, the pressure dependence of the gap to T_{SC} ratio observed by NMR, the pressure dependence of the paramagnetic limitation and of the initial slope of H_{c2} can be well explained in this scenario, and also that the pressure phase diagram of $CeCoIn_5$ is a paradigm of an (almost 2D) strongly coupled anti-ferromagnetically mediated superconductor.

With these two results we can now redraw the phase diagram we speculate for $CeCoIn_5$ (figure 3.30). We have obtained experimentally two points on the quantum critical line that would appear in the absence of superconductivity. At p= 0.4GPa, H= 0 from the fit of the upper critical field under pressure (maximum of $m^\star$, $T^\star$,

g) and from the measurements of the Fermi-liquid domain under magnetic field at p= 0GPa, H= 4.8T. The quantum criticality would arise from an AFM transition as suggested in [Zaum 10].

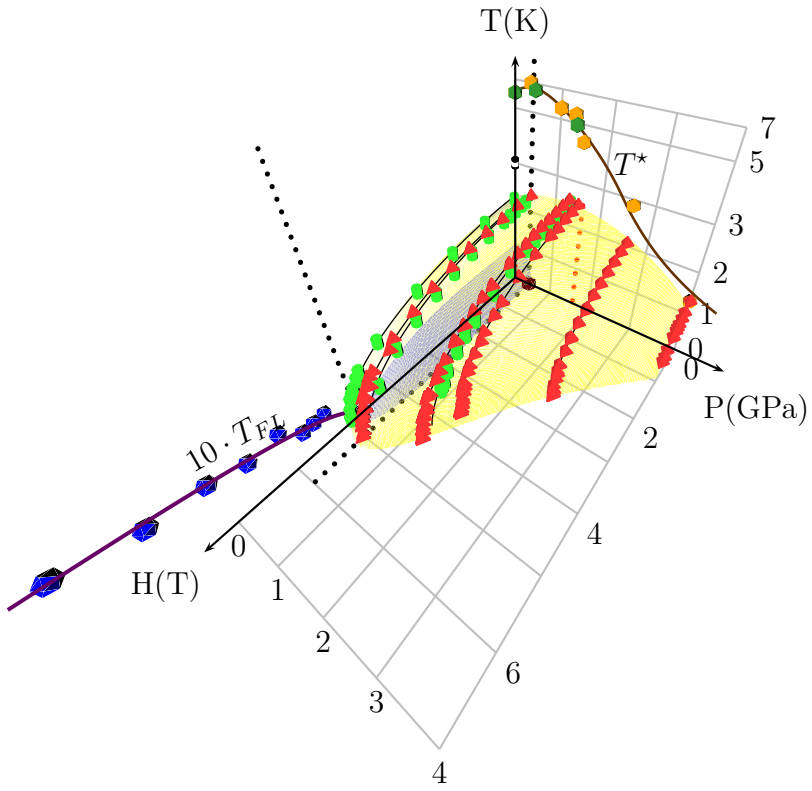

Figure 3.30: New phase diagram proposed for $CeCoIn_5$: the hypothetical QCP, corresponding to the maximum pairing strength, is not at the maximum T_{SC}, as deduced from the analysis of H_{c2} and in agreement with predictions for magnetically mediated pairing [Monthoux 99]. A possible connection with the field induced QCP observed at zero pressure is also displayed. Yellow surface extrapolated superconducting surface from data of Knebel et al. (red) and Miclea et al. (green). $T^\star$ and T_{FL} obtained as descriebed in the text and indicating the position of the pressure and field induces QCP (brown). Blue surface represent the possible AFM phase that would develop in absence of superconductivity and cause quantum criticality.

One of the issues of the scenario that was pointed out is the absence of any phase transition inside the superconducting region that would correspond to our scenario. Indeed, the speculated magnetic phase of figure 3.30 has never been observed, no anomaly is detected at the speculated QCP inside the superconducting phase. For example we could expect an increase of the Sommerfeld coefficient γ or an anomaly

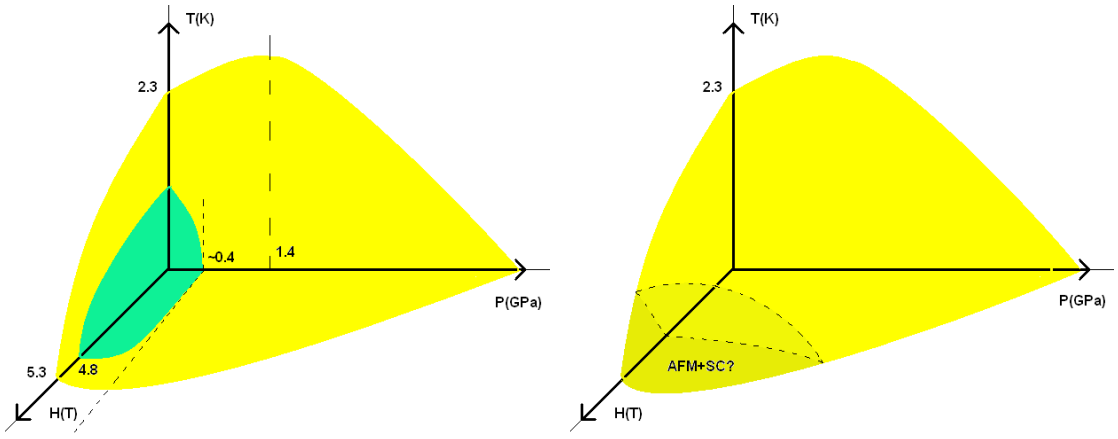

(a) (b)

Figure 3.31: (a) In the absence of superconductivity, an anti-ferromagnetic phase would develop through a second order phase transition. This gives rise to the non Fermi-liquid domain observed in the paramagnetic phase. (b) In the superconducting region another phase seems to emerge with coexistence of superconductivity and magnetism (FFLO).

in magnetization curve versus magnetic field. I want to clarify in this discussion that we do not expect any of these effects to be realized in our scenario. The reason is that appearance of the superconducting phase completely changes the magnetic scenario. Indeed, the magnetic susceptibility is modified at the transition.

We propose a scenario for quantum criticality in $CeCoIn_5$ as describe in figure 3.31.

We can look at the problem from two different angles:

- In the paramagnetic phase, the system "feels" that its ground state would smoothly become anti-ferromagnetic (AFM is taken as an example but it could also be another phase) at low Pressure and low field. The transition would be second order and therefore, associated with quantum criticality (line of QCP in (H,P,T=0) phase plane). A phase diagram with this AFM phase is displayed on figure 3.31a for H$\|$c-axis. A similar phase diagram is expected for the other field orientation even if less physical evidence is present. The fluctuations associated with this QCP give rise to the non Fermi-liquid behaviour observed in the PM phase. But before reaching a pressure or a field low enough, the ground state of the system abruptly (via a first order phase transition) becomes superconducting (figure 3.31a).

- In the superconducting phase, there are several pieces of evidence for coexisting superconductivity and anti-ferromagnetism in the high field, low temperature part of the superconducting region at least when a magnetic field is applied in the a-axis direction (figure 3.31b). This phase could be a FFLO state or a more complicated interaction between superconducting and magnetic order (as proposed for example in ref. [Ikeda 10]). The coexisting AFM-SC phase is not

directly related with the previously discussed AFM phase that would exist in the absence of superconductivity. Indeed, superconductivity will change the dynamical susceptibility of the medium and the free energy of a coexisting AF+SC phase will be different from that of the AFM phase alone. So if there is a true QCP in the superconducting phase, it can only be induced by the coexisting AFM-SC phase and will have no effect in the PM phase above H_{c2}. Superconductivity cannot cause quantum criticality as the transition is first order and the instability observed in the paramagnetic phase is suppressed by the appearance of superconductivity.

However, as discussed in the introduction, superconductivity, magnetism and quantum criticality are very probably linked together: Magnetic fluctuations as a "glue" between charge carriers allowing for pairing of the quasi-particles and quantum criticality responsible for these fluctuations which are also a pair-breaking mechanism for superconductivity when thermally excited. The difference with other system as $CeRhIn_5$ is the value of the strong coupling constant λ. Indeed, the difference between maximum of T_{SC} and QCP is predict to be large and observable only in the case of strong coupling (large λ).

4 Thermal conductivity on URhGe and UCoGe

4.1 Background

In the last ten years, four compounds with coexistence of ferromagnetism (FM) and superconductivity (SC) have been reported. UGe_2 [Saxena 00], URhGe [Aoki 01], UIr [Akazawa 04] and UCoGe [Huy 07], have a superconducting phase that develops as the compounds are already ferromagnetic. A proof that the two phenomenon coexist on a microscopic scale was recently given by Nuclear Quadrupole resonance (NQR) [Ohta 10] for the compound UCoGe. Indeed, the ^{59}Co resonance frequency is completely shifted at the FM transition (for a single crystal) indicating that the full sample becomes ferromagnetic. Then no modification in the frequency is observed at the SC transition (figure 4.3a), indicating that ferromagnetism persists when superconductivity appears. T_1 relaxation time performed on the same resonance peak displays the characteristic superconducting slow decay rate below T_{SC}, indicating FM and SC coexistence (figure 4.3b). However, only about 50% of the amplitude of the resonance follows this rate, which suggests that only 50% of the charge carriers are superconducting. Moreover, ferromagnetism has been shown by NMR to arise from the 5f electrons of uranium ions [Ihara 10], and superconductivity is clearly due to heavy quasi-particles (large specific heat jump $\frac{\Delta C}{C}$, large H_{c2}, ...). So in these compounds, ferromagnetism and superconductivity are due to the same (5f) charge carriers.

But, the most spectacular result in this family of compounds is that under

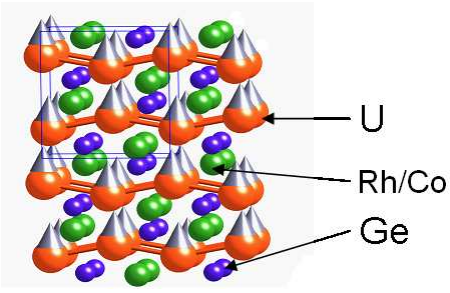

Figure 4.2: Unit cell of URhGe or UCoGe. Both compounds crystallize in the in the orthorhombic structure with TiNiSi-type. c-axis is the easy axis for magnetization in opposition to a-axis (hard axis). In the a-axis direction, the U chains form a small zig-zag.

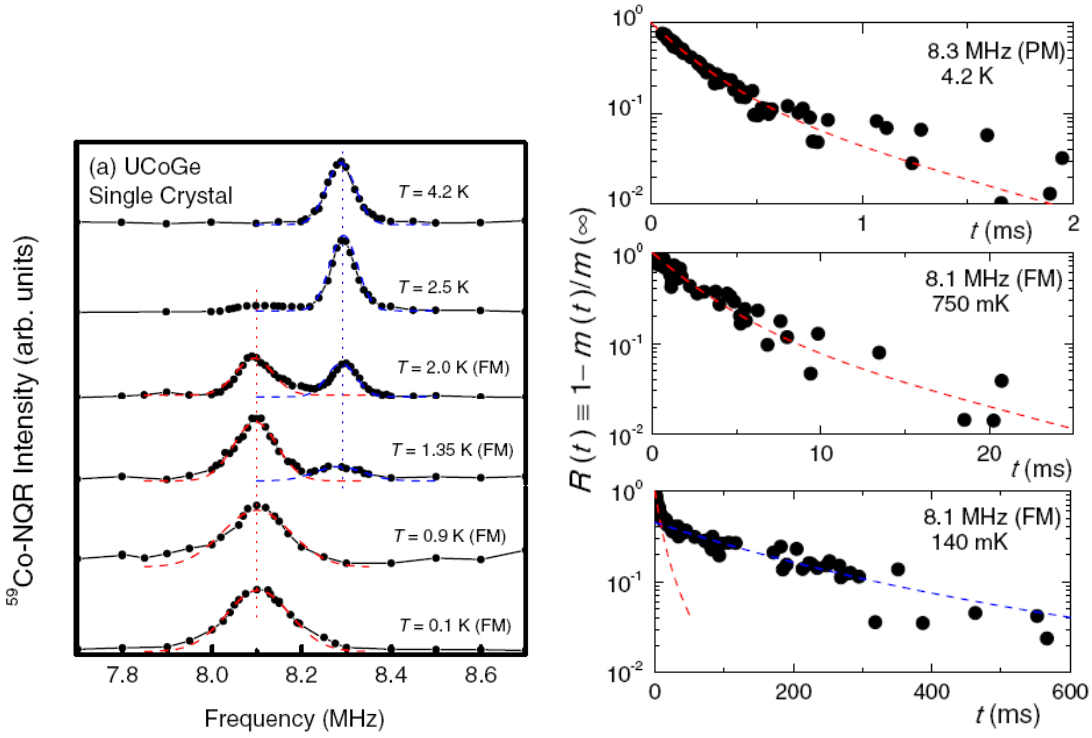

(a) (b)

Figure 4.3: NQR measurements on UCoGe. (a) the full NQR resonance frequency is shifted indicating that the sample is fully ferromagnetic. (b) the long T_1 relaxation time is characteristic of superconductivity and represents only about 50% of the signal at 140mK. This indicates that only 50% of the quasi-particles are superconducting at this temperature. Figures from [Ohta 10].

magnetic field, a so called "re-entrance" of superconductivity is observed. In URhGe two different pockets of superconductivity can clearly be identified when field is applied along the $\vec{b}$ crystallographic axis (figure 4.4b). A similar phase diagram has been detected in UGe_2 and UCoGe (figures 4.4a and 4.4c), with two superconducting domes, even if in these cases the two pockets remain connected.

It is interesting to point out that in these three systems the maximum of superconductivity appears close to a phase transition.

- In UCoGe FM disappears under applied pressure. The maximum superconducting transition temperature is reached at a pressure close (if not at) the FM-PM QCP [Hassinger 08] (figure 4.5a).

- In URhGe, under magnetic field applied along the $\vec{b}$ crystallographic direction, a re-orientation of the ferromagnetic moments from c-axis (easy axis) to b-axis happens around 11 Tesla. At the same field the maximum of superconductivity in the re-entrant phase is observed. The amplitude of the magnetic moments in the b-axis direction was followed by neutron scattering and is showed in figure 4.6 [Lévy 07]. The re-orientation of the magnetic moments

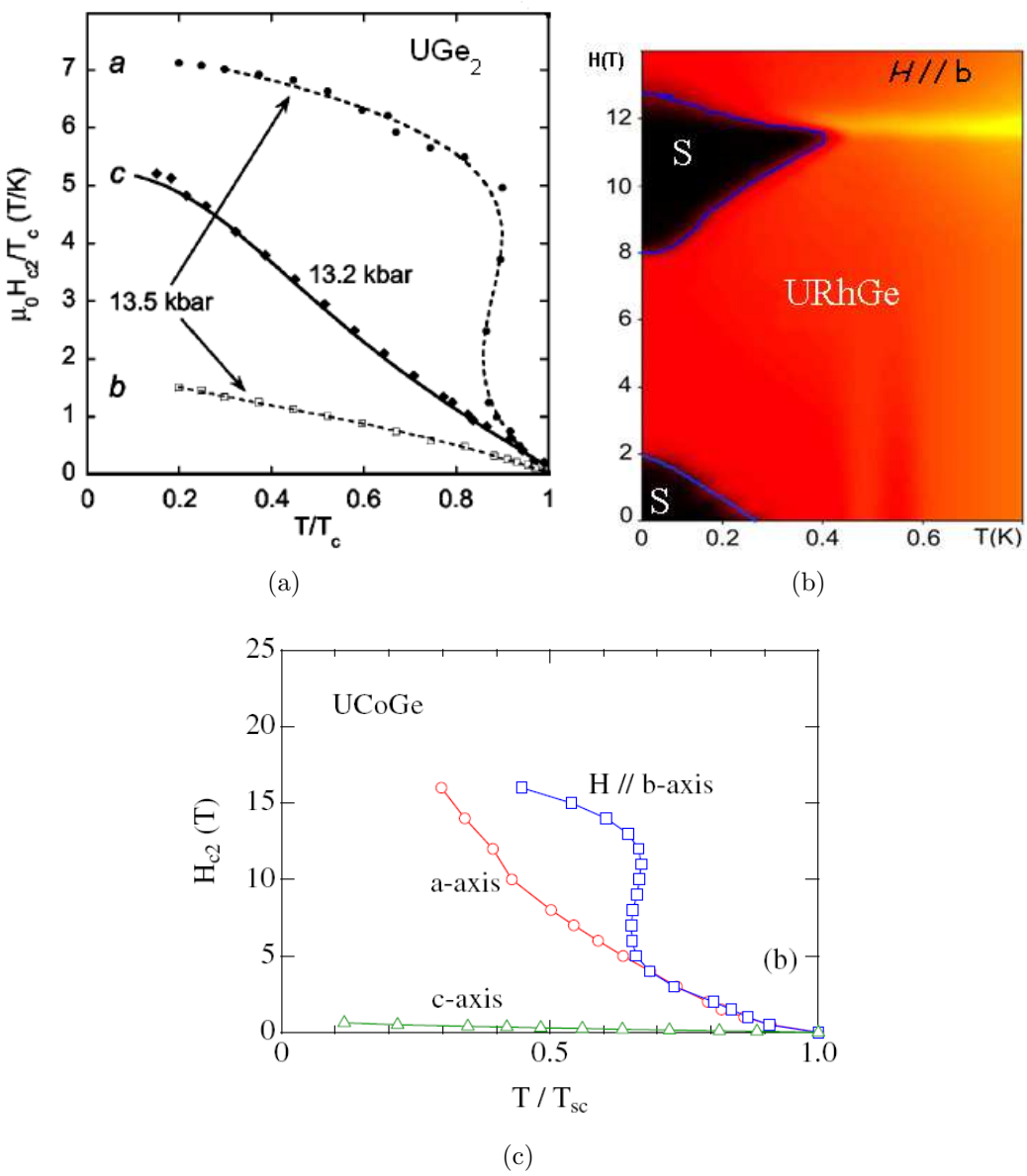

(a) (b)

(c)

Figure 4.4: Re-entrance of superconductivity in (a) UGe_2, (b) URhGe and (c) UCoGe. Graphics from [Sheikin 01, Lévy 07, Aoki 09]

is associated with a maximum in resistivity. The transition obtained from the resistive measurements is shown in figure 4.5b. The maximum was measured under pressure [Miyake 09] and found to coincide with the maximum of superconducting temperature observed in the re-entrant phase. Due to the similarities between the two compounds (chemical structure, phase diagram, orientation of FM moment,...) a similar re-orientation of the moments is expected in UCoGe and is often associated to the transition observed at 11T with a maximum of magneto-resistance.

- Finally in UGe_2 at the maximum of superconductivity, a phase transition between two FM phases with different moments is observed (figure 4.5c).

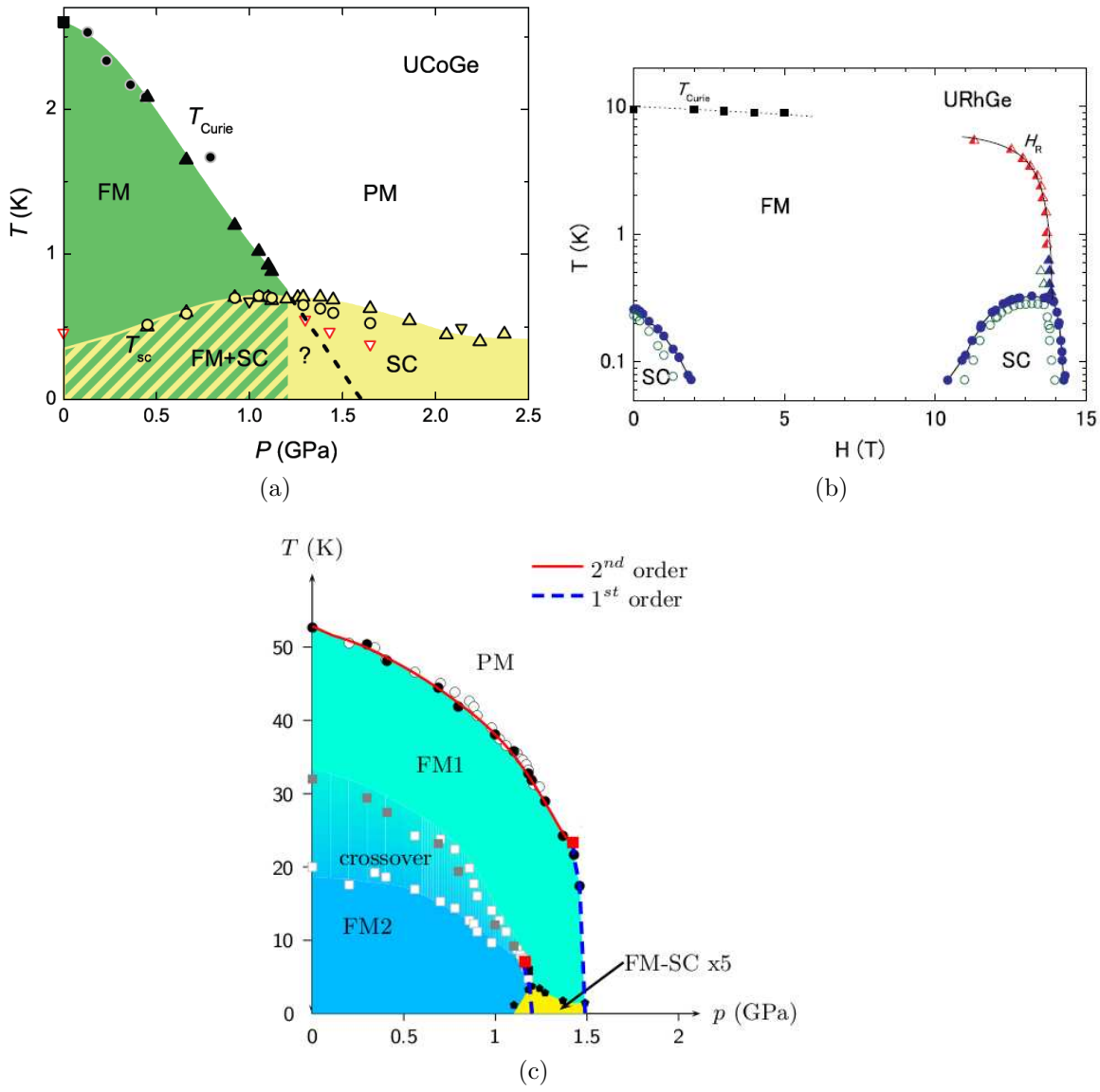

Figure 4.5: Phase diagrams showing the interplay between superconductivity (SC) and the ferromagnetic phases (FM) controlled by pressure or magnetic field. Graphics from [Hassinger 10, Miyake 08, Taufour 10]

URhGe and UCoGe are superconducting at ambient pressure, and are hence suitable for thermal conductivity measurements. Before ending this brief introduction on this family of compounds, here is a small summary of the principal characteristics of the two compounds:

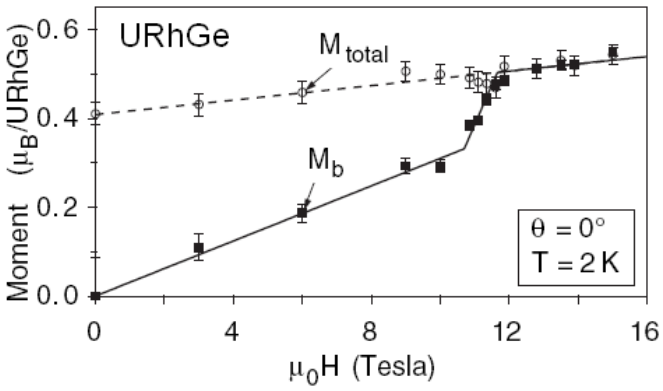

Figure 4.6: Re-orientation of the ferromagnetic moments in UCoGe arround 12 Tesla. Figure from [Lévy 07]

	UCoGe	URhGe
T_{SC}	0.7 K	0.26 K
T_{Curie}	2.5 K	9.5 K
γ	$55\mu JK^{-2}$*	164 μJK^{-2} †
m_0	$\sim$0.07 μ_B/U-atom ‡	0.4 μ_B/U-atom §
a	6.85Å*	6.87Å¶
b	4.21Å*	4.33Å¶
c	7.22Å*	7.51Å¶

Similar properties between the two compounds were expected as they share the same electronic configuration Rh being just below Co in the Mendeleiev table of elements. The main expected difference is the distance between ions, with the unit cell dimension which increases from UCoGe to URhGe. This small effect can have an important influence on the degree of hybridization of the U-5f electrons, a key point as these electrons are responsible simultaneously for the ferromagnetism, large effective mass (Kondo effect, ...) and superconductivity. It should be noted that the parent compound UIrGe, increasing one more step in the electronic configuration, has an anti-ferromagnetic ground state with $T_N \cong$16K [Prokeš 99], and similar lattice parameters (6.86, 4.30, 7.58 Å) as URhGe. This suggests that U-5f electrons hybridization is not the only relevant parameter of the problem. No superconductivity has been observed in UIrGe up to now.

Above the ferromagnetic transition, the anisotropy of magnetic susceptibility is estimated as follows:

- in URhGe $\chi_c/\chi_a \propto\sim 80$ and $\chi_c/\chi_b \propto\sim 2$ [Prokes 02]

*[Huy 07]
†[Hagmusa 00]
‡[Huy 08]
§[Lévy 07]
¶[Prokes 02]

- in UCoGe $\chi_c/\chi_{\perp c} \propto\sim 2.3$ [Troć 10].

Due to the anisotropy they are often viewed as Ising systems, with only longitudinal spin fluctuations possible. However, we can see that the anisotropy between b and c is weak and may allows magnetic fluctuations as magnons.

4.2 Aim of this study

A large number of open question are raised by these compounds. But like in the previous chapter on $CeCoIn_5$, we will focus our interest on the relation between phase transition and superconductivity. Indeed, in the AFM heavy fermions, it is believed that a quantum critical point is at the origin of the "glue" of superconductivity. Hence probing physical and especially bulk properties of these systems is of special interest for the understanding of superconducting mechanisms.

We used, for the first time thermal conductivity on these systems as it combines the advantages of:

- being a bulk probe,
- achievable down to relatively low temperature (30mK in our case),
- sensitive to anisotropy,
- probing the low energy excitations of the superconducting phase.

Quality of the samples remains an issue for these compounds even if a significant progress was achieved in the last years. We performed our measurements on the samples presenting the largest RRR and specific heat jump at the superconducting transition, but obtained a residual term about half of the normal state thermal conductivity. Whether this is an intrinsic phenomena with a large universal limit due to nodes of the gap or an artifact due to sample quality is unclear at present and needs to be further investigated. Consequently, our different analysis and conclusions still need to be confirmed on other samples.

4.3 Samples

We performed thermal conductivity measurements on two samples grown by V. Taufour and D. Aoki in the laboratory. The first one is a large URhGe crystal of dimensions about: 5x0.26x0.76 mm for a,b,c-axis directions. Resistivity was measured along a-axis direction at different positions on the sample by Dai Aoki. The RRR was found to vary across the sample with a best part of RRR$\cong$40 in the centre of the crystal (about 0.72mm, with a geometrical ratio S/l$\cong$ 280μm.). Even if this inhomogeneity makes its bulk characterization difficult, we used this sample as its large dimension allows to apply a uniform heat current and to glue the sample on a relatively large surface. Indeed for thermal conductivity only the cold end is fixed to the sample holder, and as the sample is ferromagnetic a torque is formed when magnetic field is not collinear with the ferromagnetic moments. We

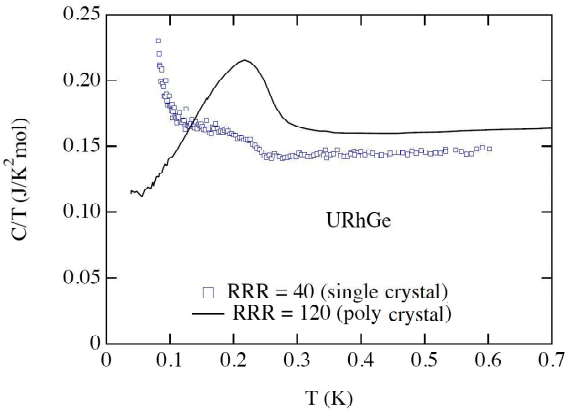

Figure 4.8: Specific heat measured on a sample of URhGe of the same batch and with identical RRR than the one used in this study compared to a higher quality polycrystal [Aoki 01].

were therefore afraid that the sample would fly off if the glued surface was too small. Alignment is also easier with a larger sample. For the measurement, we used the setup described in section 2.2. Thermal conductivity is measured with the standard two thermometers one heater method. Resistivity can be measured using the same contacts, and two continuous (4K-300K) copper wires allow simultaneous measurement of thermopower. On this sample we perform the measurements, with the heat and electric current in the a-axis direction. Magnetic field was applied in the b-axis direction.

For characterization, specific heat was measured on a sample coming from the same batch with an identical RRR (figure 4.8). Increase of $C(T)/T$ at low temperature is due to the nuclear hyperfine contribution. The value of the Sommerfeld coefficient $\gamma \cong 150\text{mJK}^{-1}$ below 1K (in the ferromagnetic state) corresponds to the previously reported values [Hagmusa 00]. In comparison a polycrystal with better RRR$\cong$120 [Aoki 01], shows a higher and sharper transition peak together with a smaller residual value. It points out the problem of sample quality for single-crystals. Nevertheless, the superconducting transition can clearly be identified in the specific heat curve which indicates bulk superconductivity.

A second experiment was performed on a sample of UCoGe. This sample is smaller than the previous one with a total length of about 2mm and a geometrical factor S/l$\cong 180\mu$m. Specific heat characterization was carried out on this sample and shows a sharp transition (figure 4.10), and a large improvement on sample quality compared to previous growth. As superconducting transition is higher, we expected more accurate thermal conductivity measurements than in the case of URhGe. On this sample we performed measurements with field applied in both c-axis and b-axis directions.

In the following I will present our results on two different samples (URhGe and UCoGe), in three different configurations: (summarized in figure 4.11),

- (Rh-B) URhGe heat and electrical current in a-axis direction, magnetic field applied in b-axis direction.
- (Co-C) UCoGe heat and electrical current, and magnetic field applied in c-axis direction.
- (Co-B) UCoGe heat and electrical current in c-axis direction, magnetic field applied in b-axis direction.

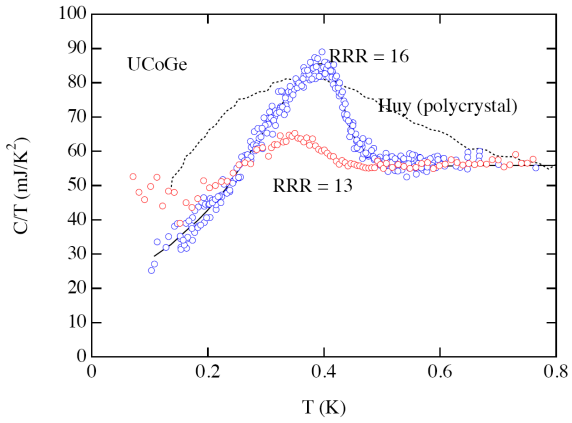

Figure 4.10: Specific heat measured on several samples of UCoGe. Sample with RRR≅16 was used in this study. Here compared with an other monocrystal RRR≅13 and a polycrystal [Huy 07].

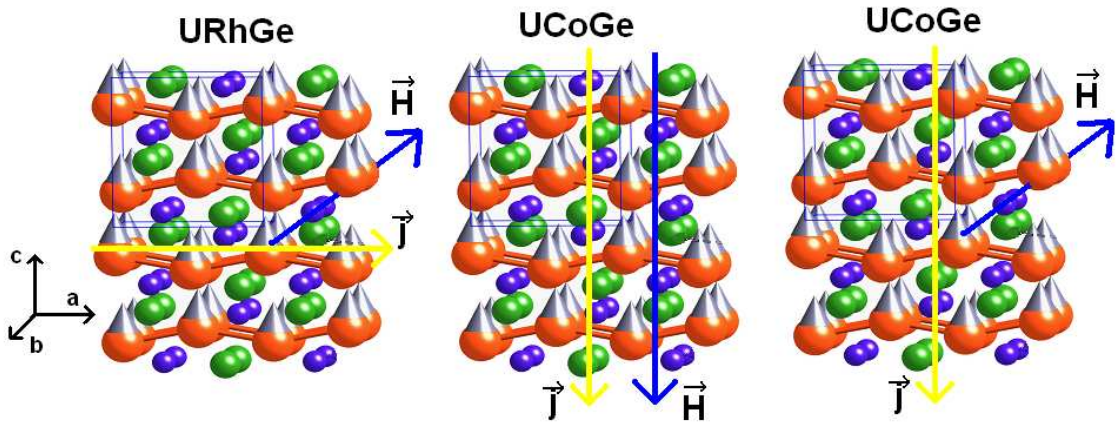

Figure 4.11: Schematic view of the three samples configuration investigated in this thesis, with current (heat and charge) and Magnetic field directions.

For simplicity I will from now refer to them as Rh-B, Co-C and Co-B respectively.

4.4 Results of this measurement

Thermal Conductivity

In the three configurations, we observed a sharp kink in thermal conductivity $\kappa(T)$ at the superconducting transition temperature T_{SC}. The sharpness is an indication of good sample quality. Indeed it indicated a small distribution of T_{SC}. To test the validity of the measurements, curves with different ΔT (1-5%) were taken at some fields. No difference is observed in the obtained thermal conductivity (see for example on figure 4.14 curves at H=0T or 1T).

On the other hand, it is clear from graphics 4.12 and 4.14 that the residual value $\kappa_{Superconducting}/\kappa_{Normal}(T \to 0) \cong 1/2$ is large. The extrapolated value κ_S/T in the superconducting state corresponds in the two cases to about half of the thermal conductivity measured at H=1T (respectively H=2.5T) in the normal state for sample Co-C (Rh-B). Whether this residual term comes from the universal limit and reflects ungapped region of the Fermi surface (lines of nodes) and impurities or

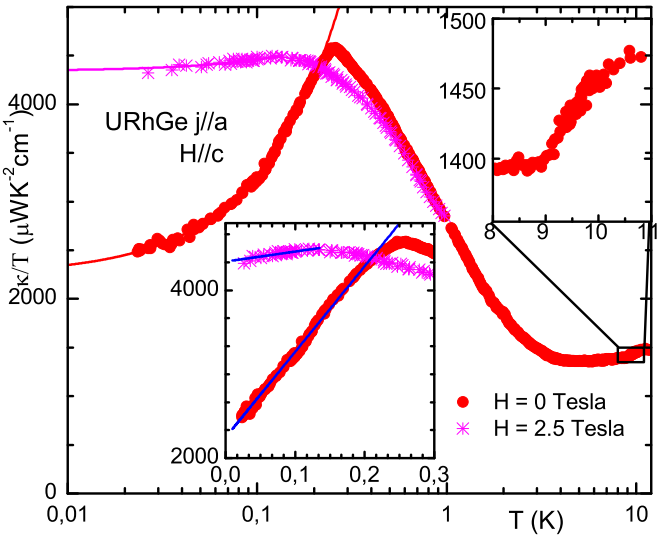

Figure 4.12: (Rh-B) Thermal conductivity of URhGe. Heat current $\overrightarrow{j} \parallel$ a-axis, magnetic field $H \parallel$ b-axis. Ferromagnetic phase transition at 9.5K, superconducting one at 260mK. In the superconducting phase the residual value represent half of the normal state contribution $\kappa_S/T(T \to 0) \cong \kappa_N/T(T \to 0)$.

is due to sample quality cannot be settled until severals samples will be compared. If this value is intrinsic, it would mean that only 50% of the quasi-particles can be superconducting at T=0. Such a small proportion of superconductivity was already reported from NQR measurements (figure 4.3 [Ohta 10]) and a large residual term (possibly 50%) is also obtained from specific heat on the UCoGe sample (figure 4.10). However, if thermal conductivity is sensitive to all quasi-particles independently of their effective masses, specific heat measures the density of states and mainly probes heavy quasi-particles. Hence identical residual values are not expected for the different measurements except if half of the Fermi surface is ungapped, with the effective mass of the two halfs identical. Such a case can happen when only one of the bands splitted by Zeeman energy is superconducting similarly to the A1 phase of He^3. However such scenario seems unlikely as it has a lot of constraints. Notably, the strong spin-orbit coupling present in heavy fermions systems (very weak for He^3) should couple both Fermi sheets, and induce superconductivity everywhere as in usual two-band superconductors,

The ferromagnetic phase transition is clearly seen in the two compounds. At 9.5K in URhGe, thermal conductivity is decreased (figure 4.12). In contrary in UCoGe, at 2.4K the kink observed corresponds to an increase in thermal conductivity. We may attribute these different behaviours to the different heat current orientations. With ferromagnetism, spin waves, as magnons or longitudinal excitations are possible, that have a given propagation direction ($\vec{c}$ direction would be

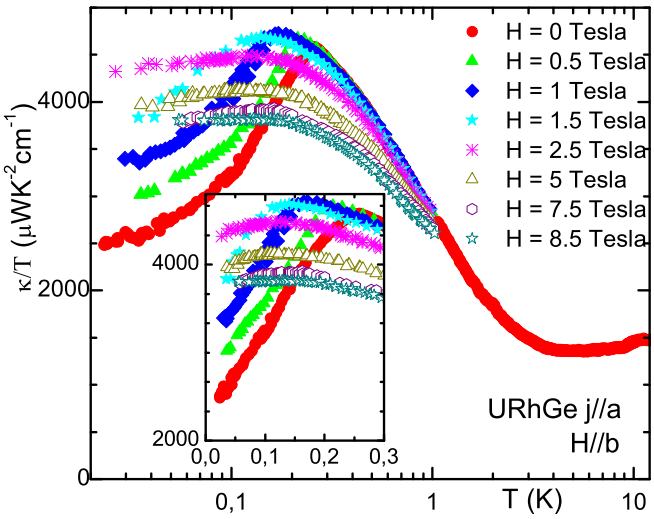

Figure 4.13: (Rh-B) Thermal conductivity of URhGe. Heat current $\overrightarrow{j} \parallel$ a-axis, magnetic field $H \parallel$ b-axis. The decrease observed in κ/T under magnetic field in the normal state is the effect of magneto-resistance. See the Lorenz number in figure 4.23.

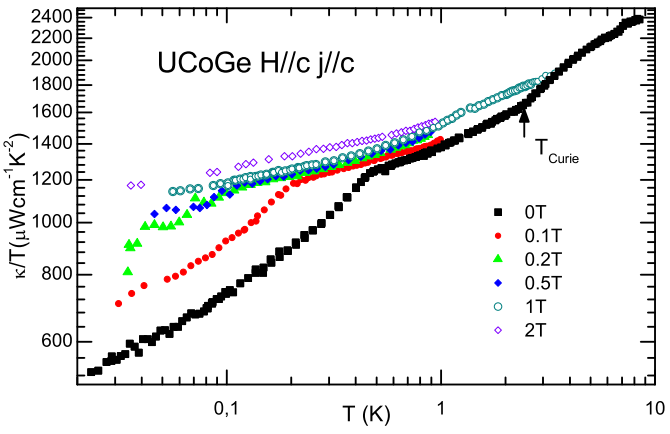

Figure 4.14: (Co-C) Thermal conductivity of UCoGe. Heat current and magnetic field $\overrightarrow{j} \parallel H \parallel$c-axis. Ferromagnetic transition T_{Curie} at 2.4K clearly observed at H=0 (kink in $\kappa(T)/T$) and disappears under magnetic field (no sign of transition a 1T). Superconducting transition at 460mK.

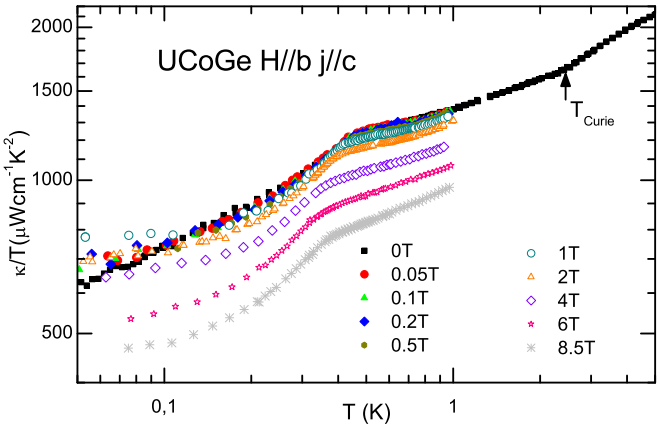

Figure 4.15: (Co-B) Thermal conductivity of UCoGe. Heat current $\overrightarrow{j}$ ∥c-axis, magnetic field H ∥ b-axis. The decrease observed in κ/T under magnetic field is the effect of magneto-resistance.

needed here). But as the system is Ising, longitudinal excitations are more likely and such excitations which are expected to be overdamped, should have little contribution to thermal conductivity [Doman 66] in contrary to magnons which thermal conductivity is $\kappa_{magnons}(T) \propto T^2$. Under magnetic field applied in c-axis direction (direction of the ferromagnetic moments), the anomaly at the ferromagnetic transition disappears as no symmetry can be broken anymore, and the phase transition is replaced by a continuous crossover.

Resistivity

The main interest of resistivity measurements in this experiment was for comparison and control of the validity of the thermal conductivity ones. This is done in the next section with the Wiedemann-Franz law. It is nevertheless interesting to present and discuss the bare data.

We measured resistivity in the same configuration as for the thermal conductivity. The ferromagnetic transition is clearly observed in zero field, and disappears when a field is applied along the c-axis direction (figures 4.17 and 4.19). In each region ($H = 0$ & $T < T_C$, $H = 0$ & $T > T_C$, $H \neq 0$), the resistivity can be fitted with a Fermi-liquid law $\rho(T) = AT^2 + \rho_0$ (orange lines on figures 4.17 and 4.19). Only one region is fitted for the sample (Rh-B) due to the temperatures range of our measurements. The A coefficient is increased inside the ferromagnetic domain, as expected as quasi-particles with different masses are created by the Zeeman spliting, and decreased again to a value similar to the paramagnetic state when field is applied along the c-axis direction.

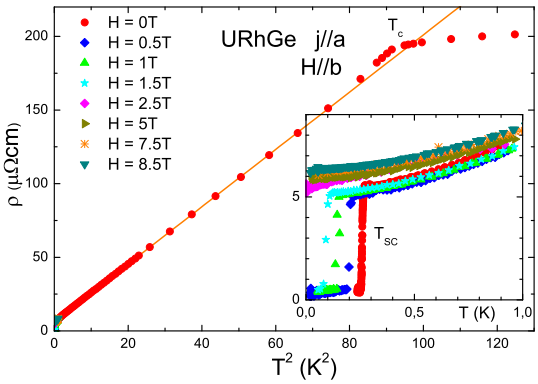

Figure 4.17: (Rh-B) Resistivity of URhGe. Electrical current $\overrightarrow{j} \parallel$ a-axis, magnetic field $H \parallel$ b-axis. Ferromagnetic transition at 9.5K, superconducting one showed in the inset at 260mK in 0 field. In the ferromagnetic region, resistivity can be fitted with a Fermi liquid law $\rho \propto T^2$. From the mean square values, the interval where such a law is observed is: $T \in [1.5K; 8.5K]$.

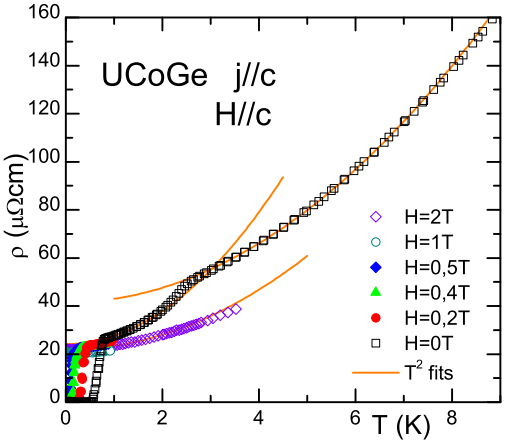

Figure 4.19: (Co-C) Resistivity of UCoGe. Electrical current and magnetic field $\overrightarrow{j} \parallel H \parallel$ c-axis. Ferromagnetic transition at 2.4K clearly visible at H=0T and disappears under magnetic field, superconducting one below 700mK. In each different regime, a Fermi liquid temperature dependence $\rho(T) \propto T^2$ is observed. From the mean square values, the intervals in between the deviation to such a law are: $T \in [0.8K; 1.9K]$ and $T \in [3.7K; 6.3K]$ at H=0T and $T \in [0K; 2.3K]$ at 1T.

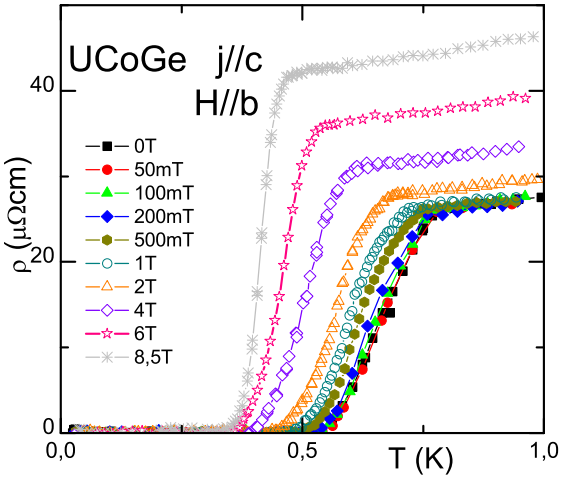

Figure 4.21: (Co-B) Resistivity of UCoGe. Electrical current $\overrightarrow{j} \parallel$c-axis, magnetic field $H \parallel$ b-axis. Under magnetic field, resistivity is increased due to magneto-resistance.

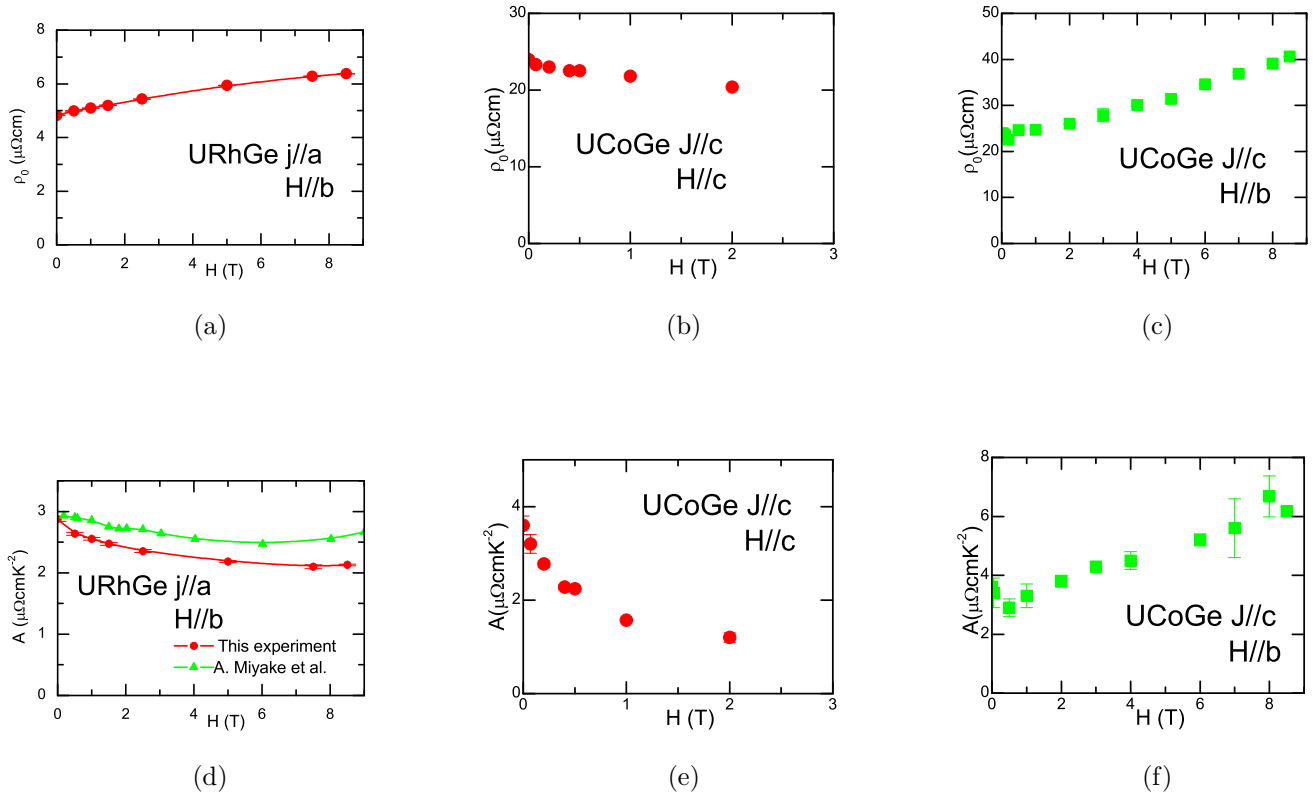

(a) (b) (c)

(d) (e) (f)

Figure 4.22: Evolution of the parameters for a Fermi liquid fit $\rho(T) = AT^2 + \rho_0$ under magnetic field for the three configurations, in a temperature range: $T \in [T_{SC}, 1K]$.

$$A = \begin{cases} 3.43 \pm 0.01 (\mu\Omega\text{cmK}^{-2}) & \text{if } T < T_{\text{Curie}} H = 0 \\ 1.538 \pm 0.001 (\mu\Omega\text{cmK}^{-2}) & \text{if } T > T_{\text{Curie}} H = 0 \\ 1.56 \pm 0.01 (\mu\Omega\text{cmK}^{-2}) & \text{if } T \in [0, 2.3] H \parallel \vec{c} = 1\text{T} \end{cases}$$

Fits of the resistivity with a Fermi-liquid law $\rho(T) = AT^2 + \rho_0$ can be done in the three configurations in the ferromagnetic domain (figure 4.22). For consistency between the data, the fits are now done in the interval: $T \in [T_{SC}, 1K]$. If we consider the scattering between electrons and the "spin-flip" channel (longitudinal fluctuations), we expect the scattering rate to be decreased when a magnetic field is applied along the "flipping" direction (c-axis in our case). This is in good agreement with the observed decrease of the A coefficient in figure 4.22e. In contrary, few effects are expected when a magnetic field is applied perpendicularly to this direction and indeed, the variation of the A coefficient is much less in figures 4.22d and 4.22f. In clean sample when the magnetic field is applied perpendicularly to the electrical current magneto-resistance effects can be important ($\omega_c \tau > 1$). A significant increase of ρ_0 is indeed observed in this configuration, figures 4.22a and 4.22c, compared to the collinear case: figure 4.22b. Finally, the variation of field dependence of the A coefficient with a magnetic field applied in the b-axis direction must be linked to

another effect, and it is natural to believe that this effect is the one responsible for the re-entrance of superconductivity observed at higher field. Indeed Miyake et al. observed a maximum of the A coefficient at the re-entrance [Miyake 08].

So the resistivity analysis suggests good quality samples (enough for the condition $\omega_c\tau > 1$ to be true), and an important effect of the "spin-flip" channel in the interactions with electrons. In UCoGe half of the A coefficient could be due to these interactions. Our data are consistent with the scenario of longitudinal uni-axial spins fluctuations in this compound.

Wiedemann-Franz Law

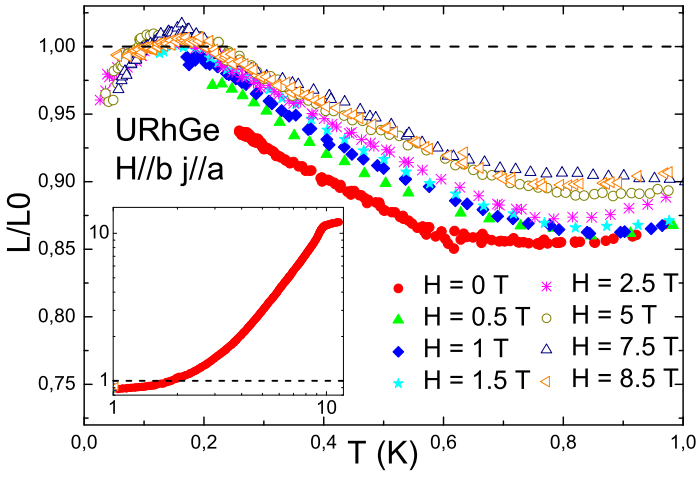

Figure 4.23: (Rh-B) Wiedemann-Franz ratio L/L_0 for URhGe sample. At $T \to 0$ $L/L_0 \to 1$, which is a good indication of the validity of the measurement. Above 2K $L/L_0 > 1$ due to the phonons contribution. Bellow 2K, $L/L_0 < 1$, due to a large number of inelastic scattering. This sample displays the expected behaviour of L/L_0 for a metal.

Check of the Wiedemann-Franz law for the three sample's configurations is presented in figures 4.23, 4.24 and 4.25. In the three cases, the ratio $L(T)/L_0$, where L_0 is the Lorenz number and $L(T) = \kappa(T)\rho(T)/T$ extrapolates to 1 at zero temperature within 5%. This is expected when both heat and charge are transported by the same carriers. This is expected at low temperatures in a metal, with the electrons as the only carriers. The good validity of this law, is an indication of the accuracy of the experiment.

In URhGe, L/L_0 follows the expected temperature dependence for a metal. At high temperature $L/L_0 > 1$ as heat conduction is larger than electrical conduction due to the contribution of phonons. The situation is reversed below 2K due to the large quantity of inelastic scattering (mainly electrons-electrons interactions), and the fast drop of the phonon contribution ($\kappa_{ph} \propto T^2$).

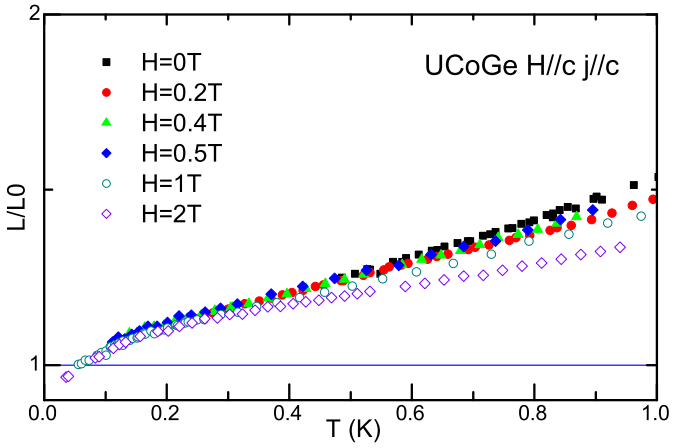

Figure 4.24: (Co-C) Wiedemann-Franz ratio L/L_0 for UCoGe sample (H‖c-axis). At $T \to 0$ $L/L_0 \to 1$, which is a good indication of the validity of the measurement. In contrary to the case of sample Rh-B (figure 4.23), L/L_0, increases with temperature and stays above 1 since the lowest measured temperatures. This indicates that an other mean of heat transport than the charge carrier (quasi-particles) is present in the sample at low temperature.

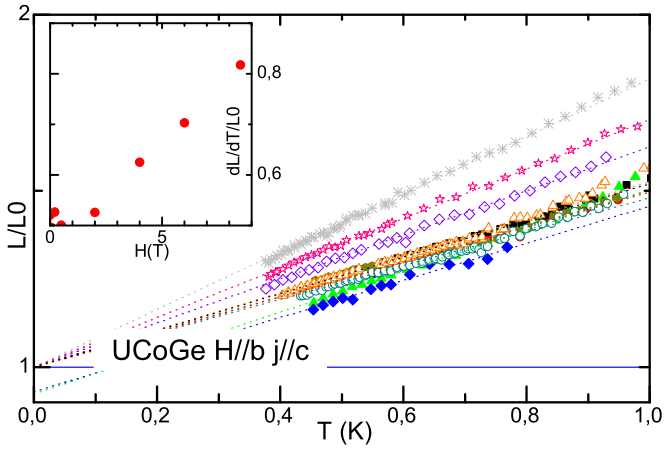

Figure 4.25: (Co-B) Wiedemann-Franz ratio L/L_0 for UCoGe sample (H‖b-axis). As for the other field direction L/L_0 is always larger than 1. The evolution of the slope $dL(T)/dT$ corresponds to the variation in magneto-resistance of resistivity.

For UCoGe the temperature dependence of L/L_0 is unusual as $L/L_0 > 1$ since the lowest temperature. Moreover, the Lorenz number increases linearly with tem-

perature. This implies that an other contribution than electrons is active at these temperatures for heat transport. The linear temperature dependence of $L(T)/L_0$ indicates a T^2 temperature dependence of this "other" contribution, which could be due either to magnons, or phonons. In the case of phonons the temperature dependence should switch to T^3 for the lowest temperatures.

Superconducting upper critical field

We have checked the validity of our thermal conductivity measurements, so we can now use them to obtain the bulk superconducting upper critical field H_{c2} and compare these results with the resistive transitions (figures 4.27, 4.29 and 4.28). Thermal conductivity is sensitive to the normal state quasi-particles and hence insensitive to filamentary superconductivity contrary to resistivity. A transition in thermal conductivity implies that an important fraction of the quasi-particles become superconducting. For this reason, the transition observed in thermal conductivity is a measurement of the bulk superconducting upper critical field. To obtain the transition temperature, we extrapolate the normal state thermal conductivity using the Wiedemann-Franz law:

$$\frac{\kappa_{\text{Normal}}}{T} = \frac{L(T)}{\rho(T)} \tag{4.4.1}$$

We either assume a linear dependence of the Lorenz number, dotted line figure 4.25, for configuration Co-B, or we simply used the Lorenz number obtained in the normal state at high field for configurations (Rh-B) and (Co-C). We also assume a $\rho(T) \propto T^2$ dependence for resistivity. This process is better than using directly the normal state value of thermal conductivity obtained at high magnetic fields, as it corrects for magneto-resistance effects. Then we subtract the normal to the superconducting state thermal conductivity and divided it by the normal contribution, to obtain the transition as the deviation from zero (explained on figure 4.26). This process allows to suppress the effects of the residual term (κ_0) and temperature dependence of the normal state. Indeed, in a two fluids model we have:

$$\begin{aligned} \kappa_{\text{Measured}}(T) &= \alpha\kappa_{\text{S}}(T) + (1-\alpha)\kappa_{\text{N}}(T) + \kappa_0 \\ \kappa_{\text{Normal}}(T) &= \kappa_{\text{N}} + \kappa_0 \\ \frac{\kappa_{\text{Measured}}}{\kappa_{\text{Normal}}} - 1 &= \alpha \left(\underbrace{\frac{\kappa_{\text{S}}(T)}{\kappa_{\text{Normal}}(T)} - \frac{\kappa_{\text{N}}(T)}{\kappa_{\text{Normal}}(T)}}_{=0 \text{ for } T > T_{SC};\ < 0 \text{ for } T < T_{SC}} \right) \end{aligned} \tag{4.4.2}$$

With $\kappa_{\text{Measured}}(T)$ the measured value of the thermal conductivity. $\kappa_{\text{Normal}}(T)$ is an extrapolation with $L(T)/L_0 \propto T$ and $\rho(T) \propto T^2$ of the Normal phase with the Wiedemann-Franz law. $\kappa_{\text{S}}(T)$ is the thermal conductivity of the quasi-particles that will be superconducting at $T = 0$, $\kappa_{\text{N}}(T)$ the thermal conductivity of the portion that stays in the normal state and α is the ratio of superconducting quasi-particles.

We also determined the $H_{c2}$from the resistive transition, using as a criterion 50% of the normal state resistivity.

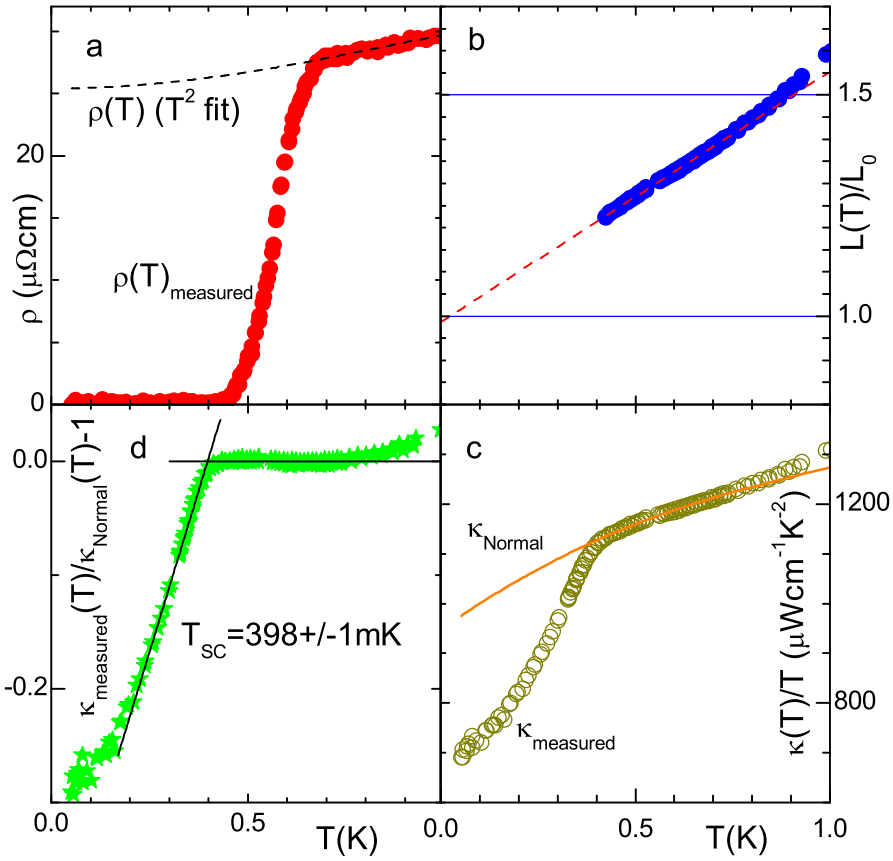

Figure 4.26: Method used to extrapolate the superconducting transition from thermal conductivity measurements: example with UCoGe $H = 2\text{T}\| \vec{b}$-axis (a) We fit the resistivity in the normal phase with a Fermi liquid law. (b) With the data of thermal conductivity in the normal state, we calculate the Wiedemann-Franz ratio $\frac{L(T)}{L_0}\frac{\kappa(T)\rho(T)}{TL_0}$, and fit it linearly. (c) With the fits of the Wiedemann-Franz ratio and resistivity we calculate the normal contribution to thermal conductivity $\kappa_N/T = L(T)/\rho_{\text{fitted}}(T)$. (d) Finally we obtain the onset of superconductivity as the deviation to 0 of $\kappa_S/\kappa_N - 1$.

In URhGe (figure 4.27), the upper critical field is linear in temperature (H ||b-axis), this is difficult to understand within a simple model as the curvature of H_{c2} should change at low temperature as $\frac{\partial H_{c2}}{\partial T}\big|_{T=0} = 0$ for the orbital limitation. The bulk superconducting transition is in perfect agreement with the resistive one, suggesting very homogeneous samples, and a good indication of a high quality crystal. This linear behaviour of H_{c2} is not predicted by conventional theories. However, the situation, from this respect, is even worse in UCoGe.

Indeed, in configuration Co-C (figure 4.28), H_{c2} obtained from resistivity transition, present a clear positive curvature from T_{SC} down to $T \to 0$. Such a curvature is very difficult to explain. In strong coupling scenarios (see in e.g. [Glémot 99]) a positive curvature can be observed but never on such a broad temperature range (curvature changes at low field). Some positive curvature can also be obtained in a

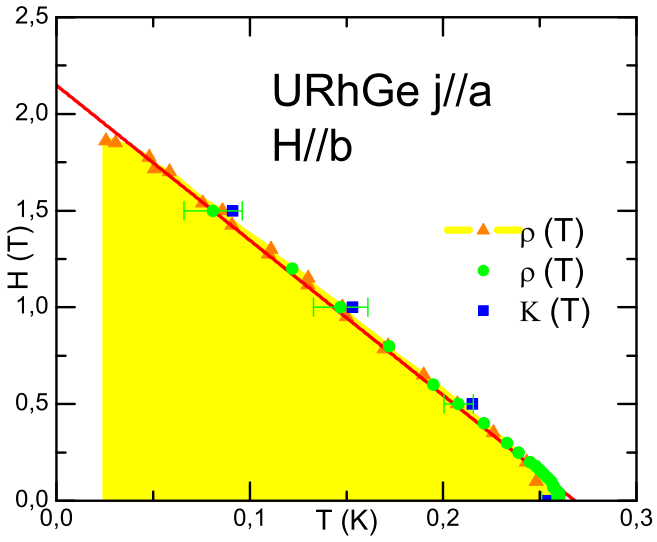

Figure 4.27: (Rh-B) Upper critical field of URhGe $\overrightarrow{j} \parallel$ a-axis, $H \parallel$ c-axis.

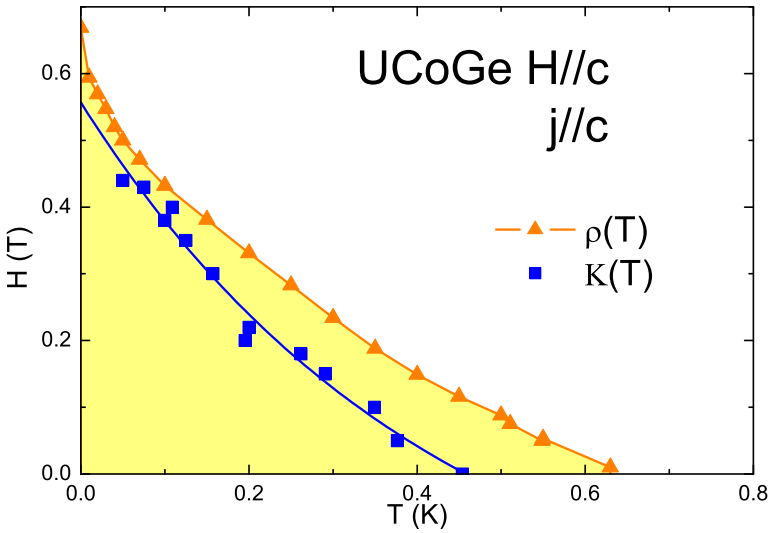

Figure 4.28: (Co-C) Upper critical field of UCoGe $\overrightarrow{j} \parallel H \parallel$ c-axis. The unusual positive curvature of H_{c2} is confirmed by bulk measurements. Blue square is the bulk transition, orange triangles the resistive transition.

multi-gaps scenario (for an example of a two gaps fitting see [Shulga 98]), but due to the extremely broad range where this effect is observed in UCoGe, in particular down to $T \to 0$ it will not be enough. Bulk transitions happen at a much lower temperature, but with a curvature that seems similar except close to T_{SC}. The three highest field data point for the bulk transition were obtained from field dependence

of thermal conductivity at fixed temperature where the normal to superconducting transition still induces a net change of slope of $\kappa(H)/T$.

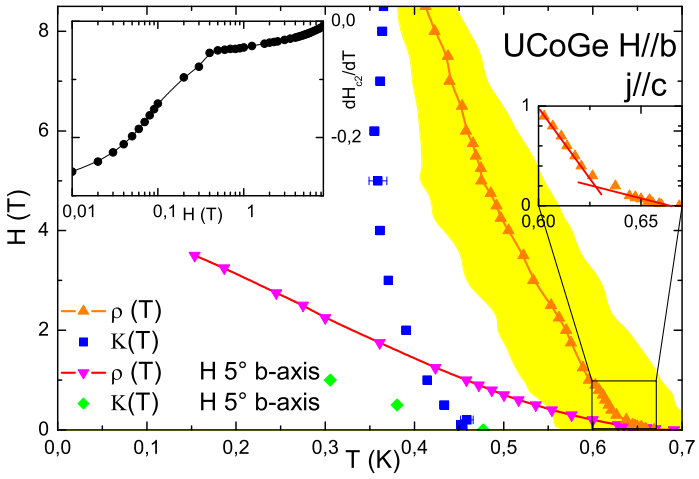

Figure 4.29: (Co-B) Upper critical field of UCoGe $\overrightarrow{j}$ ||c-axis, H ||b-axis. Re-entrance and strong angular anisotropy is confirmed by the bulk measurement. left inset show the derivative of the upper critical field dH_{c2}/dT. A clear change of behaviour is observed at 400mT.

For configuration Co-B (figure 4.29), the "re-entrance" of superconductivity is clearly observed at a lower field by bulk method than in resistivity. The strong angular dependence observed in resistivity is also present in the bulk data. Indeed, the first experiment we performed was 5 ° miss-aligned in the c-axis direction (pink triangle and green diamond) which greatly decreased the upper critical field values.

On figure 4.29 the resistive transition (orange triangle), has a width (yellow domain 10%-90% of transition), which contrary to usual cases is reduced with increasing field. The sharpening of the transition goes together with a reduction of the temperature difference between the bulk and resistive transition. This δT probably indicates a region of filamentary superconductivity that is suppressed upon applying field. One possibility for this very broad δT (more than 200mK at $H = 0$), may be that superconductivity first develops at ferromagnetic domain walls. In resistivity we note a change of slope around 200mT in the H_{c2} curve. It is probably the indication of a modification of the superconducting phase and is expected in a two bands scenario. We will discuss this point in more details when analysing the temperature dependence of the thermal conductivity. A similar discussion can be done for configuration Co-C figure 4.28.

Miyake et al. [Miyake 08] suggested that the "re-entrance" of superconductivity in URhGe could be due to an associated increase of the effective mass. This gives a good qualitative explanation to the "re-entrance" of superconductivity in URhGe but cannot explain the anomalous curvature obtained for example in configuration Co-C. In this case the slope of H_{c2} has a strong positive curvature which suggests

a decrease of the Fermi velocity incompatible with the observed strong decrease of the effective mass given by the A coefficient of resistivity for example.

$$\left(\frac{dH_{c2}}{dT}\right)_{T=T_{SC}} \propto \frac{T_{SC}}{v_F^2}, \quad v_F = \frac{\hbar k_F}{m^\star}. \tag{4.4.3}$$

Non electronic contribution to thermal conductivity

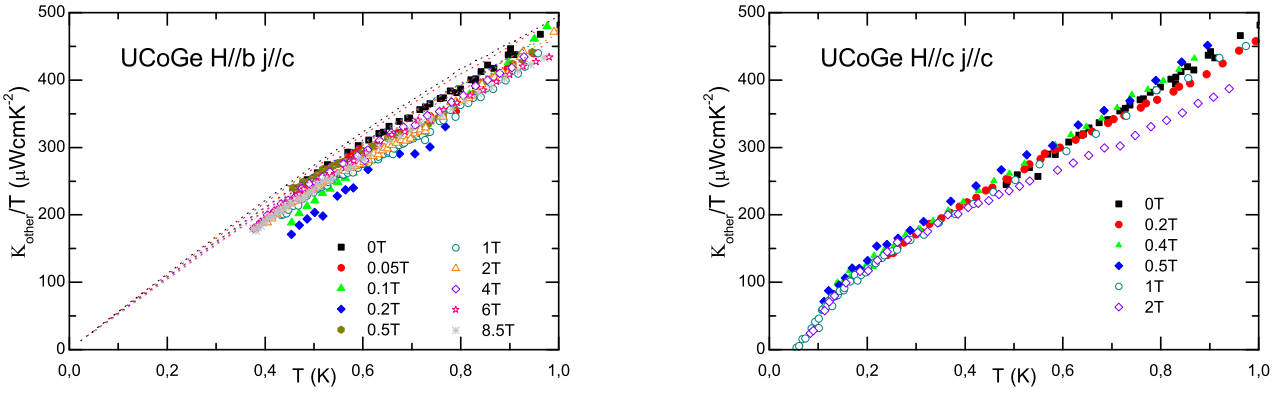

(a) (b)

Figure 4.30: The unusually high value of the Lorenz number measured in UCoGe suggests that another contribution than the charge carriers, transport heat in this system. We estimated this "other" contribution as: $\kappa_{\text{other}}/T = L_0/\rho(T)(L(T)/L_0 - 1)$ from the measurement of $\kappa(T)$ and $\rho(T)$

We found in section: Wiedemann-Franz Law, on page 96, that for the sample of UCoGe, the Lorenz number was unusually large down to the lowest temperature. We can attribute this large value to a heat channel other than the charge carriers in this compound:

$$\begin{aligned} \kappa_{\text{measured}} &= \kappa_{\text{charge carriers}} + \kappa_{\text{other}} \\ \frac{L}{L_0}(T) &= \frac{\kappa(T)_{\text{measured}}\rho(T)}{L_0 T} \\ \frac{\kappa_{\text{other}}}{T} &= \frac{L_0}{\rho(T)}\left(\frac{L}{L_0}(T) - \underbrace{\frac{\kappa_{\text{carriers}}(T)\rho(T)}{L_0 T}}_{\sim 1}\right) \end{aligned} \tag{4.4.4}$$

This "other" contribution was estimated from the different curves of L/L_0 and from resistivity: figures 4.30a,4.30b. The dotted lines in figure 4.30a comes from the extrapolation of the normal state value of $\kappa_{\text{Normal}}(T)$ as described in section: Wiedemann-Franz Law, and a $\rho(T) \propto T^2$ extrapolation. We obtain that the "other" contribution to thermal conductivity is well described by a $\kappa_{\text{other}}(T) \propto T^2$ law.

Surprisingly, the "other" contribution shows little field dependence both for b and c-axis applied field directions. κ_{other} is decreased by about 15% at 2T along c-axis direction and diminish at low temperature for 0.1T and 0.2T in b-axis direction.

One possibility is that the "other" contribution is a magnon contribution. Thermal contribution of spin fluctuations in weakly ferromagnetic metals, as well as in ferromagnetic insulators, have been found to vary as $\kappa_{\text{magnons}} \propto T^2$ [Ueda 75, Kumar 82]. However, the magnetic susceptibility of UCoGe is anisotropic ($\chi_c > \chi_a, \chi_b$) making it an Ising-like system, unfavorable for magnons. For this reason, uni-axial (along c-axis) spin fluctuations have been suggested for this system. But uni-axial spin fluctuations should precisely be strongly suppressed when field is applied in the $\vec{c}$ direction, which is not observed in the case of this "other" thermal contribution. The spin reorientation from c to b-axis (as observed around 10T H||b-axis) provides another possible fluctuations mechanism but this type of fluctuations is then expected to increase with magnetic field applied in the b-axis direction due to the proximity to the moments re-orientation field. Moreover, the strongest problem with uni-axial spin fluctuations is that in contrary to usual magnons, theoretical considerations suggest that these fluctuations do not participate to heat transport.

The other possibility is that "other" contribution is a phonon contribution. Thermal conductivity of phonons can be of the form $\kappa_{\text{phonons}} \propto T^2$ if their mean free path is limited by electron-phonon collisions. The change of slope observed at low temperature in figure 4.30b could then be explained, as the mean free path is limited by the size of the crystal when electron-phonon collisions decrease below a certain threshold and lead to: $\kappa_{\text{phonons}} \propto T^3$ for the lowest temperature. The fact that we observe this contribution would mean that the electronic thermal conductivity in this compound is small for a metal (comparable to the phonon thermal conductivity). And indeed at low temperature ($\sim 0.2K$) thermal conductivity of UCoGe is more than twice smaller than the one of URhGe which in turn is about 10^4 times smaller than copper. These variations of thermal conductivity are due to different electronic thermal conductivities and would explain why the phonon contribution cannot be neglected in UCoGe.

Different temperatures dependences of the thermal conductivity in the superconducting phase

We are now interested in the temperature and field dependences of the thermal conductivity in the superconducting phase. In principle, it is this quantity which should help identify the order parameter symmetry of the superconducting state. In this part we will mainly consider the sample of UCoGe as the temperature range that can be used in UCoGe is about a decade (40mK-400mK), whereas in URhGe only the zero field data have such a range (25mK-250mK). We are interested in the charge carrier contribution to the thermal conductivity and more precisely in the ratio between the superconducting and normal contribution. For UCoGe, we subtract the "other" contribution to thermal conductivity found previously ($\kappa_{\text{other}} \propto T^2$),

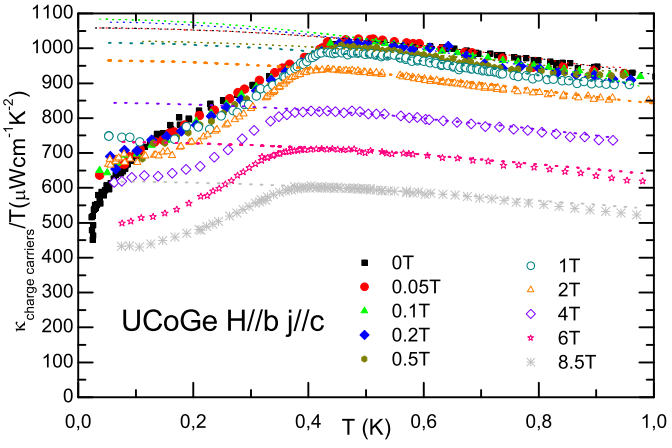

Figure 4.31: (Co-B) Charge carrier contribution to thermal conductivity

and normalize by the normal state behaviour:

$$\begin{aligned} \kappa_{\text{charge carriers}}(T) &= \kappa_{\text{measured}}(T) - \kappa_{\text{other}}(T), \\ \frac{\kappa_{\text{Normal charge carriers}}}{T} &= \frac{L(T)}{\rho_{\text{Normal}}(T)} \\ L(T) &= L_0 \end{aligned} \tag{4.4.5}$$

Of course, this is a rather crude estimation, as inelastic scattering should influence differently $\kappa(T)$ and $\rho(T)$, or in other words, $L(T) = L_0$ should not be exactly constant with temperature and because $\kappa_{\text{other}}(T)$ is only a rough estimation, but this should not influence significantly the discussion and conclusion. For this reason L_0 was adjusted of a few percent (0-3%) for each curve to obtain $\kappa_{\text{charge carriers}}(T_{SC}) = \kappa_{\text{Normal charge carriers}}(T_{SC})$. The normal state resistivity is extrapolated in the superconducting phase from a Fermi-liquid value: $\rho_{\text{Normal}}(T) \propto T^2$. The normal and superconducting part of the thermal conductivity are obtained from 4.4.5 and display on figure 4.31.

Figure 4.32 shows the obtained ratio for the charge carriers contribution: $\kappa_{\text{Superconducting}}/\kappa_{\text{Normal charge}}$ (called κ_S/κ_N for simplicity) versus the reduced temperature T/T_{SC} for magnetic field in b-axis direction. Clearly two different regimes can be identified. At fields above 0.5 Tesla, $\kappa_S/\kappa_N \propto (T/T_{SC})^2$. Below that field κ_S/κ_N decreases faster and almost linearly: $\kappa_S/\kappa_N \propto T/T_{SC}$. Even if we can clearly separate two regimes (solid line shows the first set of points of the other regime in figures 4.32a and 4.32b), we don't detect any phase transition, thermal conductivity evolving smoothly from one temperature dependence to an other. Such a crossover between two regimes is observed in case of a multigaps system. Under large magnetic field, only the bigger gap is effective and the observed thermal conductivity $\kappa_S \propto T^3$ with an additional residual constant κ_0/T term, is consistent for a gap with lines of nodes. At low field and low temperature the small gap governs the temperature dependence of the thermal conductivity.

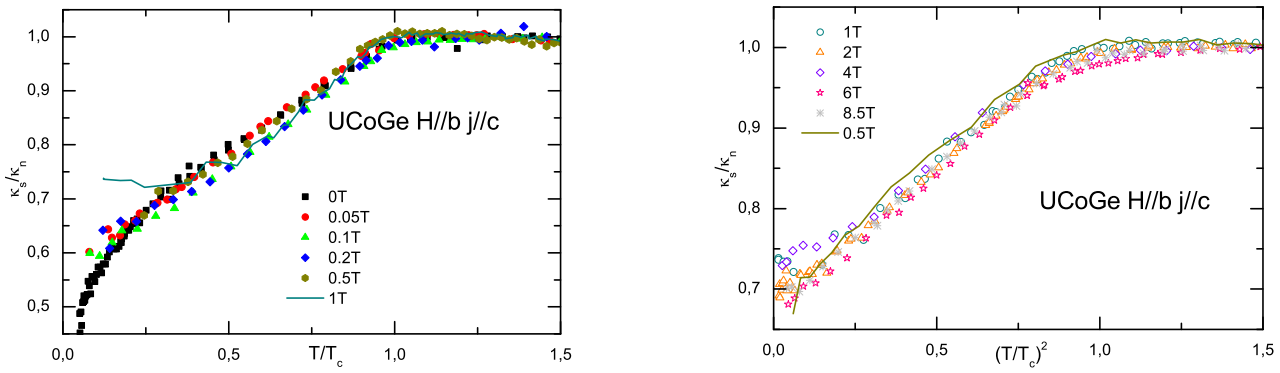

(a) (b)

Figure 4.32: (Co-B) $\kappa_{\text{Superconducting}}/\kappa_{\text{Normal}}$ versus the reduce temperature. Two different regimes can be identify $\kappa_S/\kappa_N \propto T/T_{SC}$ $H < 0.5T$ and $\kappa_S/\kappa_N \propto (T/T_{SC})^2$ $H > 0.5T$.

At this point we can notice that for URhGe (figures 4.12, and 4.13 page 91),the temperature dependence of thermal conductivity in the superconducting state is the same as that of UCoGe at low fields: $\kappa_S/\kappa_N \propto T$ (In this case the analysis is easier as there is no significant "other" contribution, and the normal state thermal conductivity is linear in temperature: $\kappa_N(T)/T \cong$ const..) In URhGe we did not measure the thermal conductivity in the "re-entrant" phase contrary to UCoGe, where the measure of the upper critical field indicates that the high field data are in the "re-entrant" domain. So there are some reasons to believe that the two superconducting domes (overlapping in the case of UCoGe) map to the two different temperature dependences of the thermal conductivity. We can move one step further in our interpretation if we believe in a multigap scenario. Then, at low field, the two gaps would be responsible for superconductivity. This is what we would measure in URhGe (Rh-B) and below about 0.5T in UCoGe (Co-B). Only one of these gap would then account for superconductivity at higher field: above 0.5T in UCoGe (Co-B) and above our experimental possibility in URhGe.

We can try to estimate both gap contributions in the case of UCoGe (Co-B), by assuming that each gap value refers to bands providing parallel channels (ignoring interactions between the bands):

$$\begin{aligned} \kappa_{\text{high field}}(H,T) = &\ \kappa^N_{\text{small }\Delta}(T,H) + \alpha\kappa^S_{\text{big }\Delta}(T,H) + (1-\alpha)\kappa^N_{\text{big }\Delta}(T,H) \\ \kappa_{\text{low field}}(H,T) = &\ \beta\kappa^S_{\text{small }\Delta}(T,H) + (1-\beta)\kappa^N_{\text{small }\Delta}(T,H) \\ &+\alpha\kappa^S_{\text{big }\Delta}(T,H) + (1-\alpha)\kappa^N_{\text{big }\Delta}(T,H) \end{aligned} \tag{4.4.6}$$

Where κ^i_j are the thermal conductivity for $j =$ (big Δ, small Δ), the two gaps contributions and $i =(S,N)$, the superconducting and normal contribution. We supposed that the field dependence of the thermal conductivity (for fields low com-

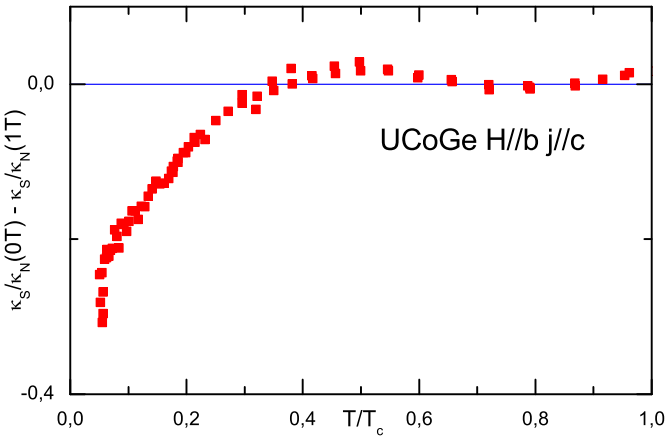

Figure 4.33: (Co-B) In a multigaps scenario, a small magnetic field can supress the effect of one gap. We believe that at 1Tesla, only the large gap contribute to superconductivity, in contrary to 0Tesla where both the small and big gap do. So the difference $\kappa_S/\kappa_N(0T) - \kappa_S/\kappa_N(1T)$ gives an indication of the magnitude of the small gap. As the small gap contributes to thermal conductivity only at temperature below $0.3T_{SC}$ its suggests: $\Delta_{SC\ \text{small gap}} \cong 0.3k_BT_{SC}$.

pared toH_{c2}) can be neglected if we normalize each contribution to the normal state value. Such a normalization suppress the magneto resistance dependence. We want to be sensitive to $\beta(T)$ so we calculate:

$$\frac{\kappa_{\text{high field}}(1T)}{\kappa_{\text{Normal}}} - \frac{\kappa_{\text{low field}}(0T)}{\kappa_{\text{Normal}}} = \beta\left(\frac{\kappa^S_{\text{small }\Delta} - \kappa^N_{\text{small }\Delta}}{\kappa_{\text{Normal}}}\right) \tag{4.4.7}$$

This difference is displayed on figure 4.33. $\kappa^S_{\text{small }\Delta} - \kappa^N_{\text{small }\Delta}$ deviates from zero only below about $0.3T/T_{SC}$. This means that $\Delta_{\text{small gap}} < k_BT$ for $T > 0.3T/T_{SC}$ which gives an estimated value of the small gap for a multigaps scenario.

The electronic contribution to thermal conductivity κ_{el}/T under magnetic field applied in the c-axis direction is presented on figure 4.34. Under magnetic field the superconducting transition is rapidly suppress. The ratio κ_S/κ_N sensibly depends on the extrapolation of the normal phase. Indeed, for fields above 0.5T, the difference between the extrapolated normal state and the measured thermal conductivity is an artifact due to the method used to extrapolate the normal state thermal conductivity. Indeed, in equation 4.4.5 the Lorenz number $L(T) = L_0$ should not be constant in the temperature interval of the extrapolation ($L(T) < L_0$ if there is a lot of inelastic scattering), and the "other" contribution to thermal conductivity may not be simply proportional to the temperature square. For example a phonon thermal conductivity can be $\kappa_{\text{phonons}} \propto T^3$ for the lowest temperatures.

Finally, figure 4.35 shows the field dependence of $\kappa_S/\kappa_N(T \to 0)$. This indicates the proportion of superconducting charge carriers (1 in normal state, 0 fully super-

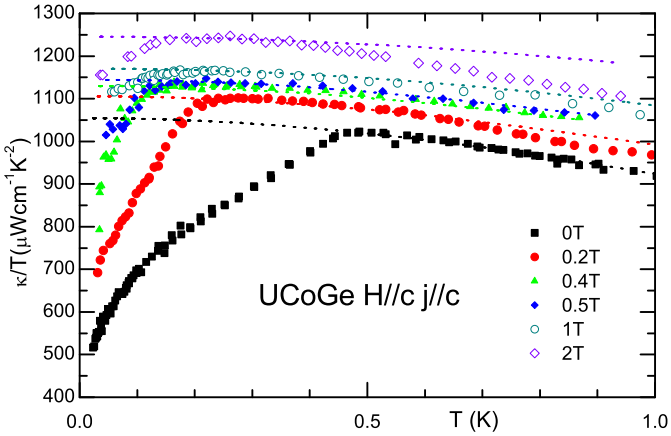

Figure 4.34: (Co-C) Electronic contribution ($\kappa_{el}(T)/T = \kappa_{\text{measured}}(T)/T - \kappa_{\text{other}}(T)$) to thermal conductivity for field applied along c-axis. The contribution of the normal state is calculated from the Wiedemann-Franz law. At low temperature a linear extrapolation gives rise to a normal state contribution that is different from the observed thermal conductivity even above $H_{c2}(0)$, in the normal state. This gives an estimation of the error of our technique to obtain the normal state electronic contribution $\delta\kappa \cong 8\%$.

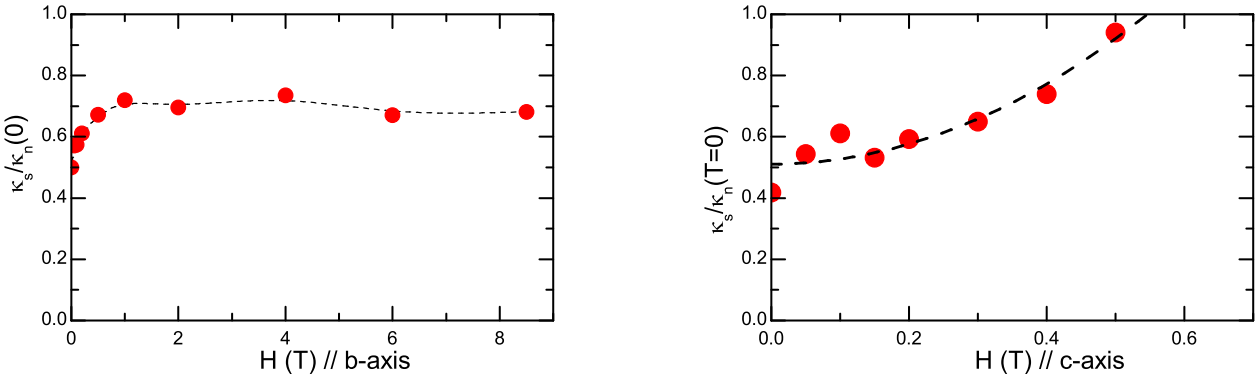

(a) (b)

Figure 4.35: κ_S/κ_N for configurations Co-B and Co-C

conductor). For fields applied along c-axis, the superconducting portion is rapidly suppressed with a field dependence $\kappa_S/\kappa_N \propto H^2$ (dashed line in figure 4.35b). For the field applied in the b-axis direction (figure 4.35a), the result is in good agreement with the two gaps model presented previously. Initial (low field) dependence

due to the suppression of the small gap, high field regime (plateau) controlled by the big gap. For field applied along c-axis the field range is too small to distinguish the two contributions.

Thermoelectric power

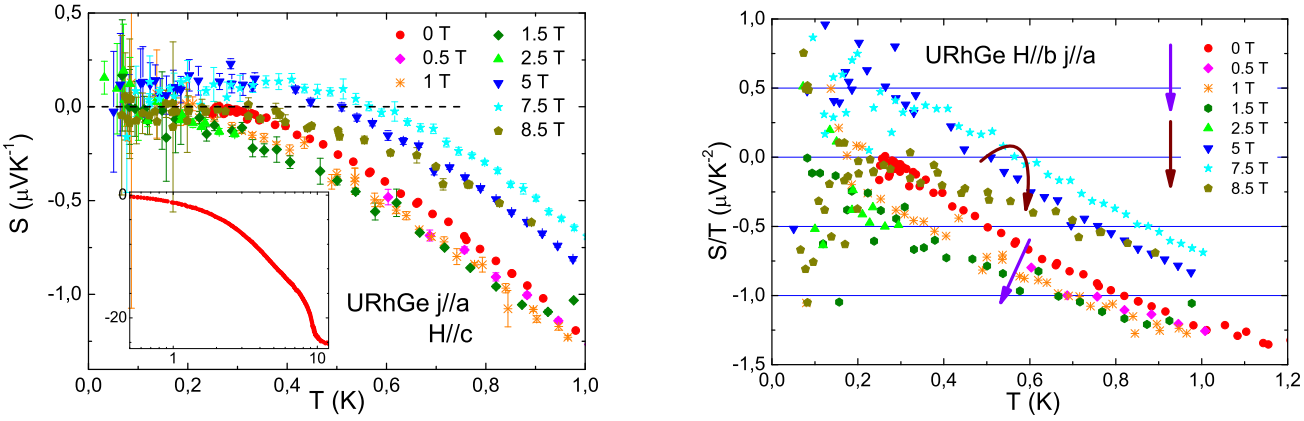

(a) (b)

Figure 4.36: (Rh-B) Thermoelectric power of URhGe. The signal vanishes at low temperature reason why the superconducting transition is invisible. (b) The ratio $S/T(T)$ does not reach the constant value expected in the Fermi-liquid regime down to 300mK.

We performed thermoelectric power measurements in the three different configurations. For URhGe the thermoelectric signal is extremely weak at low temperature and S/T does not reach a Fermi-liquid constant regime down to 300mK (figure 4.36). This behaviour is unexpected compared to the resistive data that followed the expected Fermi-liquid behaviour, but is similar to what is found in the thermal conductivity which only reaches the Fermi-liquid regime ($\kappa \propto T$) below about 200mK owing to inelastic electron-electron scattering (figure 4.13 page 92).

In UCoGe by contrast, an almost constant Fermi-liquid like value of S/T is obtained for magnetic field applied in both c direction and for low field along the b-axis (figure 4.37). With applied field along the b-axis direction the deviation from the Fermi liquid $S/T = const.$ behaviour gets stronger. However, for both field directions, the value extrapolated to $T \to 0$, has a very similar field dependence than the square root of A (figure 4.38), which is expected as both quantities are proportional to the effective mass of the quasi-particles.

With Liam Malone, we measured another sample of UCoGe at LNCMI (high magnetic field laboratory of Grenoble) in magnetic fields up to 22 Tesla. The configuration of this measurement is different than in the previous case, with the heat current applied along the a-axis direction. Magnetic field is applied along b direction.

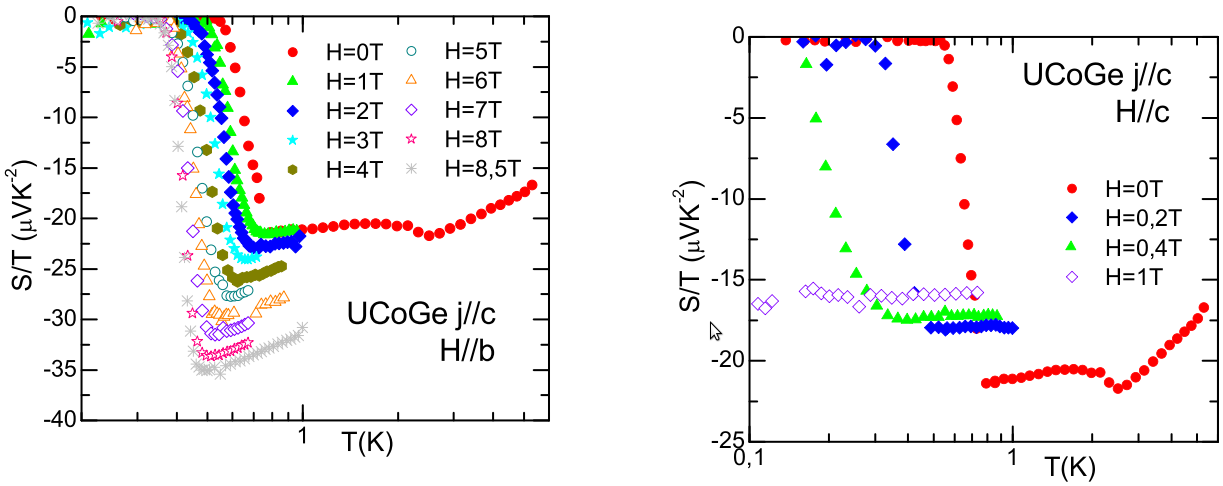

(a) (b)

Figure 4.37: Thermoelectric power of UCoGe, the signal is almost two order of magnitude bigger than for URhGe. The ratio $S/T(T)$ is roughly constant at low field as expected in the Fermi-liquid regime. The temperature dependence deviate from the Fermi-liquid one when magnetic field is applied in the b-axis direction.

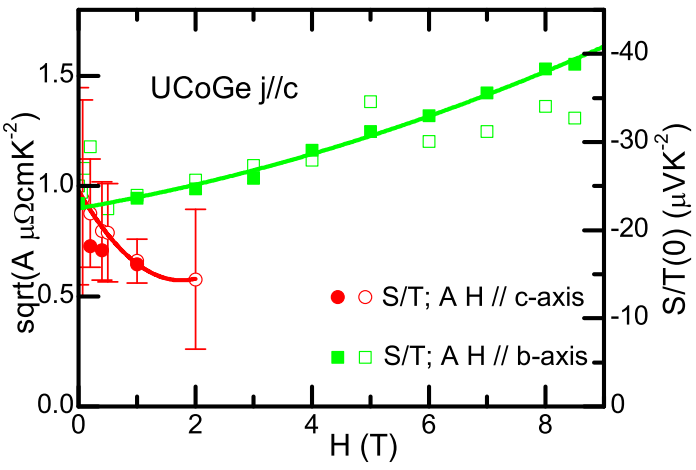

Figure 4.38: Thermoelectric power divided by temperature extrapolated at zero temperature ($S/T(0)$) for magnetic field applied in b and c axis direction. Comparison is made with the square root of the A term of resistivity and revealed a very good match.

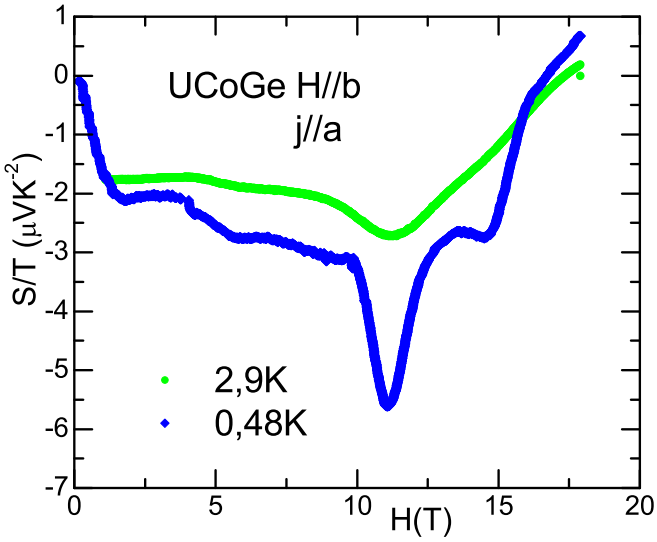

Figure 4.39: High field value of the thermoelectric power. The measurement was performed above T_{SC}, Blue curve in the FM state, green curve above T_{Curie} in the PM phase.

Figure 4.39 shows the thermoelectric power divided by temperature at a constant temperature $S/T(H, T = const.)$. The measurements were done with positive and negative field orientation to cancel any Nernst contribution. The heat gradient was measured with two RuO_2 resistive thermometers that have low magneto-resistance. The absolute value of the thermopower obtained may have a quite large error due to the difficulty to calibrate thermometers under magnetic field and the noise induced by a ramping magnetic field (dS/T ∼20%), but the field dependence is certainly correct. The anomalies observed at low field ($H \leq 4$T), are due to the switching on of the field ramp that creates high noise level and prevents any reliable measurements.

We can then calculate the "Behnia-Jaccard-Flouquet" ratio [Behnia 04] for the differents experiments on UCoGe (for URhGe we cannot extrapolate $S/T(T \to 0)$):

$$q = \frac{S}{T}\frac{N_{Av}e}{\gamma} \tag{4.4.8}$$

Where $N_{Av}e$ = 9.6x10^4 C mol^{-1}, is the Faraday number. The specific heat measured in zero field is: γ = 55mJK^{-2}mol^{-1} [Huy 07] with a decrease of about 25% for field applied in the c-axis direction (5 Tesla) [Hardy 11] and almost no effects for fields applied in the b-axis direction [Aoki 10].

The q ratio obtained is hence very anisotropic depending on the current direction ($\vec{j}$): for H=0T $q(\vec{j} \parallel \vec{c} \cong$-40, $q(\vec{j} \parallel \vec{b} \cong$-3.5. For an isotropic one band model, Behnia et al. [Behnia 04] show that the $|q|$ ratio is inversely proportional to the number of carriers. The anisotropy suggests a highly anisotropic effective mass. Indeed, the specific heat measurement is sensitive to the effective mass integrated over the

full Fermi surface, whereas thermopower probe a given direction. The high value for current applied in the c-axis direction would indicate a maximum and can even suggest the proximity to a singularity in this direction.

The large values $|q| > 1$ suggests a low carrier density in UCoGe. Such a low carrier density was already expected from the very large upper critical field. Indeed, the orbital limit vary as the Fermi velocity of the quasi-particles. The initial slope is given by:

$$\left.\frac{dH_{c2}}{dT}\right|_{T=T_{SC}} \propto \frac{T_{SC}}{v_F^2} \tag{4.4.9}$$

and is large in UCoGe for H‖b-axis. This suggest a small Fermi velocity and hence a large effective mass per quasi-particles. But the specific heat value per mole is rather modest which requires a low density of quasi-particles, in order to be consistent with the large effective mass.

When magnetic field is applied along the b direction, the absolute value of the thermopower divided by temperature ($|S/T|$) is increased up to $H_1 \cong 12$ Tesla where a strong maximum is observed (minimum of S/T). This field correspond to the maximum of the "re-entrant" superconducting phase and roughly to the transition observed in resistivity [Aoki 09] (possible moments reorientation or upper critical field for the ferromagnetic phase). In this case however, the transition is clearly still present above T_{Curie} and H_1 is unaffected by temperature 4.39. At higher field $H_2 \cong 15$ Tesla another minimum is observed that this time disappears above T_{Curie} and can certainly be associated with some properties of the ferromagnetic phase. Finally around $H_3 \cong 16$ Tesla a change of sign of S/T is observed which certainly indicates a strong modification of the Fermi surface at this point.

The two most remarkable features in this experiment are the strong anisotropy with respect to the current direction and the strong minimum observed at a fixed field H_1. As we will discuss in more detail in the next section we attribute these two features to a Lifshitz transition.

4.5 Discussion

Review of the results

We have measured the bulk superconducting transition of UCoGe and URhGe by means of thermal conductivity. Bulk transitions confirm the unusual "re-entrant" shape of the upper critical field. If in URhGe, the bulk transition coincide with the resistive transition, it is absolutely not the case in UCoGe where bulk transition is observed more than 200mK below the resistive one. Such a difference cannot be explained by sample inhomogeneities as the thermal conductivity transition is very sharp, and suggests a large region of filamentary superconductivity. Surprisingly this region is decreased with applied magnetic field.

Thermal conductivity in UCoGe clearly indicates two different regimes for low and high magnetic fields. Two behaviours are observed in the temperature dependence, field dependence and on the upper critical field, with a crossover at about

$H = 0.5T$. These two regimes are consistent with a two-band scenario. For spin triplet superconductivity, in a ferromagnet, it is tempting to map these two superconducting bands with the minority and majority spin bands of the ferromagnetism. A large residual value ($\kappa(T \to 0)$) is observed and indicates that only about 50% of the quasi-particles are superconducting. This may reveal an issue in sample quality and stresses the need to confirm these measurements with higher quality samples.

The temperature dependence of the thermopower in URhGe is unusual (very small value S/T never constant). For UCoGe, we found that $S/T(T \to 0)$ scales with the effective mass determined from A coefficient of resistivity, even if the temperature dependence is not completely constant as expected in the case of a Fermi-liquid. The large value of S/T suggests a low carriers density in this compound. The strong anisotropy and the deep minimum observed around 12 Tesla made us belie that this compound undergoes a Lifschitz transition at this field with an anomaly in the Fermi surface in the [001] direction. Let us now discuss and explain this point.

Interpretation with a Lifshitz transition / Van Hove singularity

Following an idea of Vincent Michal, PhD student from V. Mineev, I want to discuss how a Lifschitz transition / Van Hove singularity can explain several of the features observed in the two compounds: UCoGe and URhGe.

A Lifshitz transition is a modification of the topology of the Fermi surface. The implications of such modifications are anomalies in the density of states (DOS) in the proximity of the Fermi energy. A Van Hove singularity happens if there is a maximum in the DOS.

We can consider a cigar like Fermi surface oriented in the c-axis direction such that the two extremal $(0, 0, k_z)$ points of the Fermi surface are close to the boundary of the Brillouin zone ($k_z < \pi/c, k_z \sim \pi/c$). If the volume of such a Fermi surface is increased, as for example due to the Zeeman energy under magnetic field, the Fermi surface can cross the Brillouin zone. In this case it will undergo a Lifshitz phase transition (figure 4.40).

In a tight binding model such a Fermi surface can be described by:

$$E_{min} - (\mu + Acos(k_x a) + Bcos(k_y b) + Ccos(k_z c)) = 0 \tag{4.5.1}$$

With E_{min} the energy of the bottom of the conduction band, μ the chemical potential, a, b, c the lattice dimensions and A, B, C three constants. For an almost two dimensional Fermi surface as described before we have: $A, B >> C$. One dispersion relation and the DOS are sketched on figure 4.41.

At the Van Hove singularity the DOS diverges weakly (Only two points of the Fermi surface have a singularity). Similarly at $E = E_c$ for the wave vectors $\vec{k} = (0, 0, \pm\pi/c)$, the effective mass diverges and hence the Fermi velocity vanishes. We should note that for higher energy $E > E_c$ there will always be a group of directions in which the derivative of the dispersion relation vanishes and hence where the effective mass diverges. But for these wave vectors, the gradient of the energy will not vanish ($|\vec{\nabla} E| \neq 0$) so that the DOS will remain finite.

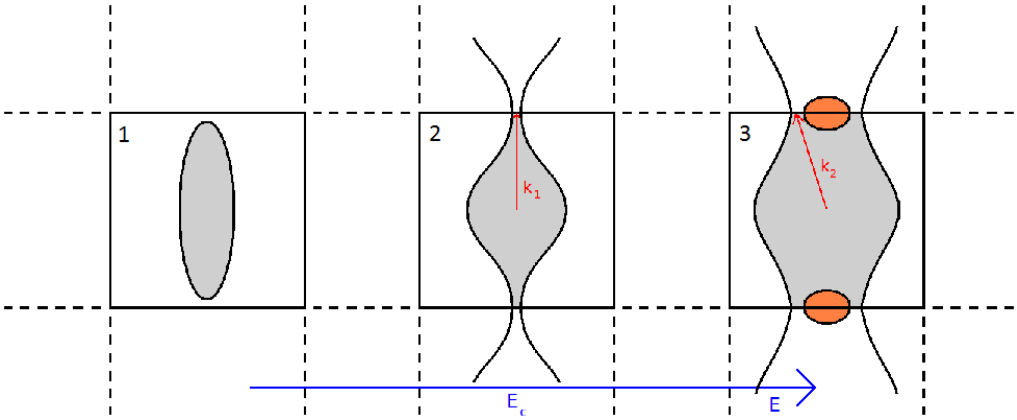

Figure 4.40: Sketch in k-space of a Lifshitz transition. (a) We start with a strongly anisotropic Fermi surface in the first Brilouin zone ($k_x < \pi/a, k_y < \pi/b, k_z < \pi/c$). (b) On increasing the Fermi energy level we reach a point ($E = E_c$) where $k_z = \pi/c$. It is a Lifshitz phase transition as the Fermi surface is modified from a closed one to an open one. $\partial E(k_1)/\partial k_z = 0$ so that the effective mass diverges at this point but also $\vec{\nabla} E = 0$ and the DOS diverges. (c) For higher energy level, the initial Fermi surface is divided in two: an open one (gray) and another small one in the next Brillouin zone (orange). There is still a divergence at the two "hot spots" lines (k_2) but no divergence of the DOS ($\vec{\nabla} E \neq 0$). Hence, the energy E_c corresponds to a Van Hove singularity.

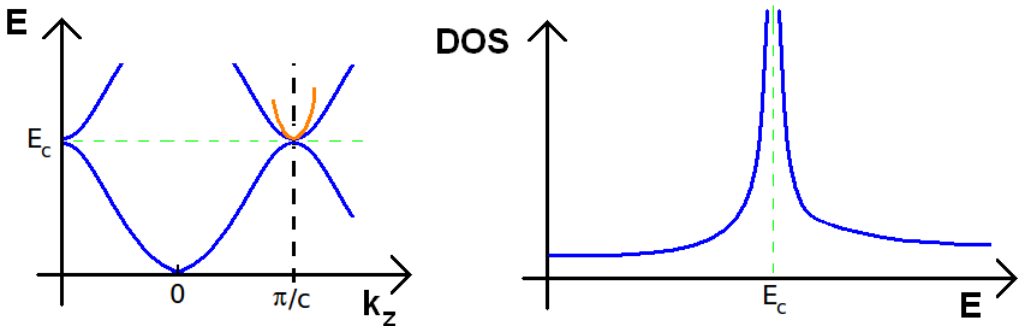

Figure 4.41: Sketch in k-space of a van Hove singularity. On the left the dispersion relation. The singularity happens at E_c. The density of states is calculated as: $DOS(E) = \frac{L^3}{(2\pi)^3} \int_{FS} \frac{dk_1 dk_2}{|\vec{\nabla} E|}$ with $dk_1 dk_2$ an element on the constant energy surface. The DOS vanishes if $|\vec{\nabla} E| = 0$ which happens at E_c for the saddle point: $\vec{k_D} = (0, 0, \pm\pi/c)$. The blue line is the dispersion relation along k_z, the orange one the dispersion relation along $k_{x,y}$ for $\vec{k_D}$.

Such an anomaly in the density of state is in good agreement with the strong minimum measured in thermoelectric power in high field at H_1 and suggest $E = E_c$ at $H \perp \vec{b} \cong 12$ Tesla. The anomaly in the c direction may explain the strong anisotropy. An other interesting property demonstrated by Sandeman et al. [Sandeman 03] is that within the Stoner model, when the density of state shows a maximum a mag-

netization jump can be observed under magnetic field. This is in good agreement with the moments reorientation observed in the URhGe compound at the superconducting "re-entrant" field and also speculated for UCoGe.

We can now analyze the implication of this model on the superconducting upper critical field. Up to date, the models which have been proposed to explain the unusual H_{c2} try to explain an increase of the coupling constant under magnetic field. Miyake et al. [Miyake 08] have mapped this increase to the increase of the effective mass and Mineev [Mineev 10a] calculates the effect of a field applied perpendicularly to the magnetization. Our approach is to consider the effect of this hypothetical Lifshitz transition on the limitation of the superconducting state, namely for triplet superconductors, the orbital limit.

The orbital limitation depends on the Fermi velocity and goes as $\left(\frac{T_{SC}}{v_F}\right)^2$. If the Fermi velocity vanishes the orbital limitation is suppressed. The Fermi velocity entering in the orbital limitation is the cyclotronic one, given by the cyclotronic effective mass: the integrated effective mass over the external diameter of the Fermi surface, perpendicular to the applied field.

With the previous model, on figure 4.43 we plot the Fermi velocity at position $v_{Fx} : (k_x, 0, 0)$, $v_{Fy} : (0, k_y, 0)$ and $v_{Fz} : (0, 0, k_z)$. The energy is taken from the bottom of the conduction band so that we have two different Fermi levels (red lines) for majority (up) and minority (down) spins. When an external magnetic field is applied, the splitting is increased and the Fermi levels are displaced as indicated by the magenta and gray arrows. For a given field, the extremal Fermi velocity v_{Fz} vanishes for the spin up band. So does also the cyclotronic Fermi velocity for a magnetic field applied in the a-b plane and the orbital limitation is suppressed. In our model, this suppression would be at the origin of the unusual shape of H_{c2} and "re-entrance", for fields applied in the a-b plane. We should note that in this model the high field vanishing of the Fermi velocity and corresponding "re-entrance" of superconductivity only happen for Cooper pairs formed with electrons of the up spin band. This corresponds to the two different bands observed with thermal conductivity measurements. The absence of real "re-entrance" for field applied along the a direction can be explained as the band splitting from such a field is a factor two smaller than for fields applied along the b direction, as deduced from the different magnetizations curves. Complete suppression of the orbital limit and hence superconductivity should then be observed around 30 Tesla for UCoGe. This has not been observed maybe because this field is too high for usual experimental setups, but at such a high field superconductivity might also be limited by the paramagnetic limit. Indeed, even for triplet superconductivity this limit still exist for fields perpendicular to the magnetization and is of the order of the exchange field [Mineev 10b].

Gor'kov et al. [Gor'kov 06] calculate that the divergence of the cyclotronic effective mass is logarithmic in energy in this model. Even if in a less pronounced manner, we should note that the Fermi velocity is also decreased, with applied field, for Cooper pairs formed from electrons of the down spin band. This decrease may explain the unusual curvature of H_{c2} for fields applied in the c-axis direction. In this case the variation of Fermi velocity is linear ($k_{Fa} << \pi/a$ and $k_{Fb} << \pi/b$).

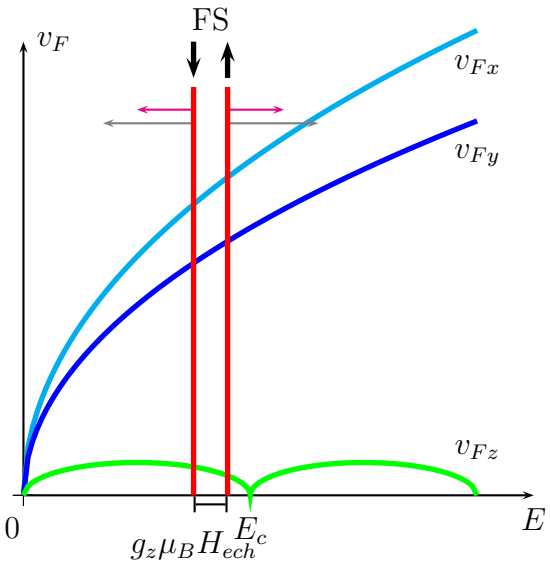

Figure 4.43: Extremal Fermi velocity and Fermi levels (red lines) versus the energy from the bottom of the conduction band for majority and minority spins. Upon applying magnetic field the splitting is increases (magenta and gray arrow). At a critical value, the Fermi velocity for the majority band vanishes ($\vec{k} = (0, 0, \pi/c)$). Scales between the different directions are not respected in this scheme, the anisotropy should be much larger.

Similarly to the case of $CeCoIn_5$, we can fit the upper critical field within an Eliashberg strong coupling model:

$$T_c(H=0)/\Omega = \Psi(\lambda_{11}, \lambda_{22}, \lambda_{12}, \lambda_{21}, \mu^\star), \tag{4.5.2}$$

$$T_c(H) = \Phi(T_c(H=0), \lambda_{11}, \lambda_{22}, \lambda_{12}, \lambda_{21}, \mu^\star, v_{F1}(H), v_{F1}(H)), \tag{4.5.3}$$

Where Ψ and Φ are calculated numerically in a two-band model. Ω a characteristic temperature of the coupling mechanism is assumed to be constant. The coupling in the two bands is set to the same values as the two bands represent the splitting of a unique one : $\lambda_{11} = \lambda_{22} = 2$. We expect the coupling between band to be much weaker and set $\lambda_{12} = \lambda_{21} = 0.5$. $\mu^\star$, the coulomb pseudo-potential is fixed to a typical value of 0.15. So that the only free parameters are $v_{F1}(H)$ and $v_{F2}(H)$.

To account for the divergence of the effective mass when the magnetic field is applied in the a-b plane, the Fermi velocity is set to vary as:

$$\begin{aligned} m^\star(H)_i &= m_0 + x \cdot \log\left(1 + \frac{|H - H_{\text{crit, }i}|}{a}\right) \quad i = 1, 2 \\ v_{Fi}(H) &= v_{F0} \frac{1 + \alpha \cdot \log\left(1 + \frac{|H^i_{\text{crit}}|}{a}\right)}{1 + \alpha \cdot \log\left(1 + \frac{|H - H^i_{\text{crit}}|}{a}\right)} \end{aligned} \tag{4.5.4}$$

Hence the parameters of the problem becomes: v_{F0} set to be identical for the two bands and given by the initial slope of H_{c2}, $\alpha = x/m_0$,a and H^i_{crit}.

When the magnetic field is applied along the c-axis, we reduce the model to one band, assuming only the one which Fermi velocity decreases is important. The Fermi velocity is taken to vary linearly (no singularity in this direction):

$$v_F = v_{F0} \frac{m^\star(H=0)}{m^\star(H)} = v_{F0} \frac{1}{1 + tH} \tag{4.5.5}$$

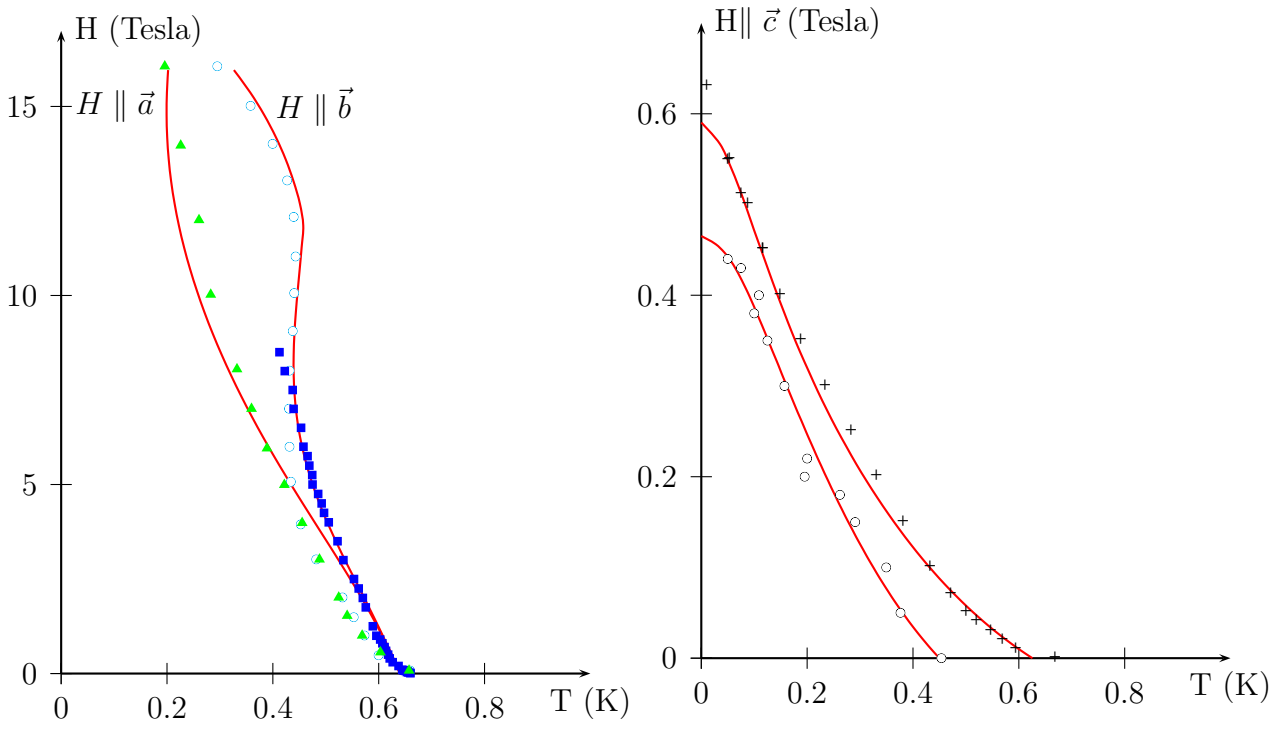

(a) (b)

Figure 4.44: Fits (red lines) of H_{c2} for UCoGe. The dependence of the Fermi velocity given by a tight-binding model with a Lifshitz singularity. The fits are compared with experimental resistive superconducting transitions from this experiment ($H \parallel \vec{c}$ crosses and $H \parallel \vec{b}$ squares) and from [Aoki 09] ($H \parallel \vec{a}$ and $H \parallel \vec{b}$ circles). In the c-axis direction also made the comparison with the bulk transition obtained from $\kappa(T)$ circles.

t is another parameter of the problem. Fits given by adjusting manually the different parameters are shown compared to resistive data on figure 4.44. The parameters used are the following:

	$H \parallel$ b-axis	$H \parallel$ a-axis	$H \parallel$ c-axis *
Ω	3.3 (K)	3.3 (K)	2.8 (K)
$\lambda_{11} = \lambda_{22}$	2	2	2
$\lambda_{11} = \lambda_{21}$	0.5	0.5	-
v_{F0}	$2.7 \cdot 10^3$ (m/s)	$2.7 \cdot 10^3$ (m/s)	$17 \cdot 10^3$ (m/s)
α	25	25	-
a	2 (T)	2 (T)	-
$H^1_{\text{crit.}}$	-5 (T)†	-5 (T)†	-
$H^2_{\text{crit.}}$	12 (T)	30 (T)	-
t	-	-	1.03 T^{-1}
$\mu^\star$	0.15	0.15	0.15

Even if the fits are not perfect, the qualitative agreement is surprisingly good and for the first time we suggest a mechanism for the unusual curvature of H_{c2} for UCoGe that can account for the anomalies in the three fields directions. The fit is especially good for the re-entrance when field is applied along the b-axis. We observed some deviation in the a-axis direction but we also found that the transition curve H_{c2}measured by resistivity depends on the sample. For the c-axis an increase of 40% (35%) of the mass of the up band at 0.5 Telsa is needed to fit correctly the resistive data (and bulk transition respectively). This would corresponds to a decrease of the volume of the minority band of a similar amount and seems unlikely as no saturation is observed up to 5 Tesla in the magnetization in this direction [Huy 08]. Due to the large numbers of parameters, the fits are not a proof of the validity of this model, but they demonstrate that such a model can account for the unusual positive curvature of H_{c2}.

Of course a quantitative fitting with a full simulation of the problem as well as comparison to bulk transition measurements up to high field are still needed to improved and check this model. Nevertheless, the Lifshitz transition scenario can clearly explain several of the features observed in the ferromagnetic superconductors UCoGe and URhGe. Of course the best way to check this idea would be to measure directly the Fermi surface with de Haas van Alphen measurements for example.

*One band model in this case.

†Negative value for spin down band as Zeeman splitting drive the system away from the singularity

5 Conclusion

5.1 Achievements

In this thesis, we investigate the superconducting phase diagram of the compounds $CeCoIn_5$, UCoGe and URhGe. In these compounds we try to relate the superconducting phase and quantum criticality.

In heavy fermions, one usually finds that superconductivity appears at a magnetic phase transition, with the maximum of superconductivity occuring close to the point where one could extrapolate the phase transition at $T = 0$ in the absence of superconductivity. Because in this region of the phase diagram physical quantities as specific heat, resistivity and others do not follow the temperature dependences expected for a Fermi-liquid, it is believed that a quantum critical point (QCP) would occur, at this point, in the absence of superconductivity. The proximity of the two phenomena also suggests that the interaction responsible for the pairing in the superconducting state originates from spin and not charge polarization as in the BCS theory.

This image was challenged by the pressure phase diagram of the compound $CeCoIn_5$ in which there are not one, but two characteristic pressures between the maximum of T_{SC} and other physical anomalies that can be related to a QCP. This unusual behaviour had triggered unconventional propositions for the link between superconductivity and quantum criticality. One of them was that, in $CeCoIn_5$, quantum criticality was limiting the superconducting phase notably at $H_{c2}(0)$. With precise measurements of the position of the QCP wit respect to H_{c2}, we could rule out this proposition.

The inconsistency between $H_{c2}(0, p)$ and $T_{SC}(p)$ had never been treated, hence, using previously published data [Miclea 06] and the new measurements from G. Knebel up to higher pressures [Knebel 10] we proposed a new scenario for this compound. We suggest that if at a QCP the coupling constant and the superconducting gap Δ are indeed maximum, thermal fluctuations in the vicinity of the QCP also acts as a pair-breakers and hence the maximum of T_{SC} is not necessarily located at the QCP. Two different positions for the QCP and maximum of T_{SC} were already predicted by Monthoux and Lonzarich [Monthoux 01] for magnetically mediated superconductivity. The effect of pair-breaking by magnetic impurities was also observed in $CeCoIn_5$ through the unusually large specific heat jump [Petrovic 01, Kos 03]. We demonstrate that this scenario can explain the unusual shape of H_{c2} in $CeCoIn_5$.

Another issue for the understanding of the relation between a QCP and superconductivity is the type of QCP that would occur in the absence of superconductivity. With our resistive measurements on $CeCoIn_5$ we obtained the field dependence of the Fermi liquid boarder (T_{FL}). This dependence is not compatible with the conventional spin fluctuations scenario of Hertz and Millis. It suggests a dynamical exponent $z \cong 1$ contrary to the expected value of $z = 2$ for itinerant anti-ferromagnetism in 3D, and the collapse of a single energy scale for T_{FL} and the divergence of the A term of resistivity. These results are in favor of either "unconventional" scenarios or a localized magnetism in the AFM phase.

In a second part, we performed the first measurements of thermal conductivity on the ferromagnetic superconductors UCoGe and URhGe. With these measurements we probed for the first time the bulk superconducting transition and confirmed the unusual shape observed by resistivity with a linear dependence (URhGe) or even an upward curvature (UCoGe) of H_{c2}. However in UCoGe we found that the bulk transition happens at a temperature much lower ($\sim$ 200mK) than the resistive transition, indicating a large range of filamentary superconductivity. This observation together with the large ($\sim$50% normal phase) residual term of $\kappa/T(T \rightarrow 0)$ observed for both compounds may indicate some issues with the samples quality and emphasizes the need of further measurements on better quality samples.

Nevertheless, analysis of the temperatures and field dependences in UCoGe leads to two conclusions. First we observed that carriers others than electrons contribute to heat transport in this compound down to the lowest temperature. This contribution may be due to uniaxial spins fluctuations as it is weaken by a magnetic field applied along the spontaneous magnetization direction. Such uniaxial fluctuations were already observed in this compound by NMR measurements [Ihara 10]. Secondly, we found two clearly different regimes between low ($H < 0.5$T) and high ($H > 0.5$T) fields for both temperature and field dependences of $\kappa(T)/T$. The transition between the two regimes is a crossover. Such behaviour is expected in a two-band model for superconductivity with only one superconducting band at high field and in the "re-entrance" domain.

Our measurements of thermoelectric power are compatible with a low carrier density in the case of UCoGe. They reveal a strong anisotropy between the current directions $\vec{j} \parallel \vec{c}$ and $\vec{j} \parallel \vec{a}$. We also observed a strong minimum at a field similar to the one of the superconducting "re-entrance" for $H \parallel \vec{b}$. This minimum is unrelated to the ferromagnetic phase, as it is observed above and below T_{Curie}.

We show that a Lifshitz phase transition is an interesting explanation for most of the observed effects. In particular, unlike previous scenarios, it can account for the unusual dependence of H_{c2} for the different fields orientations and reproduces accurately the re-entrance observed for fields applied along the b crystallographic direction.

5.2 Prospectives

Our measurements on $CeCoIn_5$ are strongly in favor of the usual scenario for the appearance of superconductivity in heavy fermions: the interaction between quasi-

particles leading to the formation of Cooper pairs is maximum at a QCP. But as calculated by Monthoux and Lonzarich [Monthoux 01], this maximum of interaction does not coincide with a maximum of T_{SC} due to pair-breaking effects in the proximity of the QCP. The mismatch between maximum of T_{SC} and maximum of pairing is not observed in other conventional heavy fermions because it is effective only for strong coupling constant λ (remember $CeCoIn_5$ as the record T_{SC} among cerium or uranium based superconductors). We can hence predict that a similar phase diagram should be observed in other strongly correlated compounds with strong coupling constants. A first natural candidate is $PuCoGa_5$. This compound is similar to $CeCoIn_5$ but with a much higher superconducting transition: $T_{SC} = 18.5K$ in $PuCoGa_5$ instead of $T_{SC} = 2.3K$ in $CeCoIn_5$. Hence the coupling constant should also be stronger and hence, the mismatch between maximum of T_{SC} and QCP.

For the ferromagnetic superconductors, comparison with better quality samples of the thermal conductivity is very important in order to confirm our finding and extract some quantitative informations about the symmetry of the gap and the possible contribution of uniaxial spins fluctuations. Our measurements of the bulk transition of superconductivity was limited to 8.5 Tesla in this experiment. It would be very interesting to pursue these measurements to obtain the full bulk H_{c2} for both UCoGe and URhGe. Finally, we only investigate a few of the possible orientations for current and magnetic field directions in the thermal transport measurements but as the anisotropy seems to be an important parameter of the problem other configurations should certainly also be probed.

We proposed a simple model for the unusual physical properties and H_{c2} of UCoGe and URhGe with a field induced Lifshitz transition. We want to improve this model calculating the angular dependence of H_{c2} in these two compounds.

The End

6 Résumé en Français

Petit résumé en français des différents chapitres de cette thèse.

Introduction

Les composés à fermions lourds sont caractérisés par de fortes corrélations du au fait que les électrons, généralement d'orbitales atomiques 4f ou 5f, ne participent pas complétement à la bande de conduction. Le caractère " localisé"de ces électrons fait qu'ils peuvent interagir soit entre eux par interaction indirecte RKKY, soit avec les électrons de la bande de conduction par l'effet Kondo. Du fait de la compétition ente ces deux mécanismes, les fermions lourds sont proches de transition de phase, entre une phase magnétique où l'interaction RKKY dominerait et une phase paramagnétique. Expérimentalement les mesures sous pression de ces composés révèlent souvent une phase supraconductrice, à basse température, à proximité de cette transition de phase (figure 1.1).

On observe dans la phase paramagnétique que le domaine de Liquide de Fermi disparait ($T_{FL} \to 0$) exactement a la position ou serait extrapolé la transition de phase (AFM-PM par exemple) en absence de supraconductivité. De même à des températures supérieures de ce point, on observe des lois dite de non liquide de Fermi pour la dépendance en température de certaines quantités physiques ($\rho(T) \propto T$, $\gamma(T) \propto -T\log(T)$,...). Ces observations suggèrent la présence d'un point critique quantique à la transition de phase: phase magnétique - phase paramagnétique à $T = 0$ caché par l'ordre supraconducteur.

Il est généralement admis et observé que l'interaction de couplage des pairs de Cooper est maximum au point critique quantique. Cependant, si ce couplage est d'origine magnétique, des impuretés magnétiques dans le composé vont agir comme briseur de pairs. Or les fluctuations du paramètre d'ordre magnétique associées au point critique quantique vont justement agir comme des impuretés magnétiques. On ne s'attend donc pas forcément a observer un maximum dans la température de transition supraconductrice T_{SC} au point critique quantique, mais a une certaine distance constituant un compromis pour une interaction de couplage forte et des effets de brisure de pairs limités (pas trop de fluctuations magnétiques).

Dans cette thèse on a étudié l'interaction entre supraconductivité et point critique quantique. Dans un premier temps en localisant la position de points critiques

quantiques sous champ et sous pression dans le composé $CeCoIn_5$, puis en étudiant l'interaction de couplage obtenue par l'étude du second champ critique supraconducteur (H_{c2}). On s'est également intéressé à la nature du point critique quantique.

Dans les supraconducteurs ferromagnétiques URhGe et UCoGe on à également étudié le second champ critique H_{c2} en déterminant la transition supraconductrice " bulk", avec des mesures de conduction thermique. Nous proposons un modèle de transition de Lifshitz pour essayer de comprendre la forme inhabituel de H_{c2} dans ces composés. Les autres résultats expérimentaux (dépendance de la conduction thermique en champ et en température dans la phase supraconductrice, mesure de pouvoir thermoélectrique, ...) sont aussi discutés.

Montages expérimentaux

Les mesures présentée dans cette thèse sont réalisées dans un frigo à dilution. La gamme de températures utilisées avec les montages présentés est d'environ 8mK-10K pour des champs magnétiques allant de 0 à 8.5 Tesla.

Deux montages expérimentaux on été réalisés durant cette thèse pour les mesures de résistivité ainsi que pour les mesures de conduction thermique (figures 2.2 et 2.11). Les principales différence avec les montages précédents déjà monté dans le laboratoire sont les suivantes:

- Le matériel utilisé pour les montage est l'argent au lieu du cuivre utilisé précédemment. L'avantage est que la chaleur spécifique hyperfine de l'argent est beaucoup plus faible que celle du cuivre ce qui permet des changements de températures beaucoup plus rapide sous champ magnétique a basse températures.
- Installation d'un mécanisme de rotation (piezo-rotator) qui permet d'orienter a froid les échantillons par rapport au champ magnétique.

Pour améliorer la qualité des mesures de résistivité nous avons installé des transformateurs à 4K. Pour utiliser les capacités maximums de ces transformateurs (gain d'un facteur 1000), nous avons minimisé la résistance des contactes sur les échantillons en déposant par évaporation du Titane et de l'or avant de faire les contactes (micro-soudure). Nous avons également cherché a minimiser les vibrations de l'expérience par exemple en pré-refroidissant l'hélium afin qu'il pénètre dans la boite à 1K à l'état superfluide.

La conduction thermique est mesurée a l'aide d'un chauffage (résistance film métallique) connecté a un bout de l'échantillon alors que l'autre extrémité est fixée au frigo. Deux thermomètres mesurent la température de l'échantillon entre ces deux point. La conduction thermique est la puissance traversant l'échantillon divisée par le gradient thermique. Il est important que l'échantillon soit bien isolé de l'extérieur afin que le courant de chaleur passe intégralement a travers l'échantillon et que les thermomètres soient à la température de l'échantillon. Pour cela nous avons utilisé des fils intégralement supraconducteur (NbTi pure). Ces fils constituent des isolants presque parfait dans leur phase supraconductrice et ont une résistance élevée dans la phase normale. Finalement des charbons actifs ont été ajouté dans le calot de la dilution pour garantir un bon niveau de vide.

$CeCoIn_5$

Dans les fermions lourds, on observe généralement que l'interaction de couplage est maximum au point critique quantique. Un paramètre expérimental qui permet de sonder la valeur du couplage est le second champ critique supraconducteur. En effet de la constante de couplage fort λ, dépend de la valeur de la transition supraconductrice, mais aussi la renormalisation de la masse effective qui modifie la vitesse de Fermi des quasi-particules et par conséquent la limite orbitale. La valeur de λ modifie aussi le rapport Δ/T_{SC} et donc la valeur de la limite paramagnétique $H_{Pauli} = \Delta/g\mu_B$.

Dans le composé parent $CeRhIn_5$ on observe clairement que le maximum de λ correspond à la position sous pression du point critique quantique. En effet le maximum de T_{SC}, le maximum de pente initiale dH_{c2}/dT, le maximum de masse effective mesuré par le terme A de résistivité ou ou par effet de Haas, le maximum du saut de chaleur spécifique à T_{SC} $\Delta C/C$ et le maximum de $H_{c2}(0)$ sont tous observé à la même pression p_c (figure 3.7). Dans ce composé on comprend que l'interaction d'appariement est maximum au point critique quantique. p_c correspond à la pression où aurait lieu la transition AFM-PM à $T = 0$ en absence de supraconductivité.

La situation est différente pour $CeCoIn_5$. Dans ce composé, le maximum de T_{SC} est observé à $p = 1.3GPa$, alors qu'aucune phase AFM n'est directement observée et que les paramètres $(\Delta C/C)_{T_{SC}}$, ρ_0, la pente initiale dH_{c2}/dT pour les deux orientations possible du champ magnétique et $H_{c2}(0)$ pour $H \parallel [001]$ ne présentent pas d'anomalie à cette pression.

Si aucune phase AFM n'est directement observée dans $CeCoIn_5$, une phase de coexistence de la supraconductivité avec un ordre AFM est observée à haut champ basse température pour $H \parallel [100]$ (possible phase FFLO). Pour une direction de champ $H \parallel [001]$ plusieurs expérience ont suggéré la présence d'un point critique quantique exactement à $H_{c2}(0)$. Pour ces raisons, on pense que dans ce composé une phase AFM se développerait en absence de supraconductivité à bas champs basse pression mais que cette phase est entièrement cachée par la supraconductivité.

Dans une première partie nous avons mesuré la résistivité de trois échantillons juste au dessus du champ critique ($H_{c2}(0)$) pour suivre le domaine de liquide de Fermi et étudier la coexistence ou non d'un point critique quantique avec $H_{c2}(0)$. Dans un liquide de Fermi, la dépendance en température de la résistivité est: $\rho(T) = AT^2 + \rho_0$. Un des échantillons utilisé à la même géométrie qu'utilisée dans les expériences précédentes $\vec{j} \parallel [100]$, $H \parallel [001]$. Cette géométrie à l'inconvénient d'être sensible aux effets de magnéto-résistance à basse température ($\omega_c\tau > 1$), ces effets rendent impossible la détermination d'un domaine de liquide de Fermi à basse température ($T > 80mK$). Les deux autres échantillons ont une géométrie plus favorable $\vec{j} \parallel [001]$, $H \parallel [001]$. De plus le dernier échantillon est dopé (1% La a la position du Co) pour diminué le libre parcourt moyen τ.

Cette expérience nous permet de montrer clairement qu'il n'y a pas de coïncidence entre $H_{c2}(0)$ et le point critique quantique. Un régime de liquide de Fermi est en effet observé en dessous de 50/100 mK pour les deux derniers échantillons respectivement juste au dessus de $H_{c2}(0)$. Au point critique quantique, il est prédit que le terme A de la résistivité diverge. La dépendance aux paramètres de contrôle

(le champ magnétique dans ce cas) de la limite du domaine de liquide de Fermi est prédit de varier comme: $T_{FL} \propto (H - H_{QCP})^{z/2}$ avec z l'exposant dynamique. Dans les théorie SCR principalement développée par Hertz-Millis-Moriya, cet exposant vaut $z = 2$. Nous avons observé que pour que la divergence du terme A et la valeur a laquelle T_{FL} s'annule coïncide (position du point critique quantique), cet exposant devait être de $z \cong 1$ ce qui peut refléter soit le manque de prédiction théorique pour un point critique induit sous champ magnétique ou une nature différente du point critique que celle prédite par la théorie SCR. Les dépendances sous champ de T_{FL} et A correspondent par contre à l'annulation d'une seule énergie caractéristique au point critique quantique.

Cette première expérience ne permet pas d'expliquer la forme inhabituel du champ critique de $CeCoIn_5$ sous pression. Dans un deuxième temps nous avons donc chercher à expliquer les courbes de $H_{c2}(T)$ de $CeCoIn_5$ à différentes pressions. Pour cela nous avons découplé la variation du T_{SC} de la constante de couplage fort λ en ajoutant des effets de brisure de pair par des impuretés magnétiques. Ces ajouts nous permettent de " fitter"parfaitement les courbes de $H_{c2}(T)$ sous pressions pour deux orientations du champ (figures 3.21, 3.22 et 3.23). Les paramètres variables du fit sont la constante de couplage fort λ, une énergie caractérisant le nombre d'impuretés magnétiques T_M ainsi que les facteur gyromagnétiques pour les deux orientation du champ g_a et g_c. Ces paramètres sont constant sous champ mais peuvent varier avec la pression. Le résultat est que pour ces quatre paramètres un maximum est observé à $p \cong 0.4GPa$ (figure 3.28). Nous pensons qu'à cette pression un point critique quantique serait observé en absence de supraconductivité. Ce résultat suggère aussi que l'interaction d'appareillement tout comme le processus de brisure de pair sont liés au point critique quantique. Le maximum de transition supraconductrice T_{SC} est ensuite naturellement décalé du fait de la compétition des deux effets. Un pareil effet d'un point critique quantique est prédit pour une supraconductivité dont l'origine du couplage est magnétique. Pour cette raison nous pensons que $CeCoIn_5$ est le premier exemple élucidé d'un supraconducteur quasi-bidimensionnel a couplage magnétique fort et un composé modèle pour ce type de couplage. Le fait que dans des composés similaire ont observe pas ce décalage entre position du point critique quantique et maximum de T_{SC} est certainement du à la valeur de la constante de couplage forte (λ doit être grand pour que le décalage soit significatif).

Ces deux expériences nous permettent de redessiner le diagramme de phase de $CeCoIn_5$ (figure 3.30).

Supraconducteurs ferromagnétiques

Nous avons effectué les première mesures de conduction thermiques a basses températures sur les composés ferromagnétiques supraconducteurs URhGe et UCoGe. Les mesures montrent un grand terme résiduel ce qui suggère que la qualité des échantillons n'est pas parfaite. Néanmoins, la loi de Wiedemann-Franz est bien obéie ce qui montre une bonne qualité des mesures. Le principal résultat de ces mesures est la détermination de la transition " bulk"supraconductrice dans ces deux composés.

Nos mesures confirment la forme inhabituelle avec une courbure positive du second champ critique H_{c2}. Pour l'échantillon URhGe, la transition déterminée par conduction thermique correspond parfaitement (à l'incertitude de la mesure prêt) avec celle déterminée par mesure de résistivité (figure 4.27). La situation est différente pour UCoGe. Dans ce composé, la transition supraconductrice déterminée par mesures de conduction thermique est observée $\sim 200mK$ en dessous de celle observée par résistivité. Cette différence suggère une supraconductivité filamentaire dans cet intervalle (figures 4.29 et 4.28).

On ne peut tirer que des conclusions partielles de la dépendance en champ et en température de la conduction thermique du fait du problème de qualité des échantillons. Cependant, dans le composé UCoGe, on a observé une valeur élevée jusqu'au plus basses températures du rapport L/L_0 de la loi de Wiedemann-Franz ce qui suggère un autre canal que les électrons pour la conduction thermique. Nous pensons que cela reflète la présence de fluctuations magnétiques (magnons). Dans ce même composé, lorsque le champ magnétique est appliqué selon l'axe $\vec{b}$, on observe deux dépendance en température différentes pour la conduction thermique entre faible ($H < 0.5T$) et haut champ. De même la valeur résiduel a une dépendance en champ différente. Ces deux effets pourraient s'expliquer avec un scenario à deux bandes. A bas champs, les deux bandes seraient supraconductrice alors qu'a haut champ seule une bande le serait.

Finalement, nous proposons un modèle de transition de Lifshitz pour expliquer la " ré-entrance"et la courbure inhabituel du champ critique dans le composé UCoGe. Dans ce modèle, la limite orbitale est supprimée sous champ magnétique du à la divergence de la masse effective à l'instabilité de Lifshitz. Sans modifier la couplage d'appariement, la suppression de cette limite permet de reproduire le champ critique observé.

Conclusion

En conclusion, dans cette thèse on à montré que:

- Dans le composé $CeCoIn_5$ il n'y a pas de réel coïncidence entre $H_{c2}(0)$ et le point critique quantique.
- La forme du champ critique H_{c2} dans $CeCoIn_5$ peut être expliquée avec la présence d'un point critique quantique induit sous pression $p \cong 0.4GPa$ et avec l'inclusion d'effet de brisure de paires dus a des impuretés magnétiques liées au point critiques quantiques. Ces résultats nous font dire que $CeCoIn_5$ est un modèle de supraconducteur quasi-bidimensionnel d'interaction magnétique.
- Nous avons réalisé les premières mesures de conduction thermique à basse températures dans les composés URhGe et UCoGe. Ces mesures nous permettent de montrer que la courbure inhabituel du champ critique précédemment observée par résistivité est une propriété " bulk".
- Nous proposons un modèle de transition de Lifshitz pour expliquer cette courbure et la " ré-entrance"de la supraconductivité observée dans ces deux composés.

Bibliography

[Akazawa 04] T Akazawa, H Hidaka, T Fujiwara, TC Kobayashi, E Yamamoto, Y Haga, R Settai & Y Onuki. *Pressure-induced superconductivity in ferromagnetic UIr without inversion symmetry.* J. Phys.: Condens. Matter **16** (2004) L29–L32.

[Aoki 01] Dai Aoki, Andrew Huxley, Eric Ressouche, Daniel Braithwaite, Jacques Flouquet, Jean-Pascal Brison, Elsa Lhotel & Carley Paulsen. *Coexistence of superconductivity and ferromagnetism in URhGe.* Nature **413** (2001) 613–616.

[Aoki 09] Dai Aoki, Tatsuma D. Matsuda, Valentin Taufour, Elena Hassinger, Georg Knebel & Jacques Flouquet. *Extremely Large and Anisotropic Upper Critical Field and the Ferromagnetic Instability in UCoGe.* J. Phys. Soc. Jpn. **78** (2009) 113709.

[Aoki 10] Dai Aoki. *private communication* (2010.) .

[Ashcroft 76] N. W. Ashcroft & N. D. Mermin. Solid state physics. Harcourt College Publishers (1976) .

[Bang 04] Yunkyu Bang & A. V. Balatsky. *Anomalous specific-heat jump in the heavy-fermion superconductor $CeCoIn_5$.* Phys. Rev. B **69** (2004) 212504.

[Bauer 05] E. D. Bauer, C. Capan, F. Ronning, R. Movshovich, J. D. Thompson & J. L. Sarrao. *Superconductivity in $CeCoIn_{5-x}Sn_x$: Veil over an Ordered State or Novel Quantum Critical Point?* Phys. Rev. Lett. **94** (2005) 047001.

[Behnia 04] K Behnia, D Jaccard & J Flouquet. *On the thermoelectricity of correlated electrons in the zero-temperature limit.* J. Phys.: Condens. Matter **16** (2004) 5187–5198.

[Benlagra 09] Adel Benlagra. *Criticalité Quantique dans les Bi-couches d'He^3 et les composé à Fermions Lourds.* PhD thesisUniversité de Paris XI (2009) .

[Bianchi 02] A. Bianchi, R. Movshovich, N. Oeschler, P. Gegenwart, F. Steglich, J. D. Thompson, P. G. Pagliuso & J. L. Sarrao. *First-Order Superconducting Phase Transition in $CeCoIn5$*. Phys. Rev. Lett. **89** (2002) 137002.

[Bianchi 03a] A. Bianchi, R. Movshovich, C. Capan, P. G. Pagliuso & J. L. Sarrao. *Possible Fulde-Ferrell-Larkin-Ovchinnikov Superconducting State in $CeCoIn_5$*. Phys. Rev. Lett. **91** (2003) 187004.

[Bianchi 03b] A. Bianchi, R. Movshovich, I. Vekhter, P. G. Pagliuso & J. L. Sarrao. *Avoided Antiferromagnetic Order and Quantum Critical Point in $CeCoIn_5$*. Phys. Rev. Lett. **91** (2003) 257001.

[Bulaevskii 88] L. N. Bulaevskii, O. V. Dolgov & M. O. Ptitsyn. *Properties of strong-coupled superconductors*. Phys. Rev. B **38** (1988) 11290–11295.

[Coleman 07] P. Coleman. *Heavy Fermions: electrons at the edge of magnetism*. arXiv:cond-mat/0612006v3 (2007) .

[Custers 03] J. Custers, P. Gegenwart, H. Wilhelm, K. Neumaier, Y. Tokiwa, O. Trovarelli, C. Geibel, F. Steglich, Pépin C. & Coleman P. *The break-up of heavy electrons at a quantum critical point*. Nature **424** (2003) 524.

[Doman 66] B. G. S. Doman. *The thermal conductivity of a ferrodielectric*. Journal of Physics and Chemistry of Solids **27** (1966) 625 – 628.

[Donath 08] J. G. Donath, F. Steglich, E. D. Bauer, J. L. Sarrao & P. Gegenwart. *Dimensional Crossover of Quantum Critical Behavior in $CeCoIn5$*. Phys. Rev. Lett. **100** (2008) 136401.

[Doniach 77] S. Doniach. *The Kondo lattice and weak antiferromagnetism*. Physica B+C **91** (1977) 231 – 234.

[Farhangfar 97] Sh. Farhangfar, K. Hirvi, J. Kauppinen, J. Pekola, J. Toppari, D. Averin & A. Korotkov. *One dimensional arrays and solitary tunnel junctions in the weak coulomb blockade regime: CBT thermometry*. J. Low Temp. Phys. **108** (1997) 191–215. 10.1007/BF02396821.

[Fertig 77] W. A. Fertig, D. C. Johnston, L. E. DeLong, R. W. McCallum, M. B. Maple & B. T. Matthias. *Destruction of Superconductivity at the Onset of Long-Range Magnetic Order in the Compound $ErRh_4B_4$*. Phys. Rev. Lett. **38** (1977) 987–990.

[Friedemann 09] S. Friedemann, T. Westerkamp, M. Brando, N. Oeschler, S. Wirth, P. Gegenwart, C. Krellner, C. Geibel & F. Steglich. *Detaching the antiferromagnetic quantum critical point from the Fermi-surface reconstruction in YbRh2Si2*. Nature Physics **5** (2009) 465–469.

[Gegenwart 08] Philipp Gegenwart, Qimiao Si & Frank Steglich. *Quantum criticality in heavy-fermion metals.* Nature Physics **4** (2008) 186–197.

[Giesbers 09] A. J. M. Giesbers & U. Zeitler. *Angle-dependent transport measurements at high magnetic fields and mK temperatures with attocube systems rotator ANR30/LT.* Attocube Application Note **P11** (2009) .

[Glémot 99] L. Glémot, J. P. Brison, J. Flouquet, A. I. Buzdin, I. Sheikin, D. Jaccard, C. Thessieu & F. Thomas. *Pressure Dependence of the Upper Critical Field of the Heavy Fermion Superconductor UBe_{13}.* Phys. Rev. Lett. **82** (1999) 169–172.

[Goh 08] Swee K. Goh, Johnpierre Paglione, Mike Sutherland, E. C. T. O'Farrell, C. Bergemann, T. A. Sayles & M. B. Maple. *Fermi-surface reconstruction in CeRh1-xCoxIn5.* Phys. Rev. Lett. **101** (2008) 056402.

[Gor'kov 06] L. P. Gor'kov & P. D. Grigoriev. *Antiferromagnetism and hot spots in $CeIn_3$.* Phys. Rev. B **73** (2006) 060401.

[Hagmusa 00] I. H. Hagmusa, K. Prokes, Y. Echizen, T. Takabatake, T. Fujita, J. C. P. Klaasse, E. Brück, V. Sechovský & F. R. de Boer. *Magnetic specific heat of a URhGe single crystal.* Physica B: Condensed Matter **281-282** (2000) 223 – 225.

[Hardy 11] F. Hardy, D. Aoki, C. Meingast, P. Burger, H. v. Löhneysen & J. Flouquet. *Transverse and Longitudinal Magnetic Field Responses in the Ising Ferromagnets URhGe, UCoGe and UGe2.* to be publiehed in: J. Phys. Soc. Jpn. (2011) .

[Hassinger 08] Elena Hassinger, Dai Aoki, Georg Knebel & Jacques Flouquet. *Pressure–Temperature Phase Diagram of Polycrystalline UCoGe Studied by Resistivity Measurement.* J. Phys. Soc. Jpn. **77** (2008) 073703.

[Hassinger 10] Elena Hassinger. *Comptition d'états fondamentaux dans URu_2Si_2 et UCoGe.* PhD thesisUniversité de Grenoble (2010) .

[Hegger 00] H. Hegger, C. Petrovic, E. G. Moshopoulou, M. F. Hundley, J. L. Sarrao, Z. Fisk & J. D. Thompson. *Pressure-Induced Superconductivity in Quasi-2D $CeRhIn_5$.* Phys. Rev. Lett. **84** (2000) 4986–4989.

[Hensel 68] J. C. Hensel. *Microwave Combined Resonances in Germanium: g Factor of the Free Hole.* Phys. Rev. Lett. **21** (1968) 983–986.

[Huy 07] N. T. Huy, A. Gasparini, D. E. de Nijs, Y. Huang, J. C. P. Klaasse, T. Gortenmulder, A. de Visser, A. Hamann, T. Görlach & H. v. Löhneysen. *Superconductivity on the Border of Weak Itinerant Ferromagnetism in UCoGe.* Phys. Rev. Lett. **99** (2007) 067006.

[Huy 08] N. T. Huy, D. E. de Nijs, Y. K. Huang & A. de Visser. *Unusual Upper Critical Field of the Ferromagnetic Superconductor UCoGe.* Phys. Rev. Lett. **100** (2008) 077002.

[Hykel 10] Danny Hykel & Klaus Hasselbach. *Magnetic imaging of UCoGe interplay of SC-FM.* Talk at the conference on the heavy fermion road in Paris (2010) .

[Ihara 10] Y. Ihara, T. Hattori, K. Ishida, Y. Nakai, E. Osaki, K. Deguchi, N. K. Sato & I. Satoh. *Anisotropic Magnetic Fluctuations in the Ferromagnetic Superconductor UCoGe Studied by Direction-Dependent ^{59}Co NMR Measurements.* Phys. Rev. Lett. **105** (2010) 206403.

[Ikeda 01] Shugo Ikeda, Hiroaki Shishido, Miho Nakashima, Rikio Settai, Dai Aoki, Yoshinori Haga, Hisatomo Harima, Yuji Aoki, Takahiro Namiki, Hideyuki Sato & Yoshichika Onuki. *Unconventional Superconductivity in CeCoIn5 Studied by the Specific Heat and Magnetization Measurements.* J. Phys. Soc. Jpn. **70** (2001) 2248–2251.

[Ikeda 10] Ryusuke Ikeda, Yuhki Hatakeyama & Kazushi Aoyama. *Antiferromagnetic ordering induced by paramagnetic depairing in unconventional superconductors.* Phys. Rev. B **82** (2010) 060510.

[Izawa 07a] K. Izawa, K. Behnia, Y. Matsuda, H. Shishido, R. Settai, Y. Onuki & J. Flouquet. *Thermoelectric response near a quantum critical point: The case of CeCoIn5.* Phys. Rev. Lett. **99** (2007) 147005.

[Izawa 07b] Koichi Izawa, Y. Nakajima, Y. Kasahara, R. Bel, K. Behnia, H. Shishido, R. Settai, Y. Onuki, H. Kontani & Y. Matsuda. *Striking similarities between HTSC and quasi-2D HFCeRIn5.* Physica C **460** (2007) 145–148. 8th International Conference on Materials and Mechanisms of Superconductivity and High Temperature Superconductors, Dresden, GERMANY, JUL 09-14, 2006.

[Kauppinen 98] J. P. Kauppinen, K. T. Loberg, A. J. Manninen, J. P. Pekola & R. A. Voutilainen. *Coulomb blockade thermometer: Tests and instrumentation.* Review of Scientific Instruments **69** (1998) 4166–4175.

[Kawasaki 03] Yu Kawasaki, Shinji Kawasaki, Mitsuharu Yashima, Takeshi Mito, Guo qing Zheng, Yoshio Kitaoka, Hiroaki Shishido, Rikio Settai, Yoshinori Haga & Yoshichika Ōnuki. *Anisotropic Spin Fluctuations in Heavy-Fermion Superconductor $CeCoIn_5$: In-NQR and Co-NMR Studies.* J. Phys. Soc. Jpn. **72** (2003) 2308–2311.

[Kenzelmann 08] M. Kenzelmann, Th. Straessle, C. Niedermayer, M. Sigrist, B. Padmanabhan, M. Zolliker, A. D. Bianchi, R. Movshovich, E. D. Bauer, J. L. Sarrao & J. D. Thompson. *Coupled superconducting and magnetic order in CeCoIn5.* Science **321** (2008) 1652–1654.

[Kittel 96] Charles Kittel. Introduction to solid state physics seventh. John Wiley & Dons, Inc. (1996) .

[Knebel 01] G. Knebel, D. Braithwaite, P. C. Canfield, G. Lapertot & J. Flouquet. *Electronic properties of $CeIn_3$ under high pressure near the quantum critical point.* Phys. Rev. B **65** (2001) 024425.

[Knebel 04] G Knebel, MA Measson, B Salce, D Aoki, D Braithwaite, JP Brison & J Flouquet. *High-pressure phase diagrams of CeRhIn5 and CeCoIn5 studied by ac calorimetry.* J. Phys.: Condens. Matter **16** (2004) 8905–8922.

[Knebel 06a] G. Knebel, D. Aoki, D. Braithwaite, B. Salce & J. Flouquet. *Coexistence of antiferromagnetism and superconductivity in $CeRhIn_5$ under high pressure and magnetic field.* Phys. Rev. B **74** (2006) 020501.

[Knebel 06b] G. Knebel, R. Boursier, E. Hassinger, G. Lapertot, P. G. Niklowitz, A. Pourret, B. Salce, J. P. Sanchez, I. Sheikin, P. Bonville, H. Harima & J. Flouquet. *Localization of 4f state in YbRh2Si2 under magnetic field and high pressure: Comparison with CeRh2Si2.* J. Phys. Soc. Jpn. **75** (2006) 114709.

[Knebel 08] Georg Knebel, Dai Aoki, Jean-Pascal Brison & Jacques Flouquet. *The Quantum Critical Point in CeRhIn5: A Resistivity Study.* J. Phys. Soc. Jpn. **77** (2008) 114704.

[Knebel 09] G. Knebel, D. Aoki & J. Flouquet. *Magnetism and Superconductivity in CeRhIn5.* ArXiv e-prints - accepted in Kotai Butsuri (2009) .

[Knebel 10] Georg Knebel, Dai Aoki, Jean-Pascal Brison, Ludovic Howald, Gerard Lapertot, Justin Panarin, Stephane Raymond & Jacques Flouquet. *Competition and/or coexistence of antiferromagnetism and superconductivity in $CeRhIn_5$ and $CeCoIn_5$.* Phys. Status Solidi B **247** (2010) 557–562.

[Kohori 01] Y. Kohori, Y. Yamato, Y. Iwamoto, T. Kohara, E. D. Bauer, M. B. Maple & J. L. Sarrao. *NMR and NQR studies of the heavy fermion superconductors $CeTIn_5$ ($T = Co$ and Ir).* Phys. Rev. B **64** (2001) 134526.

[Kondo 64] Jun Kondo. *Resistance Minimum in Dilute Magnetic Alloys.* Progress of Theoretical Physics **32** (1964) 37–49.

[Kos 03] S. Kos, I. Martin & C. M. Varma. *Specific heat at the transition in a superconductor with fluctuating magnetic moments.* Phys. Rev. B **68** (2003) 052507.

[Koutroulakis 10] G. Koutroulakis, M. D. Stewart, V. F. Mitrović, M. Horvatić, C. Berthier, G. Lapertot & J. Flouquet. *Field Evolution of Coexisting*

Superconducting and Magnetic Orders in $CeCoIn_5$. Phys. Rev. Lett. **104** (2010) 087001.

[Kumar 82] Anil Kumar. *Low-temperature magnon thermal conductivity of ferromagnetic insulators with impurities.* Phys. Rev. B **25** (1982) 3369–3373.

[Lévy 07] F. Lévy, I. Sheikin & A. Huxley. *Acute enhancement of the upper critical field for superconductivity approaching a quantum critical point in URhGe.* Nat Phys **3** (2007) 460–463.

[Löhneysen 07] Hilbert v. Löhneysen, Achim Rosch, Matthias Vojta & Peter Wölfle. *Fermi-liquid instabilities at magnetic quantum phase transitions.* Rev. Mod. Phys. **79** (2007) 1015.

[Ltd. 10] Cambridge Magnetic Refrigeration Ltd. *LTT-h Specifications: Frequency Response.* Data sheet (2010) .

[Maehira 03] Takahiro Maehira, Takashi Hotta, Kazuo Ueda & Akira Hasegawa. *Relativistic Band-Structure Calculations for $CeTIn_5$ (T = Ir and Co) and Analysis of the Energy Bands by Using Tight-Binding Method.* J. Phys. Soc. Jpn. **72** (2003) 854–864.

[Malinowski 05] A Malinowski, MF Hundley, C Capan, F Ronning, R Movshovich, NO Moreno, JL Sarrao & JD Thompson. *c-axis magnetotransport in CeCoIn5.* Phys. Rev. B **72** (2005) 184506.

[Mathur 98] ND Mathur, FM Grosche, SR Julian, IR Walker, DM Freye, RKW Haselwimmer & GG Lonzarich. *Magnetically mediated superconductivity in heavy fermion compounds.* Nature **394** (1998) 39–43.

[Matsuda 07] Yuji Matsuda & Hiroshi Shimahara. *Fulde–Ferrell–Larkin–Ovchinnikov State in Heavy Fermion Superconductors.* Journal of the Physical Society of Japan **76** (2007) 051005.

[Miclea 06] C. F. Miclea, M. Nicklas, D. Parker, K. Maki, J. L. Sarrao, J. D. Thompson, G. Sparn & F. Steglich. *Pressure Dependence of the Fulde-Ferrell-Larkin-Ovchinnikov State in $CeCoIn5$.* Phys. Rev. Lett. **96** (2006) 117001.

[Millis 93] A. J. Millis. *Effect of a nonzero temperature on quantum critical points in itinerant fermion systems.* Phys. Rev. B **48** (1993) 7183–7196.

[Mineev 10a] V. P. Mineev. *Magnetic field dependence of pairing interaction in ferromagnetic superconductors with triplet pairing.* arXiv:1011.3753v1 (2010) .

[Mineev 10b] V. P. Mineev. *Paramagnetic limit in ferromagnetic superconductors with triplet pairing.* Phys. Rev. B **81** (2010) 180504.

[Mitrović 06] V. F. Mitrović, M. Horvatić, C. Berthier, G. Knebel, G. Lapertot & J. Flouquet. *Observation of Spin Susceptibility Enhancement in the Possible Fulde-Ferrell-Larkin-Ovchinnikov State of $CeCoIn_5$.* Phys. Rev. Lett. **97** (2006) 117002.

[Miyake 07] K Miyake. *New trend of superconductivity in strongly correlated electron systems.* J. Phys.: Condens. Matter **19** (2007) 125201.

[Miyake 08] Atsushi Miyake, Dai Aoki & Jacques Flouquet. *Field Re-entrant Superconductivity Induced by the Enhancement of Effective Mass in URhGe.* J. Phys. Soc. Jpn. **77** (2008) 094709.

[Miyake 09] Atsushi Miyake, Dai Aoki & Jacques Flouquet. *Pressure Evolution of the Ferromagnetic and Field Re-entrant Superconductivity in URhGe.* J. Phys. Soc. Jpn. **78** (2009) 063703.

[Mizutani 03] Uichiro Mizutani. Introduction to the electron theory of metals. CAMBRIDGE UNIVERSITY PRESS (2003) .

[Monthoux 99] P. Monthoux & G. G. Lonzarich. *p-wave and d-wave superconductivity in quasi-two-dimensional metals.* Phys. Rev. B **59** (1999) 14598–14605.

[Monthoux 01] P Monthoux & GG Lonzarich. *Magnetically mediated superconductivity in quasi-two and three dimensions.* Phys. Rev. B **63** (2001) 054529.

[Monthoux 07] P. Monthoux, D. Pines & G. G. Lonzarich. *Superconductivity without phonons.* Nature **450** (2007) 1177–1183.

[Moriya 95] Tôru Moriya & Tetsuya Takimoto. *Anomalous Properties around Magnetic Instability in Heavy Electron Systems.* J. Phys. Soc. Jpn. **64** (1995) 960–969.

[Movshovich 01] R. Movshovich, M. Jaime, J. D. Thompson, C. Petrovic, Z. Fisk, P. G. Pagliuso & J. L. Sarrao. *Unconventional Superconductivity in $CeIrIn5$ and $CeCoIn5$: Specific Heat and Thermal Conductivity Studies.* Phys. Rev. Lett. **86** (2001) 5152–5155.

[Nakatsuji 02] S. Nakatsuji, S. Yeo, L. Balicas, Z. Fisk, P. Schlottmann, P. G. Pagliuso, N. O. Moreno, J. L. Sarrao & J. D. Thompson. *Intersite Coupling Effects in a Kondo Lattice.* Phys. Rev. Lett. **89** (2002) 106402.

[Nakatsuji 04] Satoru Nakatsuji, David Pines & Zachary Fisk. *Two Fluid Description of the Kondo Lattice.* Phys. Rev. Lett. **92** (2004) 016401.

[Nicklas 01] M Nicklas, R Borth, E Lengyel, PG Pagliuso, JL Sarrao, VA Sidorov, G Sparn, F Steglich & JD Thompson. *Response of the heavy-fermion*

superconductor CeCoIn5 to pressure: roles of dimensionality and proximity to a quantum-critical point. J. Phys.: Condens. Matter **13** (2001) L905–L912.

[Nilsson 09] Henrik A. Nilsson, Philippe Caroff, Claes Thelander, Marcus Larsson, Jakob B. Wagner, Lars-Erik Wernersson, Lars Samuelson & H. Q. Xu. *Giant, Level-Dependent g Factors in InSb Nanowire Quantum Dots.* Nano Lett. **9** (2009) 3151–3156.

[Ohta 10] Tetsuya Ohta, Taisuke Hattori, Kenji Ishida, Yusuke Nakai, Eisuke Osaki, Kazuhiko Deguchi, Noriaki K. Sato & Isamu Satoh. *Microscopic Coexistence of Ferromagnetism and Superconductivity in Single-Crystal UCoGe.* J. Phys. Soc. Jpn. **79** (2010) 023707.

[Paglione 03] J. Paglione, M. A. Tanatar, D.G. Hawthorn, E. Boaknin, R.W. Hill, F. Ronning, M. Sutherland & L. Taillefer. *Field-Induced Quantum Critical Point in $CeCoIn_5$.* Phys. Rev. Lett. **91** (2003) 246405.

[Pekola 94] J. P. Pekola, K. P. Hirvi, J. P. Kauppinen & M. A. Paalanen. *Thermometry by Arrays of Tunnel Junctions.* Phys. Rev. Lett. **73** (1994) 2903–2906.

[Pekola 10] J.P. Pekola. *Private communication* (2010.) .

[Petrovic 01] C Petrovic, PG Pagliuso, MF Hundley, R Movshovich, JL Sarrao, JD Thompson, Z Fisk & P Monthoux. *Heavy-fermion superconductivity in CeCoIn5 at 2.3 K.* J. Phys.: Condens. Matter **13** (2001) L337–L342.

[Petrovic 02] C. Petrovic, S. L. Bud'ko, V. G. Kogan & P. C. Canfield. *Effects of La substitution on the superconducting state of $CeCoIn_5$.* Phys. Rev. B **66** (2002) 054534.

[Pfleiderer 09] Christian Pfleiderer. *Superconducting phases of f -electron compounds.* Rev. Mod. Phys. **81** (2009) 1551–1624.

[Pham 06] L. D. Pham, Tuson Park, S. Maquilon, J. D. Thompson & Z. Fisk. *Reversible tuning of the heavy-fermion ground state in CeCoIn5.* Phys. Rev. Lett. **97** (2006) 056404.

[Prokeš 99] K. Prokeš, T. Tahara, T. Fujita, H. Goshima, T. Takabatake, M. Mihalik, A. A. Menovsky, S. Fukuda & J. Sakurai. *Electronic properties of a UIrGe single crystal.* Phys. Rev. B **60** (1999) 9532–9538.

[Prokes 02] K. Prokes, T. Tahara, Y. Echizen, T. Takabatake, T. Fujita, I. H. Hagmusa, J. C. P. Klaasse, E. Brück, F. R. de Boer, M. Divis & V. Sechovský. *Electronic properties of a URhGe single crystal.* Physica B: Condensed Matter **311** (2002) 220 – 232.

[Radovan 03] H. A.. Radovan, N. A. Fortune, T. P. Murphy, S. T. Hannahs, E. C. Palm, S. W. Tozer & D. Hall. *Magnetic enhancement of superconductivity from electron spin domains.* Nature **425** (2003) 51–55.

[Reyes 09] D. Reyes, M. A. Continentino & Han-Ting Wang. *Thermodynamic quantum critical behavior of the anisotropic Kondo necklace model.* J. Magn. Magn. Mater. **321** (2009) 348–353.

[Ronning 05] F Ronning, C Capan, A Bianchi, R Movshovich, A Lacerda, MF Hundley, JD Thompson, PG Pagliuso & JL Sarrao. *Field-tuned quantum critical point in CeCoIn5 near the superconducting upper critical field.* Phys. Rev. B **71** (2005) 104528.

[Ronning 06] F Ronning, C Capan, ED Bauer, JD Thompson, JL Sarrao & R Movshovich. *Pressure study of quantum criticality in CeCoIn5.* Phys. Rev. B **73** (2006) 064519.

[Rosch 00] A. Rosch. *Magnetotransport in nearly antiferromagnetic metals.* Phys. Rev. B **62** (2000) 4945–4962.

[Sakai 10] Hironori Sakai, Seung-Ho Baek, Stuart E. Brown, Filip Ronning, Eric D. Bauer & Joe D. Thompson. *^{59}Co NMR shift anomalies and spin dynamics in the normal state of superconducting $CeCoIn_5$: Verification of two-dimensional antiferromagnetic spin fluctuations.* Phys. Rev. B **82** (2010) 020501.

[Sandeman 03] K. G. Sandeman, G. G. Lonzarich & A. J. Schofield. *Ferromagnetic Superconductivity Driven by Changing Fermi Surface Topology.* Phys. Rev. Lett. **90** (2003) 167005.

[Sarrao 07] John L. Sarrao & Joe D. Thompson. *Superconductivity in cerium- and plutonium-based '115' materials.* J. Phys. Soc. Jpn. **76** (2007) 051013.

[Saxena 00] S. S. Saxena, P. Agarwal, K. Ahilan, F. M. Grosche, R. K. W. Haselwimmer, M. J. Steiner, E. Pugh, I. R. Walker, S. R. Julian, P. Monthoux, G. G. Lonzarich, A. Huxley, I. Sheikin, D. Braithwaite & J. Flouquet. *Superconductivity on the border of itinerant-electron ferromagnetism in UGe2.* Nature **406** (2000) 587–592.

[Settai 01] R Settai, H Shishido, S Ikeda, Y Murakawa, M Nakashima, D Aoki, Y Haga, H Harima & Y Onuki. *Quasi-two-dimensional Fermi surfaces and the de Haas-van Alphen oscillation in both the normal and superconducting mixed states of CeCoIn5.* J. Phys.: Condens. Matter **13** (2001) L627–L634.

[Settai 08] Rikio Settai, Yuichiro Miyauchi, Tetsuya Takeuchi, Florence Lévy, Ilya Sheikin & Yoshichika Ōnuki. *Huge Upper Critical Field and Electronic Instability in Pressure-induced Superconductor $CeIrSi_3$ without Inversion Symmetry in the Crystal Structure.* J. Phys. Soc. Jpn. **77** (2008) 073705.

[Seyfarth 08] G. Seyfarth, J. P. Brison, G. Knebel, D. Aoki, G. Lapertot & J. Flouquet. *Multigap superconductivity in the heavy-fermion system $CeCoIn_5$.* Phys. Rev. Lett. **101** (2008) 046401.

[Shakeripour 09] H. Shakeripour, C. Petrovic & Louis Taillefer. *Heat transport as a probe of superconducting gap structure.* New J. Phys. **11** (2009) 055065.

[Sheikin 01] I. Sheikin, A. Huxley, D. Braithwaite, J. P. Brison, S. Watanabe, K. Miyake & J. Flouquet. *Anisotropy and pressure dependence of the upper critical field of the ferromagnetic superconductor UGe_2.* Phys. Rev. B **64** (2001) 220503.

[Shulga 98] S. V. Shulga, S.-L. Drechsler, G. Fuchs, K.-H. Müller, K. Winzer, M. Heinecke & K. Krug. *Upper Critical Field Peculiarities of Superconducting YNi_2B_2C and $LuNi_2B_2C$.* Phys. Rev. Lett. **80** (1998) 1730–1733.

[Si 01] Qimiao Si, Silvio Rabello, Kevin Ingersent & J. Lleweilun Smith. *Locally critical quantum phase transitions in strongly correlated metals.* Nature **413** (2001) 804–808.

[Singh 07] S. Singh, C. Capan, M. Nicklas, M. Rams, A. Gladun, H. Lee, J. F. DiTusa, Z. Fisk, F. Steglich & S. Wirth. *Probing the quantum critical behavior of CeCoIn5 via Hall effect measurements.* Phys. Rev. Lett. **98** (2007) 057001.

[Sparn 02] G. Sparn, R. Borth, E. Lengyel, P. G. Pagliuso, J. L. Sarrao, F. Steglich & J. D. Thompson. *Unconventional superconductivity in CeCoIn5–a high pressure study.* Physica B: Condensed Matter **319** (2002) 262 – 267.

[Stock 08] C. Stock, C. Broholm, J. Hudis, H. J. Kang & C. Petrovic. *Spin Resonance in the d-Wave Superconductor $CeCoIn_5$.* Phys. Rev. Lett. **100** (2008) 087001.

[Tanatar 07] Makariy A. Tanatar, Johnpierre Paglione, Cedomir Petrovic & Louis Taillefer. *Anisotropic violation of the Wiedemann-Franz law at a quantum critical point.* Science **316** (2007) 1320–1322 + *Supplementary material.*

[Taufour 10] V. Taufour, D. Aoki, G. Knebel & J. Flouquet. *Tricritical Point and Wing Structure in the Itinerant Ferromagnet UGe_2.* Phys. Rev. Lett. **105** (2010) 217201.

[Tayama 02] T. Tayama, A. Harita, T. Sakakibara, Y. Haga, H. Shishido, R. Settai & Y. Onuki. *Unconventional heavy-fermion superconductor $CeCoIn_5$: dc magnetization study at temperatures down to 50 mK.* Phys. Rev. B **65** (2002) 180504.

[Tokiwa 08] Y. Tokiwa, R. Movshovich, F. Ronning, E. D. Bauer, P. Papin, A. D. Bianchi, J. F. Rauscher, S. M. Kauzlarich & Z. Fisk. *Anisotropic Effect of Cd and Hg Doping on the Pauli Limited Superconductor $CeCoIn_5$.* Phys. Rev. Lett. **101** (2008) 037001.

[Troć 10] R. Troć, R. Wawryk, W. Miiller, H. Misiorek & M. Samsel-Czekała. *Bulk properties of the UCoGe Kondo-like system.* Philosophical Magazine **90** (2010) 2249–2271.

[Ueda 75] Kazuo Ueda & Toru Moriya. *Contribution of Spin Fluctuations to the Electrical and Thermal Resistivities of Weakly and Nearly Ferromagnetic Metals.* J. Phys. Soc. Jpn. **39** (1975) 605–615.

[Ventura 09] G. Ventura & V. Martelli. *Thermal conductivity of Kevlar 49 between 7 and 290 K.* Cryogenics **49** (2009) 735 – 737.

[Watanabe 09] Shinji Watanabe, Atsushi Tsuruta, Kazumasa Miyake & Jacques Flouquet. *Valence Fluctuations Revealed by Magnetic Field and Pressure Scans: Comparison with Experiments in $YbXCu_4$ (X = In, Ag, Cd) and $CeYIn_5$ (Y = Ir, Rh).* Journal of the Physical Society of Japan **78** (2009) 104706.

[Yashima 04] M Yashima, S Kawasaki, Y Kawasaki, GQ Zheng, Y Kitaoka, H Shishido, R Settai, Y Haga & Y Onuki. *Magnetic criticality and unconventional superconductivity in CeCoIn5: Study of (115)in-nuclear quadrupole resonance under pressure.* J. Phys. Soc. Jpn. **73** (2004) 2073–2076.

[Young 07] B.-L. Young, R. R. Urbano, N. J. Curro, J. D. Thompson, J. L. Sarrao, A. B. Vorontsov & M. J. Graf. *Microscopic Evidence for Field-Induced Magnetism in $CeCoIn_5$.* Phys. Rev. Lett. **98** (2007) 036402.

[Zaum 10] S. Zaum, K. Grube, R. Schäfer, E. D. Bauer, J. D. Thompson & H. v. Löhneysen. *Towards the identification of a quantum critical line in the (p, B) phase diagram of CeCoIn5.* arXiv:1010.3175v1 (2010) .

[Zdravkov 10] V. I. Zdravkov, J. Kehrle, G. Obermeier, S. Gsell, M. Schreck, C. Müller, H.-A. Krug von Nidda, J. Lindner, J. Moosburger-Will, E. Nold, R. Morari, V. V. Ryazanov, A. S. Sidorenko, S. Horn, R. Tidecks & L. R. Tagirov. *Reentrant superconductivity in superconductor/ferromagnetic-alloy bilayers.* Phys. Rev. B **82** (2010) 054517.